Understanding $^{40}Ar/^{39}Ar$ Age Variations in Potassium Feldspars from Low-Sulfidation Epithermal Systems in the Miocene Yellowstone Hotspot

By

Zachary Davis

A thesis submitted to the Graduate Faculty of

Auburn University in partial fulfillment of the

requirements for the Degree of

Master of Science

Auburn, Alabama

August 3, 2024

Keywords: Epithermal, Closure Temperature, Yellowstone Hotspot, Silver City District, Jumbo Mine

Committee:

Willis Hames, Professor, Department of Geosciences

Laura Bilenker, Assistant Professor, Department of Geosciences

Haibo Zou, Professor, Department of Geosciences

ABSTRACT

The inception of the Yellowstone hotspot resulted in the Columbia River Large Igneous Province (LIP), Mid-Miocene magmatism in western North America, and numerous epithermal Au-Ag deposits in the Oregon-Idaho-Nevada region. $^{40}Ar/^{39}Ar$ ages of hydrothermal K-feldspars in Au-Ag bearing veins (commonly referred to as 'adularia') are useful in understanding the relationship of mineralization to the broader regional magmatic evolution and assisting in targeting exploration and mine development efforts. Although they seem 'ideal' to date, and they are highly radiogenic and yield precise ages, $^{40}Ar/^{39}Ar$ analyses for adularia from the Trade Dollar Mine (Silver City District (SCD), Idaho) and the Jumbo Mine (Nevada) yield ages ranging from 16.27 ±0.11 to 15.79±0.02 Ma, and 16.86±0.13 to 16.15±0.07 Ma respectively. These ages are notably younger than the regional volcanic rocks - and ages for individual crystals from single hand-samples were found to vary by up to ~ 0.7 Ma. These age dates could indicate a remarkably long-lived system, with episodic precipitation of adularia. However, it is more likely that these intercrystalline variations in adularia ages are created by varying diffusive properties between adularia crystals, in combination with episodic precipitation of adularia. X-ray diffraction (XRD) data indicate adularia in the SCD, and the Jumbo Mine are high sanidine (face-centered monoclinic, C2m), suggesting rapid crystallization. Rapid crystallization would prevent the ordering of Al into its preferred T_1o site and generate defects in the crystal lattice. Fluid inclusion homogenization temperatures from the SCD range from 180-285°C (Halsor et al., 1988; Aseto, 2012), at or above the calculated closure temperatures (200-266°C) for adularia from the Trade Dollar Mine. This means that upon crystallization, the adularia crystals were partially open systems that lost some radiogenic ^{40}Ar. The range of $^{40}Ar/^{39}Ar$ closure temperatures are interpreted to be

created by effective diffusion dimensions that vary from crystal to crystal. These varying effective diffusion dimensions are likely due to the rapid precipitation of adularia from solution, generating lattice vacancies, and linear and planar defects. This study concludes that $^{40}Ar/^{39}Ar$ ages reflect the age at which the individual crystal cooled past its respective closure temperature, and not the Au-Ag mineralization age.

ACKNOWLEDGEMENTS

I would like to express my profound gratitude for Dr. Hames. He has been a constant source of guidance, wisdom, and knowledge. His mentorship allowed me to grow and prosper during my short time at Auburn.

I am eternally grateful for the community of the Auburn University Department of Geoscience. I have grown immeasurably as a geologist and a man during the last two years, which I account to the friendships and the knowledge imparted by the professors within the department.

Finally, I would like to thank my family and friends who have been a constant source of love, patience, and support. They have gotten me through many rough times and my gratitude is immeasurable.

TABLE OF CONTENTS

LIST OF TABLES

LIST OF FIGURES

INTRODUCTION

The initiation of the Yellowstone Hotspot is recorded by silicic and basaltic volcanism ranging from 14-17 Ma across the Pacific Northwest and along the northeastward progression of the eastern Snake River Plain (Christiansen and Yeats, 1992) (Fig. 1). The geological term "hotspot" was put forward by Wilson (1963) to describe linear chains of volcanoes that were interpreted to record the motions of the overlying plates. The Yellowstone Hotspot is widely accepted to be driven by an upwelling deep mantle plume, and by feedback between upper-mantle convection linked to the subduction of the Juan de Fuca Plate subducting beneath the North American Plate (Hill, 1993; Camp and Hannan, 2008; Pierce and Morgan, 2009; Camp et al., 2015). Initiation of Miocene magmatism was likely aided by viscous drag, slab rollback, and trench suction that contributed to the thinning of the crust and formation of the Columbia River Large Igneous Province (LIP) (Camp and Hanan, 2008). LIPs are defined to be responsible for the generation of 10^6-10^7 km^3 of intrusions and lava emplacement (Black et al., 2010). LIPs are widely accepted as a source of heat and metals in the development of ore deposits throughout the history of Earth. The Miocene Yellowstone Hotspot resulted in the development of the Columbia River LIP, and numerous low-sulfidation epithermal Au-Ag deposits in the Oregon-Idaho-Nevada region.

Epithermal Precious Metal Systems

Epithermal ores were first defined and named by Waldemar Lindgren (Lindgren, 1933) to identify the shallow low-temperature hydrothermal ores of any origin. Lindgren in 1933 proposed that epithermal deposits formed at low temperatures (50-200°C) and pressures (< 100 atmospheres). Fluid inclusion studies have shown that epithermal ores form in temperatures that range from 150-300°C (Sawkins et al., 1979; Buchanan, 1981; Simmons et al., 2005) with ore mineralization that occurs at depths from 50 m to 1500 m (Simmons et al., 2005; Taylor, 2007). These shallow depths result in a high risk of erosion; as a result, epithermal deposits are usually only preserved in Cenozoic formations (Taylor, 2007).

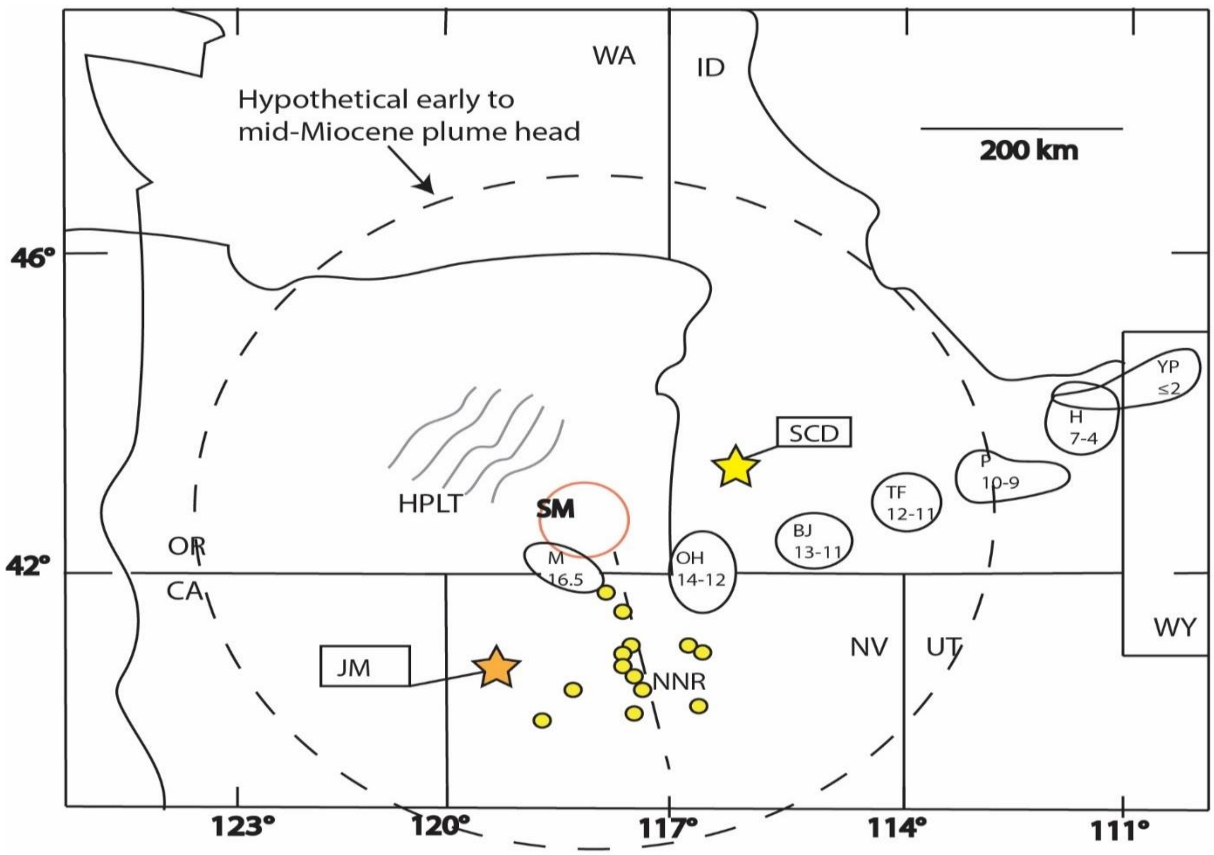

Figure 1. A generalized map showing the location of the Jumbo Mine (orange star, JM) and Silver City District (yellow star, SCD). The dashed circle represents the possible extent of flattening of the mantle plume head after Hill (1993). The orange circle represents the hypothetical hot tail of the mantle plume (original center of the Yellowstone Hotspot) after Hill (1993). Yellow circles represent Au-Ag epithermal deposits and historic Au-Ag mines. Silicic volcanic centers proposed to originate from Yellowstone Hotspot migration are outlined by dashed lines; M – McDermitt caldera; BJ – Bruneau-Jarbidge volcanic field; OH – Owhyee-Humboldt volcanic field; TF – Twin Falls volcanic field; P – Picabo volcanic field; H – Heise volcanic field; YP – Yellowstone Plateau volcanic field. Ages for the silicic volcanic centers (generally rounded to the nearest million years and are intended to be inclusive) are based on compilations of Pierce and Morgan (1992), Morgan and McIntosh (2005), and Bruseke at al. (2007), with the addition of the age for the McDermitt caldera from Henry et al. (2006). The westward-younging High Plains Lava Trend (HPLT) is shown as well. Other abbreviations: NNR, Northern Nevada Rift: SM, Steen Mountains. Figure after Hames et al. (2009).

Epithermal deposits are widely accepted as epigenetic, though they may have contemporaneous ages to their host rocks within active volcanic terranes (Taylor, 2007). Epithermal deposits are classified according to the magmatic and hydrothermal processes that formed them (Hedenquist and Lowenstern, 1994; Sillitoe and Hedenquist, 2003; Simmons et al., 2005). Epithermal deposits are usually classified into two end members: high and low sulfidation, as a function of their ore minerals, and gangue-mineral assemblage (Sillitoe and Hedenquist, 2003). High sulfidation deposits are characterized by acid alteration, are dominated by minerals such as quartz, alunite, jarosite, clays, and pyrophyllite, and typically contain gold and enargite as ore minerals. High sulfidation deposits are typically proximal to their probable magmatic source (Fig. 2) and are dominated by acidic, hotter, and saline fluids than low-sulfidation deposits (Hedenquist and Lowenstern, 1994; Sillitoe and Hedenquist, 2003; Simmons et al., 2005).

Low sulfidation epithermal deposits are formed from near-neutral pH solutions, low salinities (0.2–0.5 w.t.%), sulfide-dominated, and are distal (Fig. 2) from their likely heat source (Sillitoe, 1989; Hedenquist and Lowenstern, 1994; Sillitoe and Hedenquist, 2003; Simmons et al., 2005). Low sulfidation epithermal deposits contain quartz, sericite, calcite, adularia, and illite with typical ore minerals including electrum, arcanthite, selenides, and tellurides (Hedenquist and Lowenstern, 1994; Sillitoe and Hedenquist, 2003; Simmons et al., 2005).

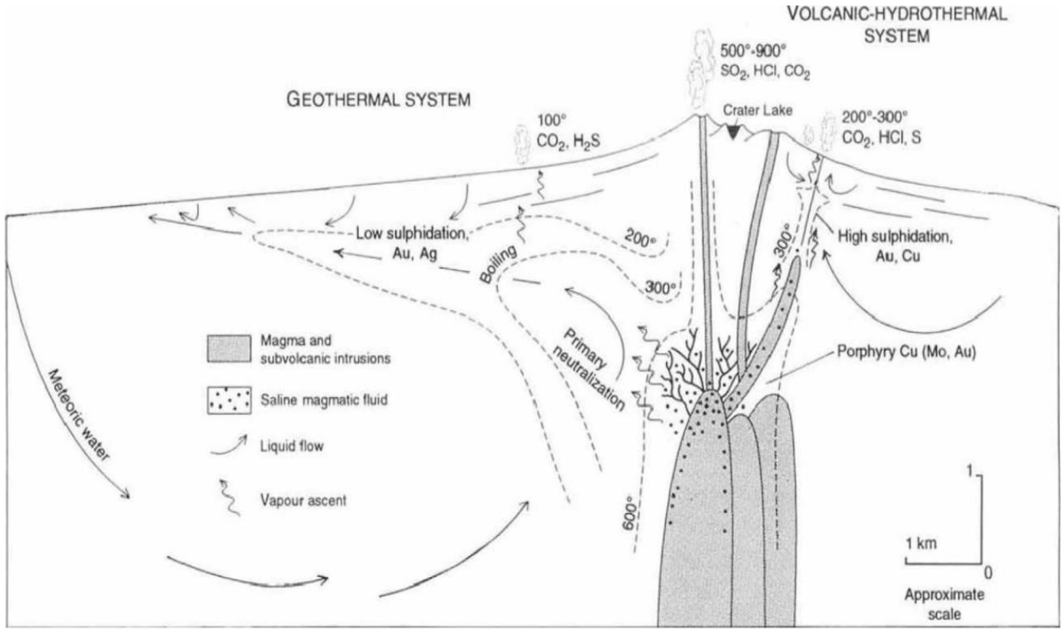

Figure 2. Cross-section of a volcanic-hydrothermal system showing the low-sulfidation epithermal deposits, high-sulfidation epithermal deposits, and porphyry deposits. Figure from Hedenquist and Lowenstern, 1994.

Previous Work and Context for Interpreting Regional Adularia Ages

Adularia ($KAlSi_3O_8$) is a gangue mineral that commonly occurs in the boiling zones of low-sulfidation epithermal systems, making it an ideal potential geochronometer to constrain the mineralization age(s) of epithermal Au-Ag deposits (John, 2001; Unger, 2008; Hames et al., 2009; Aseto, 2012). Adularia primarily occurs in low temperatures (<450°C) and is commonly triclinic but can be monoclinic; However, both symmetries have been observed to exist within single crystals (Nesse, 2012). Adularia habit is influenced by Al-Si ordering, where high dis-ordering, intermediate dis-ordering, and relatively ordered ($2t_1$ >0.84), produce pseudo-acicular adularia, rhombic adularia, sub-rhombic adularia, respectively (Dong and Morrison, 1995). Rhombic and tabular habit implies rapid crystallization conditions, with sub-rhombic reflecting slow crystallization (Dong and Morrison, 1995).

Aseto (2012) conducted $^{40}Ar/^{39}Ar$ geochronology on fresh, euhedral, and optically clear adularia from several Silver City mines (including Trade Dollar, Orofino, Poorman, Blackjack, Dewey) which yielded ages ranging from 16.17±0.08 to 15.46±0.06 Ma (ages recalculated using the decay constant from Min et al., 2000). The authors interpreted these ages to represent the crystallization age of adularia. These ages are between the ages of the youngest regional volcanic rocks which range from 16.6 to 14 Ma (Bonnichsen and Godchaux, 2006), and younger than the earliest regional basaltic to rhyolitic magmatism represented regionally by the Steens Basalts at ~16.7 Ma (Jarboe et al., 2010). Any regional volcanism could have acted as both a heat and metal source to drive the mineralization event at the Silver City District. Halsor (1988) and Aseto (2012) conducted fluid inclusion studies on adularia from the Silver City District and found homogenization temperatures that range from 180-285°C. These temperatures are above the nominal closure temperature of 200°C for alkali feldspars, indicating that upon crystallization, they were only partially retentive of radiogenic ^{40}Ar.

Mining in the Silver City District, Idaho was primarily located at DeLamar and Florida Mountains. During the lifetime of mining at the Silver City District, an estimated production of 750,000 oz. of Au and 47.5 million oz. of Ag were produced (Gillerman and Mitchell, 2005). This amounts to $1,515,750,000 for Au and $1,157,100,000 for Ag in 2023 (Kitco, 2023). The Trade Dollar vein (referred to as the Trade Dollar Mine) is located on Florida Mountain in the Silver City District, Idaho. The Silver City District is in the Owyhee volcanic field, hosted by an Upper Cretaceous granite with a K/Ar age data of ~ 65 Ma (Pansze, 1975), and is related to the Idaho Batholith (Lingdren, 1900; Ekren et al., 1982; Halsor et al., 1988). Above this, Halsor et al. (1988) describes an unconformity which is overlain by basalts of variable thickness. These basalts were reported to have $^{40}Ar/^{39}Ar$ dates of 16.1 Ma (Aseto, 2012).

The Jumbo Mine is in the northern Slumbering Hills, Nevada (Fig. 1) hosted by folded Mesozoic, slate, phyllite and quartzite (Willden, 1964). The Jumbo Deposit produced 1000 tons of Au-Ag ore between 1935 and 1937. Jumbo was mined until 1951 when the ore ran out (Willden, 1964). Geochronology of adularia from the Jumbo Mine in the Slumbering Hills of Northern Nevada has been conducted via K/Ar by Conrad et al. (1993) and $^{40}Ar/^{39}Ar$ by Hames et al. (2009). Conrad et al. (1993) found an age of 17.3 Ma, however, the bulk-sample total-fusion method utilized was incapable of resolving extraneous, non-atmospheric “excess” argon, which likely produced an older age. Hames et al. (2009) conducted $^{40}Ar/^{39}Ar$ geochronology on adularia that were clear, inclusion-free, euhedral, and fresh. Hames et al. (2009) reported an age of 16.64±0.04 Ma (age recalculated using the decay constant from Min et al., 2000), which the authors interpret as the age of crystallization of adularia.

Diffusion Theory Context for Considering Adularia; Cooling Ages or Crystallization Ages?

When utilizing $^{40}Ar/^{39}Ar$ geochronology on alkali feldspars, it is important to consider the temperature at which alkali feldspar crystals will sufficiently retain radiogenic ^{40}Ar. Dodson (1973) defines the closure temperature as the temperature at the time recorded by the sample age (Fig. 3). Dodson (1973) postulated the closure temperature (T_c) model:

(1) $$\mathrm{T_c} = R/[Eln\left(\frac{A\tau D_0}{a^2}\right)]$$

Where R is the gas constant, E is the activation energy, τ is the time constant, D_0 is the frequency factor, a is the diffusion dimension (also referred to as r^2), and A is the geometric constant equal to 55, 27, or 8.7 for the sphere, cylinder, or plane sheet model, respectively. T is related to cooling rate by:

(2) $$\tau = \frac{\mathrm{R}}{\left(\frac{\mathrm{Ed}T^{-1}}{dt}\right)} = -RT^2/\left(\frac{EdT}{dt}\right)$$

Foland (1994) conducted ^{40}Ar diffusion experiments with carefully sized alkali feldspar crystals under varying temperatures and fluid activities. Foland (1994) concluded that the diffusion of alkali feldspars is controlled by the size of the grain, with larger crystals being more diffusive. Based upon Foland's (1994) experiments on T_c, the ^{40}Ar T_c for feldspars ranges from 150 to 300°C, with the nominal closure temperature at 200°C (Fig.4).

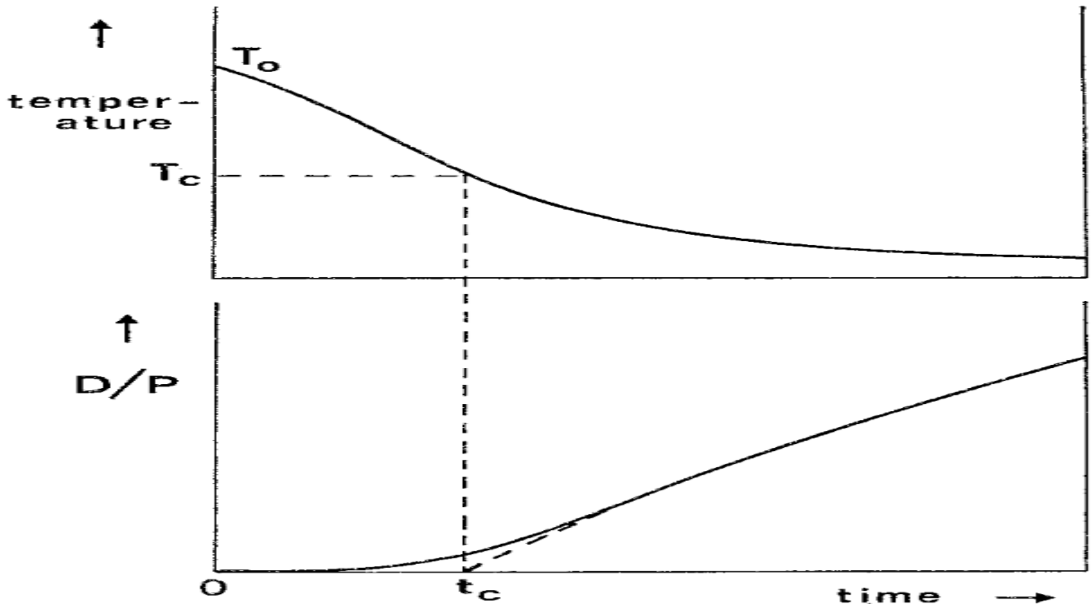

Figure 3: A graphical representation of closure temperature (T_c) where T_c is the temperature at which the age of the sample is recorded. Prior to T_c, there is partial retention and loss of radiogenic ^{40}Ar in the sample. After T_c, there is partial loss of radiogenic ^{40}Ar with the majority being retained in the sample. Figure from Dodson (1973).

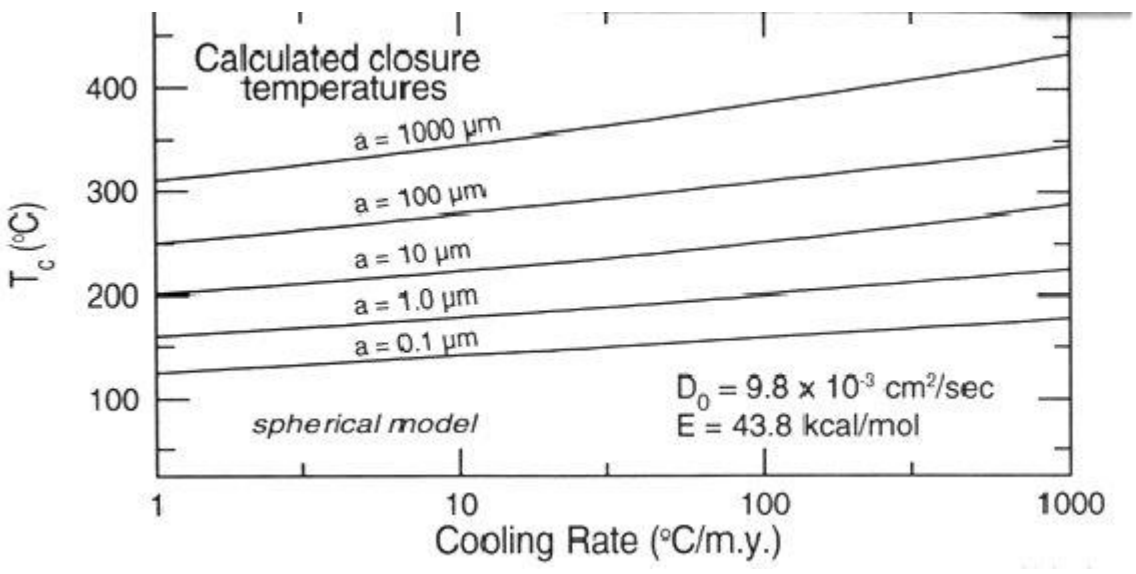

Figure 4: Foland (1994) calculation of the closure temperature for feldspars utilizing the spherical geometric model following Dodson (1973).

Objectives and Hypotheses

The present study tested the magnitude of age variation of feldspars collected from two epithermal systems along the Miocene Yellowstone Hotspot using field context, feldspar texture, feldspar geochemistry, crystallography, and $^{40}Ar/^{39}Ar$ geochronology of single adularia crystals.

Hypothesis 1

The formation of Au-Ag ores in the Yellowstone Hotspot began at 16.4 Ma with the initiation of the Yellowstone Hotspot, and young towards the progressively eastward track of the Yellowstone Hotspot. Au-Ag mineralization at the Silver City District, Idaho occurred at 15.5 Ma, about 1 m.y. later, following the interaction of the Yellowstone Hotspot with the continental lithosphere in this relatively easterly location.

Test

Single adularia crystals from the Jumbo Mine and Trade Dollar Mine were analyzed with $^{40}Ar/^{39}Ar$ geochronology using single crystal total fusion and incremental heating to determine $^{40}Ar/^{39}Ar$ ages. Samples ages at Jumbo match the initiation of the Yellowstone Hotspot (16.5 Ma) and samples at Trade Dollar will be 15.5 Ma, reflecting the relative easterly travel of the hotspot.

Hypothesis 2

As the Silver City District is more centralized along the Yellowstone Hotspot track, relative to the site of the Jumbo Mine it would be subjected to higher temperatures for extended periods. These higher temperatures would not promote the retention of radiogenic ^{40}Ar. Therefore, the Silver City adularia $^{40}Ar/^{39}Ar$ age dates of 15.5 Ma do not accurately reflect the age of Au-Ag mineralization. Instead, the $^{40}Ar/^{39}Ar$ ages reflect a thermal history that kept the adularia above the nominal 200°C closure temperature, promoting ^{40}Ar loss and creating misleadingly young $^{40}Ar/^{39}Ar$ age ages.

Test

Conducted single crystal total fusion and incremental heating on adularia from the Jumbo Mine and Trade Dollar Mine to determine $^{40}Ar/^{39}Ar$ ages. Sample ages may range from the initiation of the Yellowstone Hotspot to the youngest regional volcanic activity. These ages will reflect the time at which samples began to favorably retain radiogenic ^{40}Ar.

Hypothesis 3

As the Trade Dollar Mine was likely exposed to a stronger and perhaps longer thermal history than the Jumbo Mine which have promoted the K-feldpars from the Silver City Granite Host rock to favorably lose $^{40}Ar^{*}$. If this is true, the Silver City Granite K-feldspars would record the stronger and perhaps longer thermal history in their $^{40}Ar/^{39}Ar$ ages.

Test

Single crystals of K-feldspars from the Silver City Granite were analyzed with $^{40}Ar/^{39}Ar$ geochronology using single crystal total fusion and incremental heating to determine $^{40}Ar/^{39}Ar$ ages. Sample ages may reveal ages that match the adularia ages from the Trade Dollar Mine, which would suggest resetting of the $^{40}Ar/^{39}Ar$ ages by the magmatism and associated hydrothermal activities that drove the Au-Ag mineralization at the Trade Dollar Mine. Elemental analysis of the K-feldspars will be used to verify composition prior to $^{40}Ar/^{39}Ar$ analysis.

Hypothesis 4

Variations in the chemical composition and corresponding variations in diffusivity of ^{40}Ar of adularia are responsible for the range of $^{40}Ar/^{39}Ar$ age dates presented by Aseto (2012).

Test

Analyze the elemental composition of adularia collected from the Jumbo Mine and the Silver City District (Trade Dollar Mine) to verify the composition of adularia. Adularia with low potassium content will have lower radiogenic ^{40}Ar, resulting in ages that are highly susceptible to excess argon and fluid inclusions.

Hypothesis 5

Crystalline structure and Al-Si disordering within the crystal lattice may vary enough between the Jumbo Mine Adularia, Trade Dollar Mine Adularia, and Silver City Granite K-feldspars to generate a range of T_c between the samples and within the samples. This range of T_c would create a spectrum of ages and suggest that $^{40}Ar/^{39}Ar$ ages of adularia are cooling ages rather than the age of Au-Ag mineralization.

Test 1

X-Ray Diffraction analysis was conducted on the Jumbo Mine Adularia, Trade Dollar Mine Adularia, and Silver City Granite K-feldspars to determine crystalline structure and Al-Si disordering within the crystal lattice.

Test 2

Calculation of closure temperature of the Jumbo Mine Adularia, Trade Dollar Mine Adularia, and Silver City Granite K-feldspars was conducted to understand how the thermal history of the sample sites played a role in $^{40}Ar^{*}$ retention.

GEOLOGIC FRAMEWORK

The geology of the Northern Great Basin is a complex puzzle that has gone through numerous geologic processes. John (2001) provides an excellent discussion of the geologic history of the Northern Great Basin and the following review is largely adapted from his analysis.

The Late Proterozoic saw the breakup of the Rodina Supercontinent, which created a westward facing passive margin on the rifted edge of the Precambrian continental crust (Stewart, 1980; Karlstrom et al., 1999). Several compressional and extensional tectonic regimes occurred during the Paleozoic to Cenozoic Era, including the Late Devonian to Early Mississippian Antler and the Late Permian to Early Triassic Sonoma orogenies which thrusted sedimentary rocks of the Roberts Mountains on top of the continental shelf. The following Mesozoic and early Cenozoic Nevadan, Elko, Sevier, and Laramide orogenies were driven by east-dipping subduction beneath the North American Plate and the accretion of island-arc terranes. Orogenic development continued until an extensional tectonic regime began to dominate in the Cenozoic, which continues to the present day. Calc-alkaline subduction-related magmatism occurred in high amounts during the Jurrasic, Cretaceous, and Cenozoic (Miller and Barton, 1990; Christiansen and Yeats, 1992), which generated many prophyry-related Cu, Mo, Au deposits, and the Carlin and Getchell trend deposits (John, 2001). Cenozoic extension and magmatism have a close temporal and spatial relationship within the Great Basin (John, 2001;Gans et al., 1989; Feeley and Grunder, 1991; Morris et al., 2001). In the Late Eocene, large-scale normal faults and detachment faults began to affect the Great Basin (Proffett, 1977; Gans et al., 1989; Seedorff, 1991). Wide-spread but small-scale normal faulting began to affect the Great Basin around 17-16 Ma, which are responsible for the physiography seen today (John, 2001). Cenozoic magmatism in the Great Basin is characterized by three tectonic-magmatic assemblages (John, 2001): (1) An (Eocene to early Miocene) andesite-rhyolite, (2) an (early Miocene to early Pliocene) andesite, and (3) a (middle Miocene to Holocene) bimodal basalt-rhyolite. The older magmatic assemblages (1&2) are interpreted to have formed from back-arc extension (Christiansen and Lipman, 1972; Carlson and Hart, 1987) and with Yellowstone Hotspot interaction with the crust at ~16.5 Ma (Zoback and Thompson, 1978; Christiansen and Yeats, 1992; Pierce and Morgan, 1992; Parsons et al., 1994). The younger assemblage (3) is interpreted to be formed by lithospheric extension over the Yellowstone Hotspot (Christiansen and Yeats, 1992; Noble, 1998).

The Northern Nevada Rift (NNR) (Fig. 1) is a north- to northwest-trending aeromagnetic anomaly which extends from central Nevada northward to Oregon and Idaho (Zoback et al., 1994; John et al., 2000; Colgan, 2013). The surface of the NNR is marked by epithermal Au-Ag deposits, mid-Miocene volcanic and hypabyssal rocks that formed during west-south-west-east-northeast extension (Zoback and Thompson, 1978; Zobeck et al., 1994; John and Wallace, 2000). Zoback et al. (1994) published $^{40}Ar/^{39}Ar$ age dates from basaltic dikes along the NNR, indicating it formed primarily between 16.5 – 14 Ma. Much of the earlier $^{40}Ar/^{39}Ar$ age dates pinpoint mineralization along the NNR to have occurred in a relatively short geologic time, from 15.6 Ma – 15.0 Ma (John et al., 1999; John and Wallace, 2000), although Hames et al. (2009) showed mineralization at the western margin of the NNR to have occurred at 16.5 Ma. John et al. (2001) utilizing field relationships, volcanic geochemistry, and $^{40}Ar/^{39}Ar$ geochronology surmise that the NNR was a product of the onset of regional west-southwest-east-northeast-directed extension, and emplacement of magmas in the upper crust due to development of the Yellowstone Hotspot.

METHODOLOGY

Sample Collection

The Jumbo Mine is hosted by folded Mesozoic, slate, phyllite and quartzite (Willden, 1964). A large reverse fault crosscuts the Jumbo Mine, which acted as a conduit for fluid flow and concentrated the Au-Ag mineralization within this fault zone. As a result, most of the mining at Jumbo occurred along strike of the reverse fault. Rock samples of phyllites were collected from the Jumbo Mine in Humboldt County, Nevada from the pit wall and from nearby tailings piles (Fig. 5). Coordinates for sample locations can be found in Appendix 3. Adularia veins at Jumbo were 0.2 – 2.0 cm in diameter in the metasedimentary host rock and focused along the fault zone. Adularia at Jumbo were commonly rhombic to sub-rhombic habit, 0.1 – 0.4 cm in diameter, and vitreous to milky and perfect cleavage on (001) and good cleavage on (010) (In-situ samples can be found in Appendix 3). The Jumbo samples commonly present superficial iron-oxide staining (Fig. 5), however, adularia without superficial iron-oxide staining does occur. Accessory iron oxide minerals (limonite can be found along the fractures of the metasedimentary host rock (Fig. 5). The lack of staining on some adularia is likely due to the absence of infiltrating meteoric waters with abundant dissolved Fe^{2+} ions along the respective fractures. The small diameter of the veins (0.2 – 2.0 cm) and sub-rhombic habit (suggesting slower crystallization) at Jumbo likely would require a shorter-lived system and possibly a low to moderate heat flow within the system to generate the present vein material.

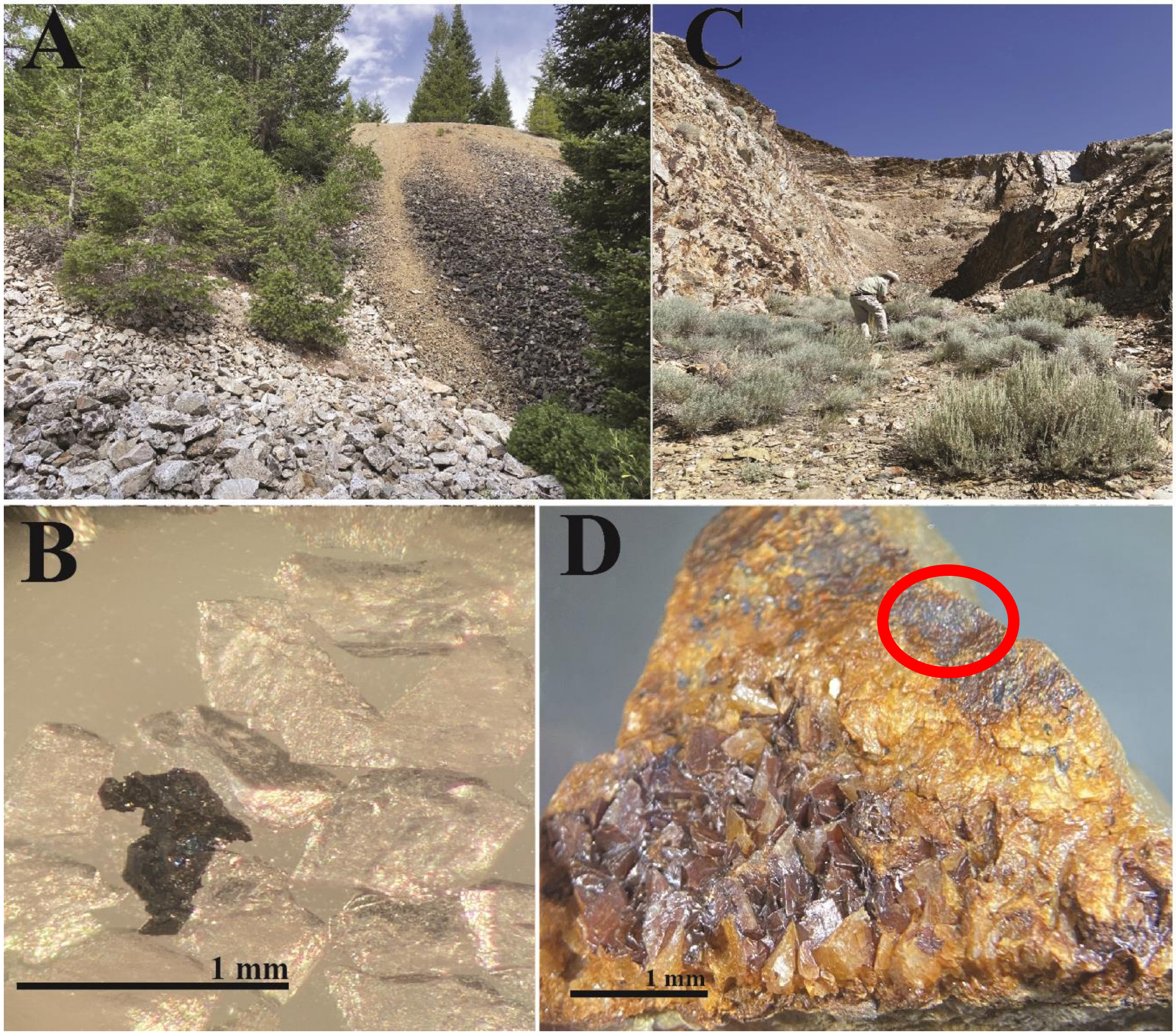

Figure 5: (A) A photo of the tailing piles of the Trade Dollar Mine, Silver City District, Idaho, with adularia collected from the granitic wall rock (gray) and the basaltic wall rock (black). (B) A photo through a binocular microscope of adularia (clear) that is free of inclusions, alteration, and no perthitization from the Trade Dollar Mine, Idaho, with a crystal of naumannite (gray black). (C) A photo of the Jumbo Mine in Humboldt County, Nevada. This photo was taken from inside the pit of the mine. Samples were collected from tailings piles from within and above the mine pit. Pictured is Dr. Hames for scale. (D) A photo though a binocular microscope of adularia with iron-oxide staining collected from the Jumbo Mine, Nevada. The red circle encapsulates the unknown accessory FeO mineral.

The Trade Dollar Mine is hosted by the Silver City Granite and a suite of basalts, which are overlain by rhyolitic tuffs at Florida Mountain. The Silver City Granite is a phaneritic bi-micaceous granite. The muscovite and biotite are euhedral, platy habit, 0.1 – 0.2 cm in diameter, and exhibit perfect cleavage on (001). The micas are commonly altered to chlorite, likely due to interactions with the hydrothermal fluids that created the Au-Ag mineralization. The alkali feldspars are largely unaltered, however, some alteration to kaolinite does occur. The alkali feldspars are euhedral to subhedral, milky to white, non-metallic, with visible striations, and perfect cleavage on (001) and good cleavage on (010). The plagioclase feldspars are largely unaltered, however, light alteration to kaolinite does occur. The plagioclase feldspars are euhedral to subhedral, milky, non-metallic, with visible striations, and perfect cleavage on (001) and good cleavage on (010). The basalt suites at Florida Mountain are aphyric and contain ~0.01 cm diameter pyroxene and plagioclase feldspars. Chloritization of the basalt suites do occur locally around the veins. Rock samples of basalts and granites were collected from the Trade Dollar Mine in the Silver City District from nearby tailings piles (Fig. 5). The vein material commonly has a brecciated texture, with host rock clasts (0.2 – 3 cm) included within the adularia vein material and contained in veins that vary from 0.1 – 10 cm (Photos of brecciated vein material can be found in Appendix 3). This texture is likely generated by hydraulic fracturing of the host rock during mineralization. Alteration to sulfide minerals commonly occurs on the rims of the basaltic host rock, with fracture infilling of pyrite within the basalt clasts also common (photos of sulfide minerals can be found in Appendix 3). The adularia can present with a rhombic or granular habit, 0.1 – 1.0 cm in diameter, vitreous to milky, and perfect cleavage on (001) and good cleavage on (010). Adularia can be found with quartz after platy calcite (QAPC) boiling textures in the vein material. Adularia in the veins can present with a layered texture, that can mimic colloform banding (textured adularia vein material photos can be found in Appendix 4). Sulfides such as pyrite (FeS_2) and chalcopyrite ($CuFeS_2$) are commonly present, with naumannite (Ag_2Se) (Fig. 5). The large diameter of the veins (0.1 – 10 cm), layered (pseudo-colloform banding) and rhombic habit (suggesting rapid crystallization) at Trade Dollar would require a longer-lived system, and possibly a high heat flow to generate the abundant vein material.

Mineral Preparation for $^{40}Ar/^{39}Ar$ Geochronology

Adularia samples were prepared by crushing quartz-adularia veins followed by sieving to sizes ranging between 250-840 μm. Crystals were hand-picked under a binocular microscope based on their morphologies and were generally free from alteration, inclusions, twinning or perthitic textures (Fig. 5).

Alkali feldspars from the Silver City Granite were prepared following the same procedures. Plagioclase feldspars from the Silver City Granite were also picked incidentally due to the similar morphological characteristics of alkali feldspars.

$^{40}Ar/^{39}Ar$ Geochronology

Crystals were loaded into a customized aluminum disk, wrapped in aluminum foil, stacked, encapsulated under vacuum in a fused silica tube (Fig. 6), and dispatched for irradiation over 16 hours at Oregon State's TRIGA reactor in Corvallis, Oregon. This irradiation generated neutron-induced $^{39}Ar_k$ from ^{39}K in the reactor facility as described by Dalrymple et al. (1981). Monitor minerals from the Fish Canyon tuff (the New Mexico Technical University separate 'FC-2'; Age: (28.2 Ma) and the GA1550 Biotite (99.44 ± 0.17 Ma) standard age data from Schaen et al., 2020) were placed in the irradiation disk to serve as a flux monitor.

This flux monitor allowed for the determination of the "J" value as defined in the $^{40}Ar/^{39}Ar$ age equation (Merrihue and Turner, 1966).

(3) $$t = \frac{1}{\lambda} ln[J * R + 1]$$

Where t is time, λ is the total decay constant for ^{40}K, J is measure of the proportion of ^{39}K converted to ^{39}Ar by bombarding a ^{39}K nucleus with a fast neutron and emitting a proton through the reaction $^{39}K(n,p)^{39}Ar$, R is ratio of $^{40}Ar^{*}/^{39}Ar$. These irradiated crystals were then placed into the Auburn Noble Isotope Mass Spectrometer (GLM-110), where a 60W CO_2 laser was applied to the samples by single crystal incremental heating and single crystal total fusion heating, following methods described by Hames (2021). Routine air measurements made during analysis provided $^{40}Ar/^{39}Ar$ isotopic ratios of 293.5 ± 1.5, with blank measurements conducted after every 5 unknown analyses (see Appendix 2 for measurements). Following the analyses, data reduction, and blank and mass discrimination following the $^{40}Ar/^{39}Ar$ isotopic ratios reported by Lee et al. (2006) were utilized to create model-age spectra, statistical ages, and isotope correlation diagrams with an Excel Spreadsheet integrated with Excel's Isoplot v. 3.75 (Ludwig, 2012).

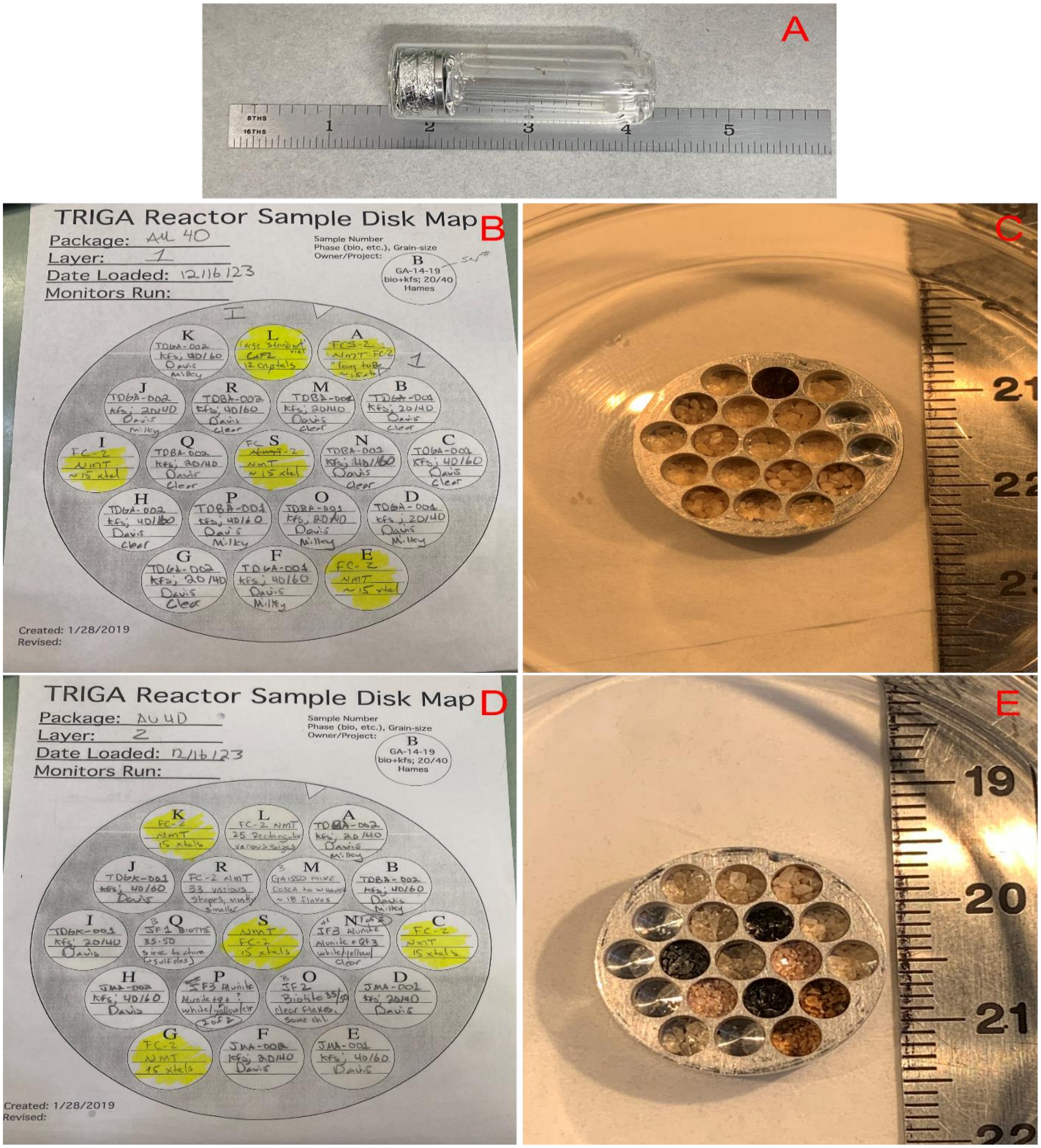

Figure 6: (A) Prepared irradiation package "AU40" composed of 2 disks including the analyzed samples of this thesis. (B) Disk Map of Layer 1 of irradiation package AU40. (C) Disk Layer 1 of AU40. (D) Disk Map of Layer 2 of irradiation package AU40. (E) Disk Layer 2 of AU40. Yellow circles in (B) and (D) represent holders occupied by the standards of FC-2, GA1550 Biotite, and CaF_2. Uncolored circles in (B) and (D) represent holders occupied by samples analyzed in this study and by other academics. Sample names (can be found in Appendix 2) refer to the package number, layer of the package, position in the respective layer (A-S) and phase of material.

Electron Microprobe Analysis

Electron microprobe quality grain mounts were prepared using the Auburn University Department of Geosciences Sample Preparation Laboratory. These grain mounts were prepared by mounting 15-20 crystals of adularia from Jumbo, 15-20 adularia crystals from Trade Dollar, and 15-20 alkali feldspars from the Silver City Granite host rock. The information collected from this analysis provides accurate classification for the end-member of alkali feldspar and provides insight into the degree of exsolution that has occurred.

Crystals within grain mounts were analyzed using the JEOL JXA-8600 Superprobe of Auburn University. This EMPA (Electron Microprobe Analyzer) is equipped with 4 WDS (wavelength dispersive X-ray spectroscopy) spectrometers, EDS (energy-dispersive spectroscopy), BSE (back-scattered electron) detectors, and the Geller System upgrade. Grain mounts were coated with carbon in a SPI Module Carbon Coater and loaded into the EMPA. The grain mounts were then analyzed with a 15 kV accelerating voltage and a ~20 nA beam current with a beam size of 1 μm. The JEOL JXA-8600 Superprobe was calibrated five times before and after each session of quantitative spot analysis on each unknown crystal using natural mineral standards (information on standards can be found in Appendix 1).

X-Ray Diffraction

X-ray diffraction data on single crystals of Fish Canyon Sanidine, Trade Dollar adularia, Jumbo adularia, and Silver City Granite alkali feldspars at 100 K were collected using a Bruker D8 VENTURE κ-geometry diffractometer system of Auburn University, equipped with an Incoatec IμS 3.0 microfocus sealed tube (Mo Kα, λ = 0.71073 Å) and a multilayer mirror monochromator. The Bruker SAINT Software package was used to determine integrated intensities; the data were corrected for absorption effects using the multi-scan method (SADABS). The structure was solved and refined using the Bruker SHELXTL software package. The unit cell constants are based on reflections with intensities above 20 σ(I). The Fish Canyon Sanidine was also included in this analysis as a standard, as it is a well-studied crystal (e.g., Cassata and Renne, 2013).

Choice of Diffusion Parameters and Calculating Closure Temperature

Cassata and Renne (2013) performed a systematic study of diffusion parameters for different feldspars to improve the accuracy of thermal modeling and $^{40}Ar/^{39}Ar$ geochronology of feldspars. The study revealed that feldspars of comparable crystalline structure (C2m, C, etc) and similar geochemical compositions have similar diffusion parameters and T_c. Therefore, a well-studied sample matching these requirements was chosen to calculate the T_c of the adularia analyzed within this study. The representative diffusive parameters were chosen from Foland (1974) of the Benson Mines Orthoclase ($An_0Ab_{3.0}Ksp_{97.0}$; C2m) to calculate the closure temperature(s) of the samples analyzed within this study. The calculation of T_c following Dodson (1973) was performed with Equation 1, with a spherical model chosen for the geometric constant (A) (Foland, 1974; McDougall and Harrison, 1999), where R is 0.0019872 kCal-mol-k , E is 43.8 kCal/mol, τ is the time constant, D_0 is 0.00982 cm^2/sec, a is a range from 0.001 – 0.2 cm , and A is 55.

RESULTS

Geochemical Analysis (EMPA)

Tables showing oxide wt% and calculated mineral chemical formulas can be found in Appendix 1. Adularia from samples TDB-A-001, JMA-001, and alkali feldspar from TDG-K-001 were analyzed. The chemical compositions of the adularia and alkali feldspars are plotted on a ternary diagram (Fig. 7). In the following summary, the term KSP or K-feldspar is subsituted for $KAlSi_3O_8$ (or alkali feldspar) to avoid connotation of structure for the potassium feldspars.

Adularia from the Jumbo Mine were found to be near end-member K-feldpsar ($An_{0.07}Ab_{2.78}Ksp_{97.1}$; Average of geochemical analysis, N=8). Calculated mineral formulas based on 8 oxygens provide Ab% ranges from 1.86 – 4.57, An% ranges from 0 – 0.19, and Or% ranges from 95.3 – 98.09.

Adularia from the Trade Dollar Mine hosted by the basaltic host rocks were found to be near end-member K-feldspar ($An_{0.1}Ab_{2.8}Ksp_{97.2}$; Average of geochemical analysis, N=5). Calculated mineral formulas based on 8 oxygens provide Ab% ranges from 2.03 – 3.44, An% ranges from 0 – 0.02, and Or% ranges from 96.56 – 97.97. Adularia from the Trade Dollar Mine is geochemically indistinguishable from the Jumbo Mine Adularia.

K-feldspar from the Silver City Granite were found to be K-feldspar ($An_{0.37}Ab_{9.84}Ksp_{89.79}$; average of geochemical analysis, N=14). Calculated mineral formulas based on 8 oxygens provide Ab% ranges from 5.00 – 15.18, An% ranges from 0.15 – 0.64, and Or% ranges from 84.54 – 94.84. The plutonic K-feldspar from the Silver City Granite is much higher in albitic and anorthitic composition (9.2% and 0.32%, respectively) than the Jumbo and Trade Dollar Mine adularia. The growth of albitic exsolution lamellae during cooling are likely responsible for the large range of observed Ab% and Or% values.

The lower An% and Ab% values observed in Jumbo and Trade Dollar adularia compared to the alkali feldspar from the SCD likely reflect the geochemical composition and temperature of their genetic systems. The presence and mobility of K^{+} within the respective hydrothermal systems and their fluids were likely much higher than that of higher Ca^{2+} and Na^{+} bearing felsic magma. This would create a more K-rich microcline (adularia) than the magmatically generated SCD alkali feldspar. Furthermore, the low temperature (150 - 350°C) of low-sulfidation epithermal systems would likely favor a simple solid solution substitution of Na^{+} or K^{+} into the 8 coordination number polyhedral site. In contrast, the higher temperatures (750 - 1000°C) of a magmatic system, would be expected to favor coupled substitution of Ca^{+2} and Al^{3+} for Na^{+}/K^{+} and Si^{4+}, generating a ternary K-feldspar with notably higher anorthite composition.

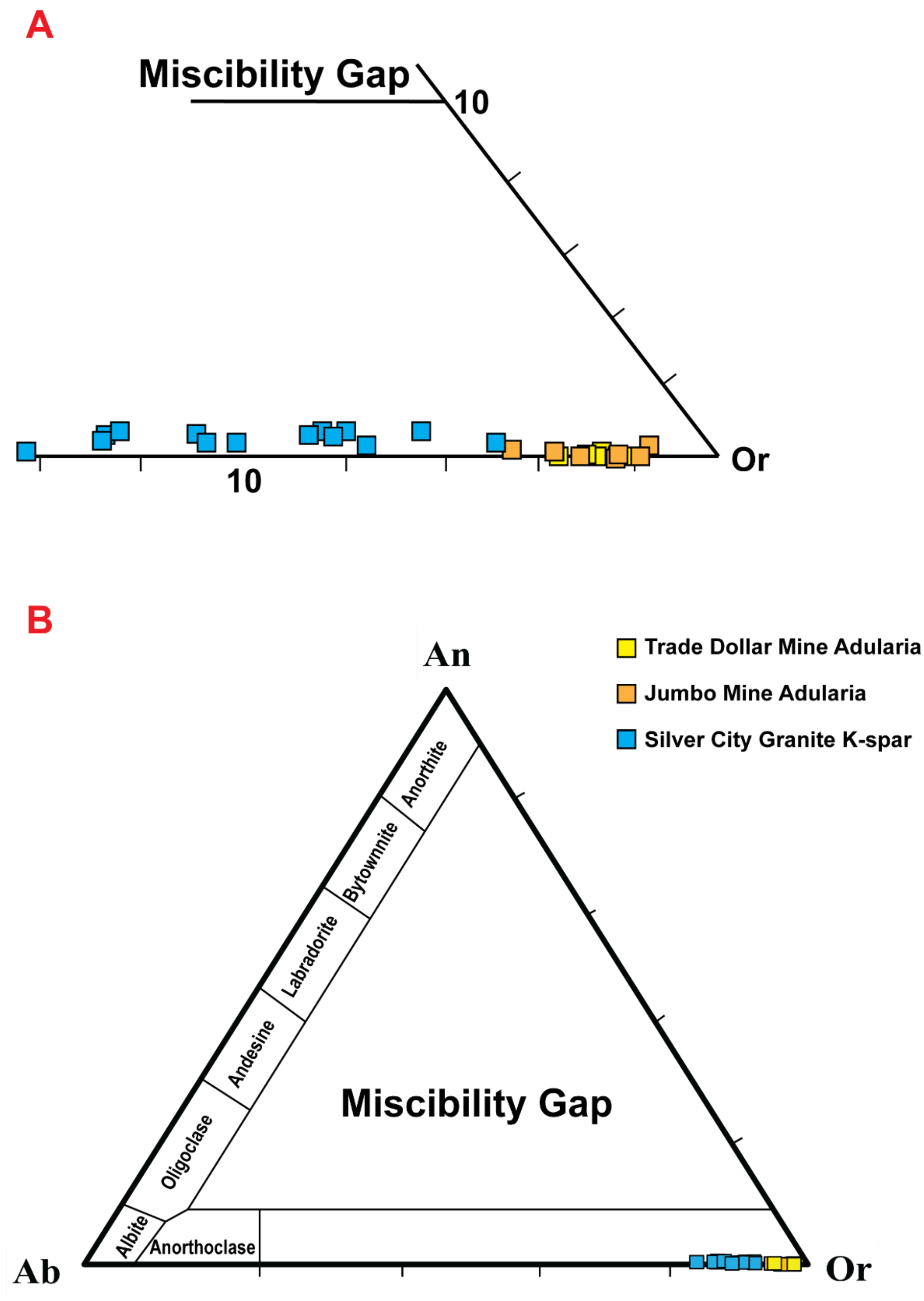

Figure 7: (A) A zoomed-in ternary diagram of the solid-solution series for plagioclase. (B) Ternary diagram of the solid-solution series for plagioclase. Blue squares represents K-Spar from the Silver City granite. The orange squares represent adularia from the Jumbo Mine. The yellow squares represent adularia from the Trade Dollar Mine.

$^{40}Ar/^{39}Ar$ Geochronology

Jumbo Mine

Five single crystals of adularia from the Jumbo Mine were incrementally step heated, and 48 crystals of adularia underwent single crystal total fusion (SCTF) (Fig. 8). The analyzed crystals were prepared from a single sample (JMA-002). Incremental step-heating of the five crystals of adularia yielded precise ages that define an average plateau age of (16.49 ± 0.15 Ma). Plateau increments were defined by a value greater than 60% of the total $^{39}Ar_k$ released. Previous studies have demonstrated that adularia crystal ages from a single sample can vary by up to 0.5 Ma, depending on the amount of extraneous argon and $^{40}Ar^*$ loss from each grain (Hames et al., 2009). Determined plateau ages range from ca. 16.66 ± 0.044 to 16.503 ± 0.03 Ma and comparable ages from SCTF of adularia (16.86 ± 0.13 to 16.159 ± 0.07 Ma) were calculated from the Jumbo Mine (ages reported within 2σ errors) (Fig. 8). $^{39}Ar/^{37}Ar$ can be used to model the composition of Ca/K, and when plotted there was not an appreciable variation. The ages for *JMA-002* range from 16.86 ± 0.13 to 16.15 ± 0.07 Ma. The oldest age (16.86 ± 0.13 Ma) is interpreted to represent the maximum temperature for cooling ages for adularia at the Jumbo Mine. The youngest age (16.159 ± 0.070 Ma) is interpreted to represent the minimum age at which the Jumbo Mine cooled below a temperature at which would favorably retain radiogenic ^{40}Ar. The mean age for the Jumbo Mine was calculated at 16.521 ± 0.021 Ma. SCTF and incremental heating methods produced $^{40}Ar/^{39}Ar$ age dates that are statistically similar (within calculated errors, Fig. 8). The release spectra for A and B (Appendix 2) reveal initial steps that are younger (11.788 ± 1.575 and 14.393 ± 1.186 Ma, respectively) than the plateau ages. These ages could represent an apparent diffusion loss profile; however, these ages are relatively sensitive to errors in measurement and blank correction as they comprise a very small fraction of the total $^{39}Ar_k$ released. The ages calculated from the present study agree with the published ages from Hames et al. (2009).

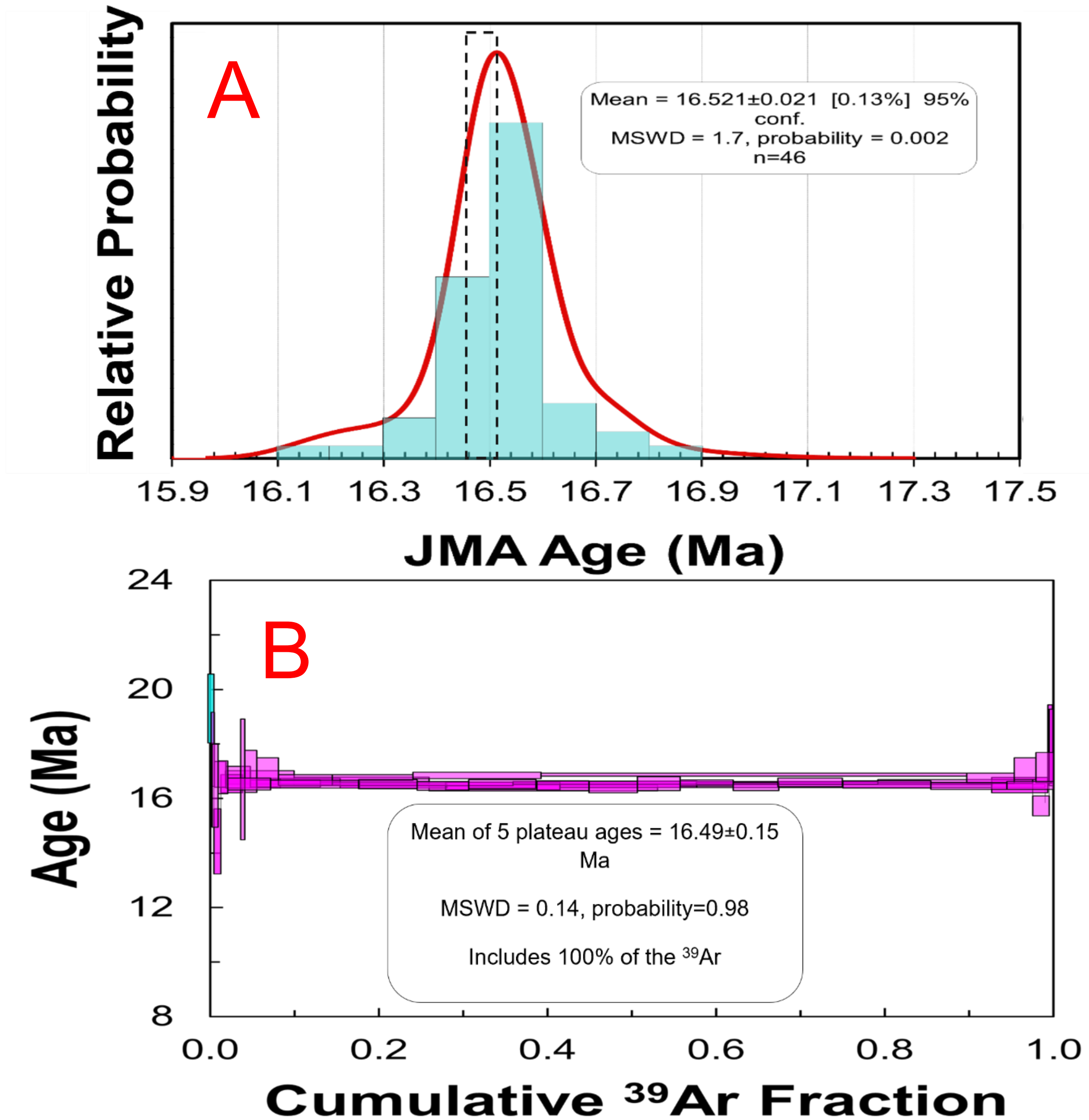

Figure 8: (A) A probability histogram of the variation of $^{40}Ar/^{39}Ar$ ages found during analysis of adularia from the Jumbo Mine. Populations of $^{40}Ar/^{39}Ar$ ages occur at ca. 16.6, 16.5, 16.4, and 16.3 Ma. (B) A compilation of the incremental heating analysis of adularia (N=5) from the Jumbo Mine, with an average age calculated at 16.49 ± 0.15 Ma. Ages are reported within 2σ, box heights represent 1σ, including J-error of 0.000012. Blue boxes were not included in the plateau age calculation, where purple was included. The dashed box represents the range of ages for the Jumbo Mine from Hames et al. (2009).

Trade Dollar Mine Adularia

Crystals of adularia were prepared from a single sample (TDGA-001) of a vein hosted by the Silver City Granite (Sample photograph can be found in Appendix 3). Five crystals of adularia were incrementally step heated, and 38 samples of adularia underwent SCTF (Fig. 9). Incremental step-heating of the five crystals yielded very precise ages that define an average plateau age of (15.92 ± 0.09 Ma). Determined plateau ages range from 15.99 ± 0.026 to 15.84 ± 0.028 Ma, and comparable ages from SCTF of adularia (16.27 ± 0.11 to 15.79 ± 0.02 Ma) were calculated (ages reported within 2σ errors). (Fig. 9). $^{39}Ar/^{37}Ar$ can be used to model the composition of Ca/K, and when plotted there was not an appreciable variation. The ages for *TDGA-001* range from 16.27 ± 0.11 to 15.79 ± 0.02 Ma. The oldest age (16.27 ± 0.11 Ma) is interpreted to represent the earliest cooling age for adularia at the Trade Dollar Mine. The youngest age (15.79 ± 0.02 Ma) is interpreted to represent the minimum age at which the Trade Dollar mine cooled below a temperature at which would favorably retain radiogenic ^{40}Ar. The mean age for the Trade Dollar Mine is 15.880 ± 0.030 Ma. SCTF and incremental heating methods produced $^{40}Ar/^{39}Ar$ age dates that are statistically similar (within calculated errors, Fig. 9). The ages calculated from the present study are older than the average age of adularia (15.7 Ma) determined by Aseto (2012).

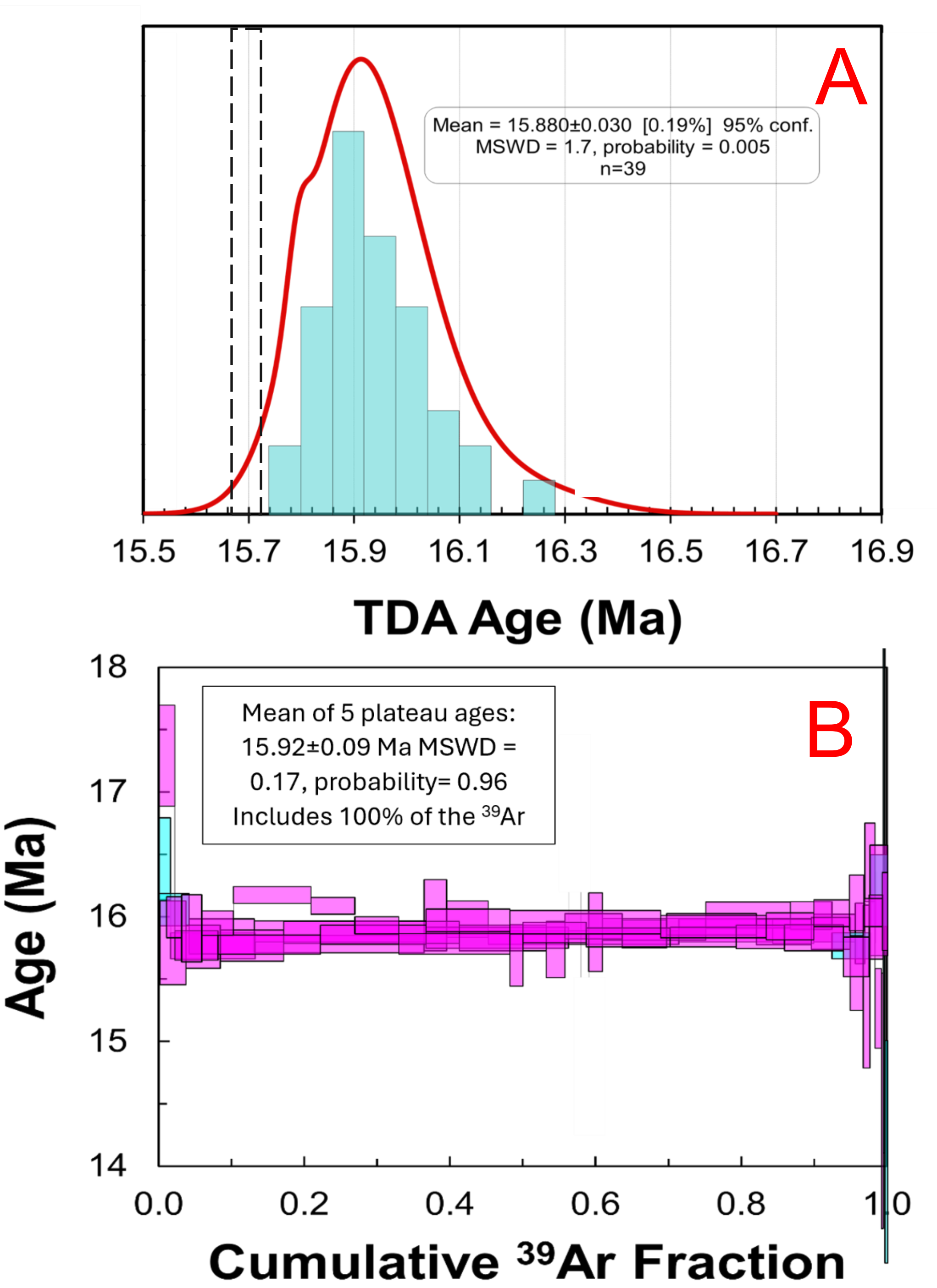

Figure 9: (A) A probability histogram of the variation of $^{40}Ar/^{39}Ar$ ages found during analysis of Trade Dollar Mine Adularia (TDA). Populations of $^{40}Ar/^{39}Ar$ ages occur throughout 16.1 – 15.7 Ma. (B) A compilation of the incremental heating analysis of adularia (N=5) from the Trade Dollar Mine, with an average age calculated at 15.92 ± 0.09 Ma. Blue boxes were not included in the plateau age calculation, where purple was included. Ages are reported within 2σ, box heights represent 1σ, including J-error of 0.000005. The dashed box represents the average age of the Trade Dollar Mine from Aseto (2012).

Silver City Granite Alkali Feldspar

Three crystals of K-feldspar and 3 crystals of plagioclase feldspar from the Silver City Granite host rock were incrementally step heated (Fig. 10). Twenty-six samples of K-feldspar, and eight samples of plagioclase feldspar underwent SCTF. These crystals were collected from the same sample as TDGA-001 and shown in Appendix 3, Fig.C. When incremental step-heating did not define plateaus, integrated ages were calculated (>70% of $^{39}Ar_k$ release). The three K-feldspar crystals yield precise ages that define integrated ages that range from 51.3 – 61.6 Ma. Radiogenic ^{40}Ar loss is observed in the incremental heating steps, with an initial release (0% - ~40% $^{39}Ar_k$) reflecting ages from 20 – 40 Ma, followed by progressively older ages that provide integrated ages of 50-60 Ma.

The three incremental step-heating age spectra (Fig. 10) for the plagioclase feldspar may reflect a radiogenic ^{40}Ar loss. This profile is observed in the incremental heating steps with an initial release (0% - ~40% $^{39}Ar_k$) reflecting ages from 20 – 40 Ma. Continued release (>40%) reveals progressively older ages that present ages of 50 – 60 Ma. The lower K content (and therefore, lower $^{40}Ar^*$) in plagioclase feldspar makes $^{40}Ar/^{39}Ar$ ages more susceptible to extraneous ^{40}Ar. Considering $^{39}Ar/^{37}Ar$ for the plagioclase feldspar from the Silver City Granite (values in Appendix 2) reveals the variation of Ca and K within the analyzed samples, with lower Ca/K ratios at initial release (0.0 – 30% $^{39}Ar_k$) and higher Ca/K ratios in subsequent steps. This may be due to the preferential release of K-rich phases radiogenic ^{40}Ar with lower temperatures steps (perhaps driven by microcrystalline exsolution developed during crystal cooling), followed by progressive degassing of high-Ca domains in plagioclase.

It is evident that the initial step heating ages for K-feldspar and plagioclase are similar (ca. 30 Ma initial release, Fig. 10: B, D), indicating final closure and retention of radiogenic ^{40}Ar in the Oligocene. However, the overall style of release differs, with the K-feldspar release seeming related to diffusive loss whereas the plagioclase release may reflect mixed Ca/K phases.

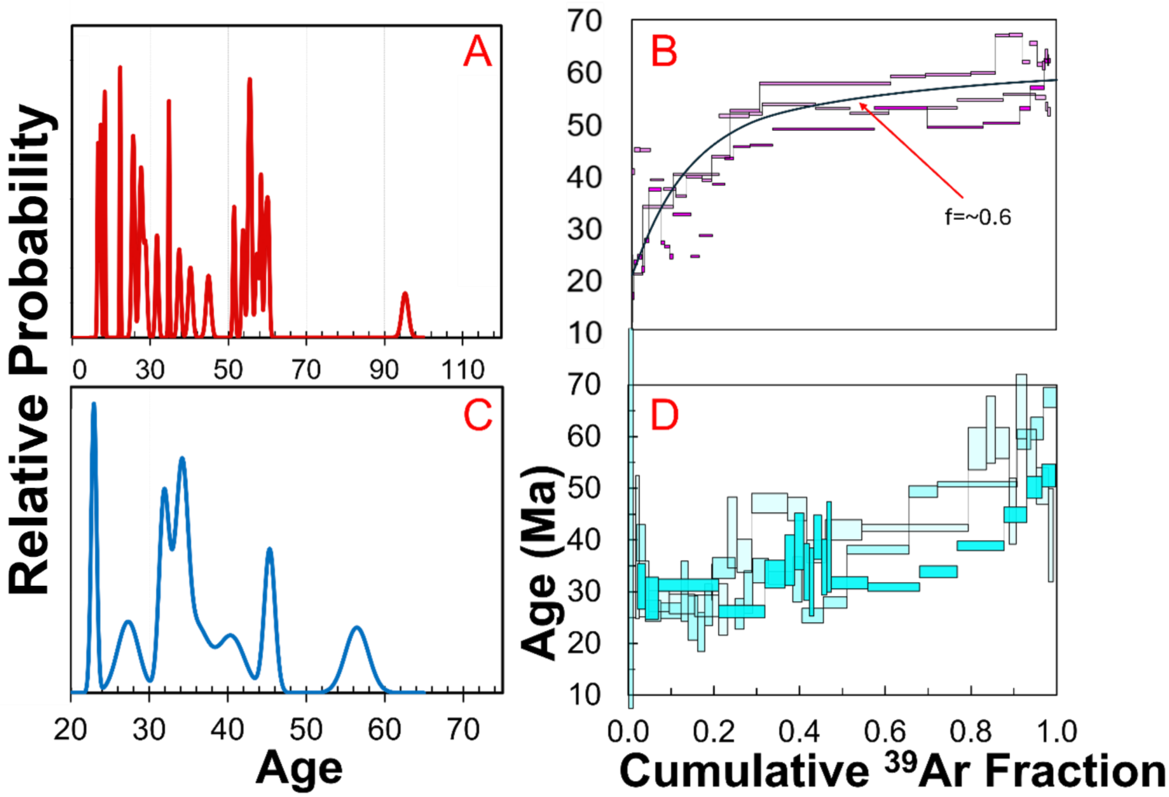

Figure 10: (A) A probability histogram of the variation of $^{40}Ar/^{39}Ar$ ages found during the analysis of plagioclase feldspars from the Silver City Granite. Populations of $^{40}Ar/^{39}Ar$ ages occur throughout 20 – 58 Ma. (B) A compilation of the three plagioclase feldspar age spectra. (C) A probability histogram of the variation of $^{40}Ar/^{39}Ar$ ages found during the analysis of alkali feldspars from the Silver City Granite. Populations of $^{40}Ar/^{39}Ar$ ages occur throughout 16 – 60 Ma. (D) A compilation of the three alkali feldspar age spectra, with radiogenic loss profile of f=~0.85 after McDougall and Harrison (1999). The age spectra for B and D reflect a diffusion loss profile, with initial release (0 – 40%) reflecting ages from 20 – 40 Ma, and subsequent release (>40%) reflecting ages from 40 – 60 Ma. Ages reported within 2σ errors, box heights represent 1σ, including J-error of 0.000012.

X-Ray Diffraction

X-ray diffraction analysis of the Fish Canyon Sanidine (FCS), Jumbo Mine Adularia (JMA-001), Trade Dollar Mine Adularia (TDGA-001), and Silver City Granite K-feldspar (TDGK-001) reveal:

Sample ID	**a** Axis Length (Å)	**b** Axis Length (Å)	**c** Axis Length (Å)	α Cell Angle	β Cell Angle	γ Cell Angle
FCS	8.48	13.02	7.18	90°	116.04°	90°
JMA-001	8.57	13.03	7.19	90°	116.07°	90°
TDGA-001	8.57	12.99	7.21	90°	116.10°	90°
TDGK-001	7.22	7.66	7.88	113.34°	104.17°	103.67°

Table 1: XRD data for the FCS, JMA-001, TDGA-001, and TDGK-001 samples including axis length and cell angles.

FCS has a space group of C2m (face-centered, monoclinic) with cell lengths of **a**=8.48 Å, **b**=13.02 Å, **c**= 7.18 Å, and cell angles of α =90°, β =116.04° γ= 90° (Table 1; Figure 11). This structure contains symmetry operations of a 2-fold rotation axis on (010), a 2-fold screw axis on (010), and an inversion center at [000]. This reveals that the FCS is structurally sanidine, which conflicts with the EMPA classification as microcline. These results match those presented by Cassata and Renne (2013) for FCS.

JMA-001 has a space group of C2m (face-centered, monoclinic) with cell lengths of **a**=8.57 Å, **b**=13.03 Å, **c**= 7.19 Å, and cell angles of α =90°, β =116.07° γ= 90° (Table 1; Figure 11). This structure contains symmetry operations of a 2-fold rotation axis on (010), a 2-fold screw axis on (010), and an inversion center at [000]. This reveals that the JMA-001 is structurally sanidine, which conflicts with the EMPA classification as microcline. JMA-001 is indistinguishable from FCS within this study and Cassata and Renne (2013).

TDGA-001 has a space group of C2m (face-centered, monoclinic) with cell lengths of **a**=8.57 Å, **b**=12.99 Å, **c**= 7.21 Å, and cell angles of α =90°, β =116.10° γ= 90° (Table 1; Figure 11). This structure contains symmetry operations of a 2-fold rotation axis on (010), a 2-fold screw axis on (010), and an inversion center at [000]. This reveals that the TDGA-001 is structurally sanidine, which conflicts with the EMPA classification as microcline. TDGA-001 is indistinguishable from FCS within this study and Cassata and Renne (2013), and from the XRD data for JMA-001 collected in the present study.

TDGK-001 has a space group of P1 (primitive, triclinic) with cell lengths of **a**=7.22 Å, **b**=7.66 Å, **c**= 7.88 Å, and cell angles of **α**=113.34°, **β** =104.17° **γ**= 103.67° (Table 1; Figure 11). This structure contains symmetry operations of an inversion center at [000]. TDGK-001 is triclinic (primitive, space group of 1) microcline, which matches the EMPA classification of microcline. This triclinic symmetry is created by the complete ordering of Al into the T_1o site, distoring the 2-fold rotation axis (mirror plane) on (010), generating the triclinic system. The distortion of symmetry in TDGK-001 generated a shorter unit cell lengths and **α**, **γ** ≠ 90° producing a triclinic system, compared to the sanidine system of the previous samples. TDGK-001 (P1) is geochemically similar to C1 samples analyzed in Cassata and Renne (2013), however the structural group is different. This may be due to microperthite within the TDGK-001 samples that modified the C lattice type, however, this is not detectable in the XRD and EMPA data.

Classification of the analyzed feldspars following Wright and Stewart (1968) based upon the unit cell lengths of axes **a** and **b**, reveal that FCS is a high (disorder) sanidine, JMA-001 lies between high (disorder) sanidine and orthoclase, and TDGA-001 lies between orthoclase and low (disorder) microcline (Figure 12). This classification reveals interesting relationships and contrasts between the C2m space group K-feldspar (FCS, JMA-001, TDGA-001) as well as the P1 space group K-feldspar (TDGK-001). FCS, JMA-001, and TDGA-001 could be expected to share similar disordering of Al within their tetrahedral sites, due to their expected rapid crystallization (Volcanic eruption, hydrothermal precipitation, and hydrothermal precipitation, respectively). However, what is revealed is a range of disordering, which may be reflect heat flow post-crystallization.

TDGK-001 is triclinic (primitive, space group of 1). This triclinic symmetry is created by the complete ordering of Al into the T_1o site, distorting the 2-fold rotation axis (mirror plane) on (010), generating the triclinic system. The complete ordering of Al into the T_1o site is likely generated by exposure to high heat flow for an extended period, before the exhumation of the Silver City Granite. It should be noted that the Bruker D8 Venture Single Crystal X-ray Diffractometer can not reliably distinguish partial substitution of Al for Si within the tetrahedral sites, however, this does not appreciably affect the results.

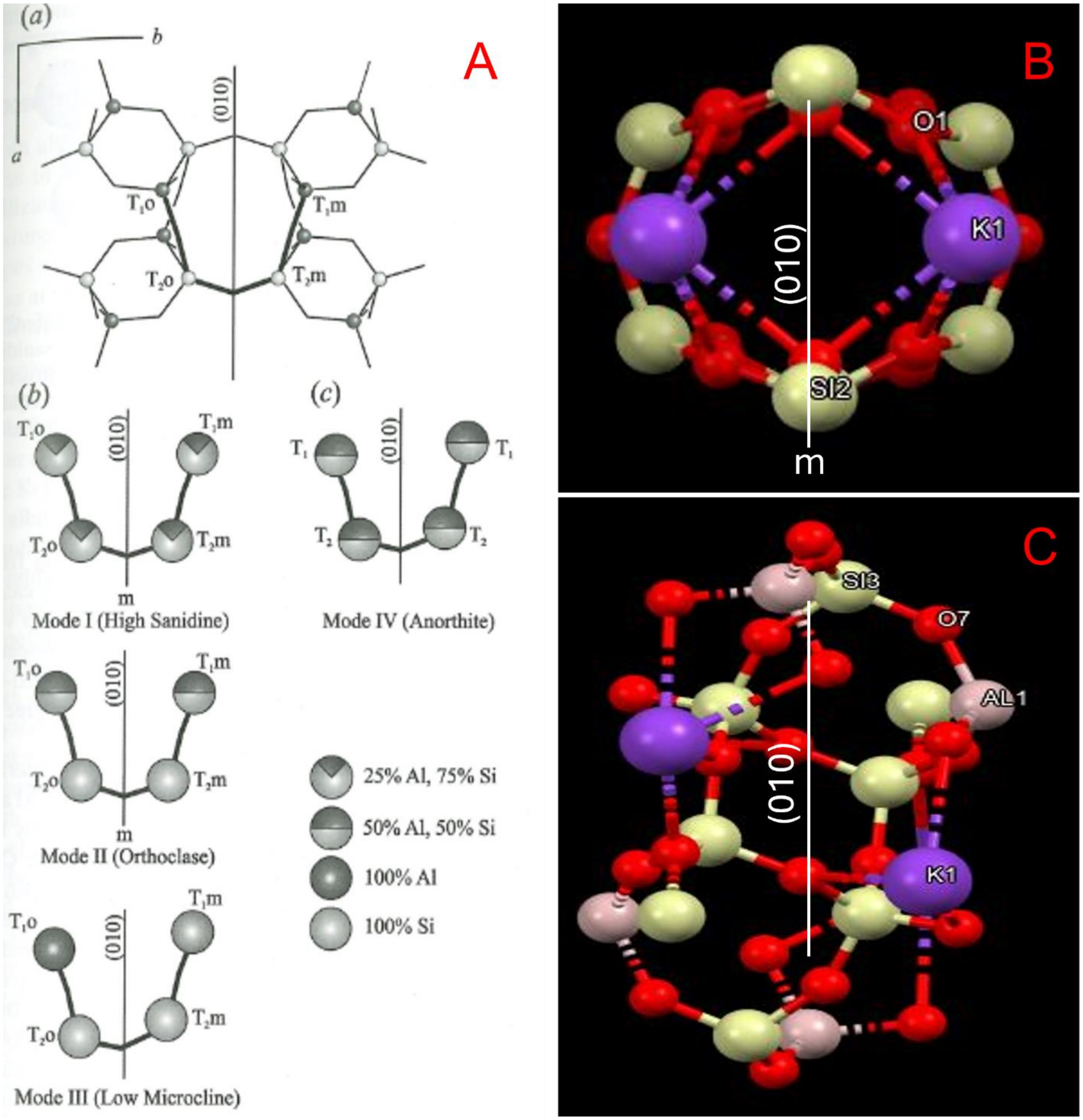

Figure 11: (A) A figure from Nesse (2012) that illustrates the ordering of Al and Si and accompanying symmetry changes among tetrahedral sites within feldspars; also described is the loss of the mirror plane on (010) as Al orders into its preferred T_1o site. Mode I (A) describes samples JMA-001 and FCS-001. Mode II (A) describes sample TDGA-001. Mode III (A) describes sample TDGK-001. (B) The molecular structure of FCS, JMA-001, and TDGA-001 with the 2-fold rotation axis on (010). The differences in unit axis length are indistinguishable at this scale. (C) The molecular structure of TDGK-001 with distortion and lack of a mirror plane across (010), by complete reordering of Al into the T_1o site.

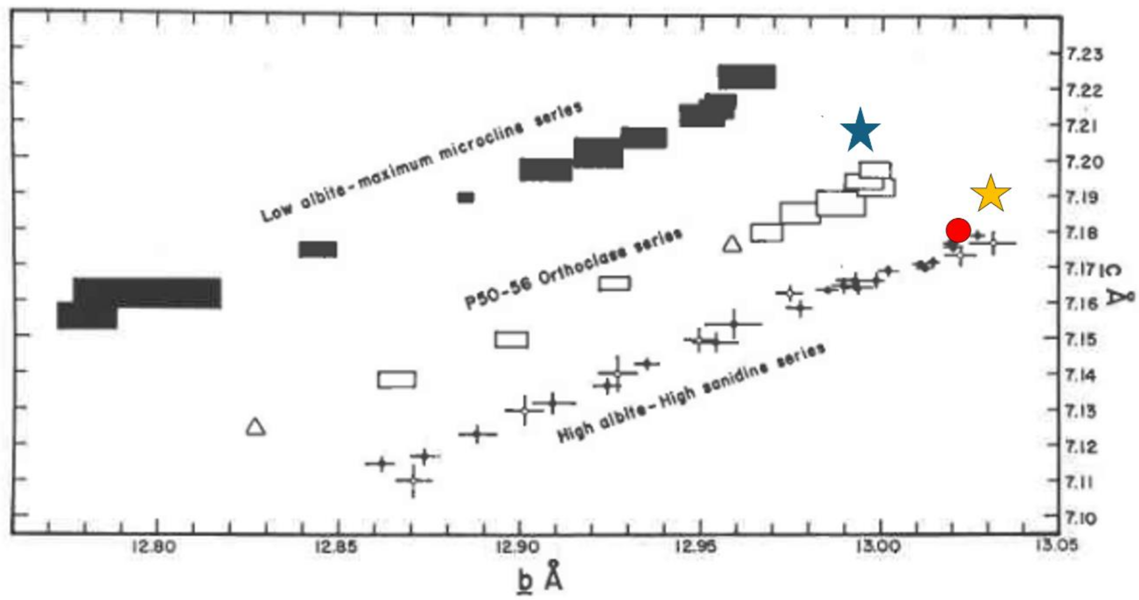

Figure 12: The relationship of the unit cell length of the **b** and **c** axis for three structurally equivalent alkali feldspars. FCS is represented by the red circle, JMA-001 is represented by the orange star, and TDGA-001 is represented by the blue star. Figure modified from Wright and Stewart (1968).

Calculated Closure Temperatures

The closure temperatures (T_c) for the adularia calculated within this study range from 200 - 290°C, as the effective diffusion dimension increases from 0.001 to 0.05 cm (Fig. 13). The hypothetical effective diffusion dimensions used to calculate and create Fig. 13 could represent a range from the physical size of the grain (0.02 – 0.5 cm) to defects in the crystalline lattices (0.001 – 0.01 cm). Calculated closure temperatures are consistent with calculated T_c of C2m minerals of similar geochemical compositions analyzed by Cassata and Renne (2013). The calculated closure temperatures shown are presented with the averaged determined homogenization temperatures for multiple mines from the Silver City District, Idaho: Florida Mountain (290°C), War Eagle Mountain (225°C), Poorman Mine (190°C) (Aseto, 2012) and Delamar Mountain (210°C) (Halsor, 1988). The homogenization temperatures for each vein may vary as most analyzed samples were collected from tailings piles preventing accurate understanding of the crystal's original location within the system. Therefore, samples from deeper in the system (crystallized at higher temperatures) were likely analyzed with samples from higher in the system (crystallized at lower temperatures). Calculated closure temperatures are above the averaged homogenization temperatures for Florida Mountain by Aseto (2012) when the effective diffusion dimension is 0.02 – 0.5 cm. When the effective diffusion dimension decreases <0.02 cm, the calculated T_c comes in line with War Eagle Mountain, but remains above the Poorman Mine, and Delamar Mountain. Cassata and Renne (2013) determined a T_c of approximately 380°C for an oligoclase ($An_{19.6}Ab_{74.2}Or_{6.2}$) with a crystal structure of C1, where $E_a \pm 1\sigma$ is 273.3 ± 12.18 (kJ/mole) and $\ln(D_o/a^2) \pm 1\sigma$ is 19.9 ± 2.8 ($\ln(s^{-1})$). As the crystal structure and geochemical signature are comparable to the K-feldspar from the Silver City Granite, a similar T_c of 380°C for the Silver City Granite K-feldspar likely exists. This relationship suggests that crystalline structure may play a role in the T_c of feldspars.

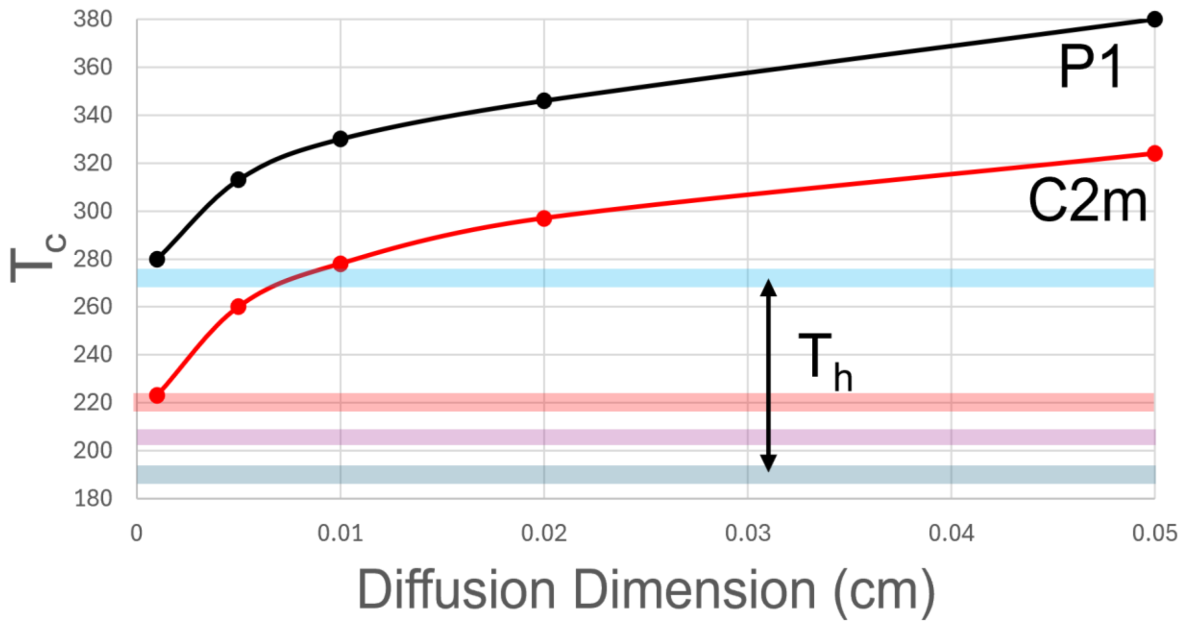

Figure 13: A graph representing the relationship of effective diffusion dimension versus closure temperatures of alkali feldspars at a constant cooling rate (10°C/Ma). Red dots represent calculated T_c for C2m minerals based on representative diffusion parameters for the Benson Mines Orthoclase obtained from Foland (1974). Black dots represent hypothetical T_c for P1 minerals following Cassata and Renne (2013). Averaged homogenization temperatures (T_h) from Aseto (2012) and Halsor et al., (1988) are represented by the colored bars. Blue is Florida Mountain (290°C, n=112, Aseto (2012)), red is War Eagle Mountain (225°C, n=26, Aseto, 2012), purple is Delamar Mountain (210°C, n=17, Halsor et al., 1988), and green is Poorman Mine (averaged homogenization temperature 190°C, n=34, Aseto, 2012).

DISCUSSION

Previous K/Ar and $^{40}Ar/^{39}Ar$ studies have constrained ages for hydrothermal mineralization, progression of the Yellowstone Hotspot, and subsequent magmatism (Armstrong et al., 1975; Pierce and Morgan, 1992). The earliest magmatism of the Yellowstone Hotspot is interpreted to be recorded by mafic magmatism of the Steens Mountain Basalt ~16.58 ± 0.18 Ma (Bruseke et al., 2007; Jarboe et al., 2010). $^{40}Ar/^{39}Ar$ age dates from the Jumbo Mine produced by this study reveal a mean cooling age of 16.521 ± 0.021 Ma, with a maximum cooling age of 16.86 ± 0.13 Ma, which is coeval to the magmatism that produced the Steens Mountains Basalt (16.58 ± 0.18 Ma). Therefore, this study interprets that the Jumbo Mine coincided in time with the earliest magmatism of the Yellowstone Hotspot and the earliest wave of Au-Ag mineralization in the Great Basin (as previously concluded by Hames et al. (2009). The lack of evidence of diffusion loss from the age spectra (Fig. 10) means that the Jumbo Mine likely experienced a rapid cooling history after the magmatism of the Steens-stage volcanism. High Al-Si disordering found in the Jumbo Mine Adularia suggests a thermal history that tapered off rapidly after precipitation of adularia, which prevented Al substitution into its preferred T_1o site. Furthermore, the lack of volcanic or plutonic rocks at the Jumbo Mine, in-conjunction with small vein diameter (0.2 – 2.0 cm) and rhombic to sub-rhombic habit suggests a low-heat flow environment that rapidly cooled post adularia crystallization.

$^{40}Ar/^{39}Ar$ ages from this study and Aseto (2012) suggest the Silver City District either experienced vein formation through a remarkably long-lived system (16.2 to 15.4 Ma), experienced multiple heating events, or experienced high enough temperatures over an extended period that caused partial loss of radiogenic ^{40}Ar from adularia over a 1 My time interval. It is noteworthy that the average $^{40}Ar/^{39}Ar$ age for the Trade Dollar Mine from Aseto (2012) of ~15.7

Ma is ~0.2 Ma younger than the average age of ~15.9 Ma found in the present study. Both studies collected Trade Dollar adularia from tailings piles, therefore, it is possible that the Aseto (2012) samples were originally lower in the system, and the present studies samples were originally higher in the system. The higher in the system samples would have cooled earlier (present study), than the lower in the system samples (Aseto, 2012), creating the older versus younger ages described in the two studies. This explanation would explain why samples collected ex-situ but from the same deposit can reveal variation in $^{40}Ar/^{39}Ar$ ages between samples. Aseto (2012) and Halsor (1988) conducted fluid inclusion studies from the Silver City District and found homogenization temperatures that range from 165-285°C. These temperatures are above the calculated ranges of T_c for the adularia based on diffusive parameters defined by Foland (1974) and as supported by the C2m structure of endmember sanidine by Cassata and Renne (2013). Furthermore, as the T_c is dependent on the effective diffusion dimension, a variety of effective diffusion dimensions may exist within a single-hand sample of adularia. As the adularia collected at the Trade Dollar Mine are rhombic to sub-rhombic habit and low to moderate disordering suggest rapid crystallization and exposure to high heat flow, lattice defects would probably be generated. These lattice defects would affect the effective diffusion dimension and create Tc that vary between individual crystals, leading to $^{40}Ar/^{39}Ar$ ages that span a wide range of time. Furthermore, due to the proximity of the Silver City District and the Trade Dollar Mine to the Yellowstone Hotspot track (Fig. 1), it is logical that the samples from the Trade Dollar Mine would be exposed to a higher temperature, and perhaps longer heating history, compared to the Jumbo Mine. This relationship of higher temperature and longer duration of heating is emphasized by the abundant volcanic suites of the Silver City District, which range from 16.1 - 15.2 Ma (Halsor, 1998; Aseto, 2012). The volcanic suites generated from 16.1 - 15.2 Ma at the Silver City District, in combination with the readily diffusive, structurally flawed adularia sampled from the Trade Dollar Mine would promote ^{40}Ar loss after crystallization and lead to younger ages as observed at the Trade Dollar Mine. However, it is noteworthy that adularia no age spectra from the present study or previous ones (Aseto, 2012; Monroe, 2021; Unger, 2008) reflect a diffusion loss profile.

The alkali feldspars and plagioclase feldspars from TDGK-001 were obtained from the same sample as the adularia from TDGA-001, however, only diffusive loss ^{40}Ar/^{39}Ar age spectra are observed in the alkali feldspars and plagioclase feldspars from *TDGK-001*. This raises the question of why diffusive loss ^{40}Ar/^{39}Ar age spectra are only observed in the host rock, and not the adularia. The age spectra from *TDGK-001* (Fig. 13) show an initial release (0% - ~40% $^{39}Ar_k$) reflecting ages from 20 – 40 Ma. Continued release (>40% $^{39}Ar_k$) reveals progressively older ages of 50 – 60 Ma, which agree with Pansze (1975), who reported a K/Ar age data of ~ 65 Ma. This age spectra profile may reflect initial T_c at ~60 Ma, with exhumation of the Silver City Granite that accelerated to result in final closure and retention of radiogenic ^{40}Ar by 20 – 40 Ma. The feldspars from the Silver City Granite have a different defect structure, as they formed from the slow cooling of a magmatic body. This slow cooling and recrystallization history allowed for ideal ordering in the K-feldspar crystal lattice (creating the P1 symmetry), which minimized structural defects in the crystal lattice. The data of Cassata and Renne (2013) suggest less diffusivity of $^{40}Ar^*$ and higher closure temperature with decreasing symmetry in K-feldspars. The trends in diffusivity imply the Silver City Granite K-feldspars are more retentive of $^{40}Ar^*$, compared to the rapidly cooled adularia of the Trade Dollar Mine. It is clear from their release spectra (Fig. 10) that the plagioclase feldspar and K-feldspar from the Silver City Granite present different records of cooling history. The release spectra of the K-feldspar from the Silver City Granite is dominated by diffusional loss of $^{40}Ar^*$, whereas the plagioclase feldspar release spectra appear to be dominated by initial release of K-rich phases, followed by subsequent degassing of Ca-rich domains, as noted in the results section. Different records of cooling between K-feldspars and plagioclase feldspars are also evident in data presented by Cassata and Rennes (2013). Analysis of labradorite ($An_{63.9}Ab_{35.4}Or_{0.7}$) with a symmetry of I1 has a T_c of ~330°C, compared to an oligoclase ($An_{19.6}Ab_{74.2}Or_{6.2}$) with a symmetry of C1 that has a T_c of ~380°C, which implies that plagioclase feldspars have lower T_c and are more diffusive than K-feldspars. Despite this, Silver City Granite feldspars reflect similar closure ages (~30 Ma), which may be driven by Oligocene tectonic events (e.g., Colgan et al., 2006). As the plagioclase feldspar from the Silver City Granite has a lower T_c, and has higher diffusivity than the K-feldspars, it could record a thermal event which served to re-open and favor $^{40}Ar^*$ loss in the plagioclase feldspars, which would not be reflected in the age spectra of the K-feldspars. However, age spectra for the feldspars (Fig. 10) both show closure at 30 Ma and reveal a gap in thermal record between 30 Ma and cooling of the Trade Dollar adularia at 16 Ma. This implies that the feldspars of the Silver City Granite reached isotopic closure for ^{40}Ar by the middle Oligocene and were not subject to appreciable ^{40}Ar loss in the Miocene. As the feldspars do not record loss in their age spectra (Fig. 10), it is logical that the magmatic and associated hydrothermal events that drove mineralization at the Trade Dollar Mine vein were relatively low in temperature and brief (perhaps some combination of temperatures below 330°C and times less than 1 million years). This hypothetical thermal history would not be sufficient to drive $^{40}Ar^*$ loss in the Silver City Granite feldspars but could prevent adularia (with effective diffusion dimensions ranging from 0.001 – 0.05 cm, see Fig. 13) from favorably retaining $^{40}Ar^*$ loss until the crystals effectively reached isotopic closure. $^{40}Ar/^{39}Ar$ ages for the Trade Dollar Mine adularia record a spectrum of cooling ages and not the timing of Au-Ag mineralization, as controlled by their diffusivity, effective diffusion dimension of the adularia, and regional thermal history.

CONCLUSION

Mid-Miocene low-sulfidation epithermal systems in the Northern Great Basin are widely accepted to be related to the development of the Yellowstone Hotspot. The earliest magmatism of the Yellowstone Hotspot is interpreted to be recorded by mafic magmatism of the Steens Mountain Basalt at 16.58 ± 0.18 Ma (Bruseke et al., 2007; Jarboe et al., 2010). The determined maximum cooling age for the Jumbo Mine of 16.86 ± 0.13, and mean cooling age of 16.52 ± 0.02 Ma of the present study showcases that Au-Ag mineralization in the Northern Great Basin either preceded or is coeval to initiation of volcanism related to the Yellowstone Hotspot. As the Yellowstone Hotspot migrated east (relatively) and away from the Jumbo Mine, the source of regional heating migrated relatively eastward. This gradual removal of the heat source likely occurred by ~16.2 ± 0.07 Ma, based on the minimum cooling age for the adularia of the Jumbo Mine. As the Yellowstone Hotspot trended east, and related magmatism occurred with an influx of heat, low-sulfidation epithermal deposits formed in the Silver City District. The Au-Ag deposit of the Trade Dollar Mine is interpreted to have formed before ^{40}Ar retention in adularia at in the area, at a maximum age of 16.27 Ma and a minimum age of 15.7 Ma. Rapid cooling and low heat flow at the Jumbo Deposit is recorded by the high Al-Si disordering, rhombic to sub-rhombic habit, small vein diameter, and lack of regional volcanics. This is contrasted by the slower cooling, and high heat flow near the Trade Dollar Mine, which is recorded by low Al-Si disordering, rhombic to granular habit, and high vein diameter, and mid-Miocene volcanics that dominate the region. The geochemical composition of adularia from the Jumbo Mine and Trade Dollar Mine does not appear to vary in amounts that would affect the precision of $^{40}Ar/^{39}Ar$ geochronology. Age spectra from the Silver

City Granite feldspars (Fig. 10) reveal a closure age of ~30 Ma, which may be driven by tectonic events in the Oligocene (as described regionally by Colgan et al., 2006). A ~14 Ma gap in thermal events is recorded between the age spectra of the Silver City Granite feldspars (30 Ma, Fig. 10) and the Trade Dollar adularia (16 Ma, Fig. 9).

Insights from fluid inclusion studies for the Silver City District (Aseto, 2012; Hastor, 1988) reveal averaged homogenization temperatures of 255°C, which is higher than calculated T_c for Trade Dollar Adularia for diffusion dimensions less than 0.02 cm and cooling rates below 10°C/Ma. The calculated T_c for the feldspars (following Cassata and Renne, 2013) from the Silver City Granite are ~330°C for k-feldspar, and ~380°C for plagioclase feldspar. These T_c are above the homogenization temperature for the Silver City District (Hastor, 1988; Aseto, 2012), which implies the feldspars from the Silver City Granite were not promoted to favorably lose radiogenic ^{40}Ar by the mid-Miocene magmatism and subsequent hydrothermal activity experienced at the Silver City District. However, these temperatures may be high enough to prevent favorable retention of $^{40}Ar^*$ within the adularia, creating a spectrum of ages that reflect the slow cooling experienced at the Silver City District.

FUTURE WORK AND IMPLICATIONS

Epithermal systems are an important source of precious metals that can include Au and Ag, making them a key resource as society becomes increasingly dependent upon electronics. In recent years, the government of the United States has strived to reduce our dependency on foreign countries to meet our industrial and commercial needs. To accomplish this, we must locate new ore deposits and/or improve our efficiency of extracting ores from existing mines. The Yellowstone Hotspot and related LIP are prime targets for this development, as they host numerous Au-Ag epithermal ore deposits that were previously or are actively mined. The societal importance of these metal deposits requires an accurate understanding of the development and timing of epithermal systems. This study revealed that $^{40}Ar/^{39}Ar$ dates for adularia do not always accurately record the date of Au-Ag mineralization. Detailed diffusion and scanning electron microscopy (SEM) analysis of the Jumbo Mine and Silver City adularia to characterize the effective diffusion mechanism and to identify defects that would facilitate $^{40}Ar^{*}$ loss past its nominal closure temperature would greatly increase our understanding of these world-class systems. Isothermal heating experiments at 700°C over a period of a month on the analyzed feldspars were conducted in 2024 using the high-temperature furnaces in the Experimental Petrology Lab in the Department of Geosciences of Auburn University, with the goal of inducing artificially driven $^{40}Ar^{*}$ loss. These samples will be irradiated and analyzed in Fall 2024 via a diode laser to measure the $^{40}Ar^{*}$ loss and diffusivity parameters of the samples. Furthermore, a detailed study of the geothermal gradient at the active, current-day Yellowstone Hotspot would allow for the reconstruction of the paleo-geothermal gradient at the Silver City District. The reconstruction of the paleo-geothermal gradient would greatly benefit the understanding of diffusion and cooling ages at the Silver City District. In-situ collection via drilling would allow for accurate recording of the depth of each adularia collected, which would be beneficial in helping to understand the ages of adularia crystals based upon where they lay within the system. These advancements would help us better understand the timing and context of Au-Ag mineralization in the classic Yellowstone Hotspot setting and to enhance the usefulness of $^{40}Ar/^{39}Ar$ age determinations of adularia as important tools in the precious metal exploration of LIPs in general.

REFERENCES

Armstrong, R.L., Leeman, W.P., and Malde, H.E., 1975, K-Ar dating quaternary and Neogene volcanic rocks of the Snake River Plane, Idaho: American Journal of Science, v.275, p.230-233.

Aseto, C.O., 2012, Geology, geochemistry and geochronology of the mid-Miocene, low-sulfidation epithermal gold-silver ores on War Eagle Mountain, Silver City District, Idaho [M.Sc Thesis]: Auburn University.

Black, B.A., Karlstrom, L., and Mather, T.A., 2010, The life cycle of large igneous provinces: Nature Reviews Earth & Environment, v. 2, doi: https://doi.org/10.1038/s43017-021-00221-4.

Bonnichsen, B., and Godchaux, M.M., 2006, Geologic map of the Murphy 30 X 60 Quadrangle, Ada, Canyon, Elmore, and Owyhee Counties, Idaho: United States, Idaho Geological Survey: Moscow, ID, United States.

Brueseke, M.E., Heizler, M.T., Hart, W.K., Mertzman, S.A., 2007, Distribution and Geochronology of Oregon Plateau (U.S.A) flood basalt volcanism: The Steens Basalt revisited: Journal of Volcanology and Geothermal Research, V. 161, p. 187-214.

Buchanan, L.J., 1981, Precious metal deposits associated with volcanic environments in the southwest: Arizona Geological Society Digest, v. 14, p. 237-262.

Camp, V.E., and Hanan, B.B., 2008, A plume-triggered delamination origin for the Columbia River Basalt group: Geosphere, v. 4, doi: https://doi-org.spot.lib.auburn.edu/10.1130/GES00175.1.

Carlson, R.W., and Hart, W.K., 1987, Crustal genesis on the Oregon plateau: Journal of Geophysical Research, v. 92, p. 6191–6206.

Cassata, W.S., and Renne, P.R., 2013, Systematic variations of argon diffusion in feldspars and implications for thermochronometry: Geochemica et Cosmochimica Acta, V. 112, doi: http://dx.doi.org/10.1016/j.gca.2013.02.030.

Christiansen, R.L., and Lipman, P.W., 1972, Cenozoic volcanism and plate tectonic evolution of the western United States. II. Late Cenozoic: Philosophical Transactions of the Royal Society of London, Series A, v. 271, p. 249–284.

Christiansen, R.L., and Yeats, R.S., 1992, Post-Laramide geology of the U.S. Cordilleran region, in Burchfiel, B.C., Lipman, P.W., and Zoback, M.L., eds., The Cordilleran orogen: Conterminous U.S.: Boulder, Colorado, Geological Society of America, Geology of North America, G-3. 261–406, doi: https://doi-org.spot.lib.auburn.edu/10.1130/DNAG-GNA-G3.261.

Colgan, J.P., Dumitru, T.A., Reiners, P.W., Wooden, J.L., and Miller, E.L., 2006, Cenozoic tectonic evolution of the Basin and Range Province in Northwestern Nevada: American Journal of Science, v. 306, doi: 10.247/08.2006.02

Colgan, J.P., 2013, Reappraisal of the relationship between the northern Nevada rift and Miocene extension the northern Basin and Range Province: Geology, v. 41, p. 211-214, doi: https://doi.org/10.1130/G33512.1.

Dalrymple, G.B., and Lanphere, M.A., 1969, Potassium argon dating Principles techniques and applications to geochronology: W.H. Freeman and Company, San Fransisco, p. 258.

Dalrymple, G.B., Alexander, E.C., Lanphere, M.A., and Kraker, G.P., 1981, Irradiation of samples for $^{40}Ar/^{39}Ar$ dating using the Geological Survey TRIGA Reactor: USGS Professional Paper 1176, p. 55.

Dodson, M.H., 1973, Closure temperature in cooling geochronological and petrological systems: Contributions to Mineralogy and Petrology, v. 40, p. 259-274, doi: https://doi.org/10.1007/BF00373790.

Dong, G., and Morrison, G.W., 1995, Adularia in epithermal veins, Queensland: morphology, structural state and origin: Mineralium Deposita, v. 30, p. 11-19.

Ekren, E.B., Mcintyre, D.H., Bennett, E.H., and Malde, H.E., 1982, Cenozoic stratigraphy of western Owyhee County, Idaho, in Bonnichsen, B. and Breckenridge, R.N. eds., Cenozoic Geology of Idaho: Idaho Bureau of Mines Geology Bulletin 26, p. 215-235.

Feeley, T.C., and Grunder, A.L., 1991, Mantle contribution to the evolution of middle Tertiary silicic magmatism during early stages of extension: the Egan Range volcanic complex, east-central Nevada: Contributions to Mineralogy and Petrology, v. 106, p. 154–169.

Foland, K.A., 1994, Argon diffusion in feldspars: Feldspars and their reactions: Springer Dordrecht, p. 415-447.

Gans, P.B., Mahood, G.A., and Schermer, E., 1989, Synextensional magmatism in the Basin and Range province: A case study from the eastern Great Basin: Geological Society of America Special Paper 233, p. 53.

Gillerman, V.S., and Mitchell, V. E., 2005, New developments in a new century for Idaho's precious metal districts, in Rhoden, H.N., Steininger, R.C., and Vikre, P.G., eds., Geological Society of Nevada Symposium 2005: Window to the World, Reno, Nevada, May 2005, p. 663–672.

Griffin, K., 2018, $^{40}Ar/^{39}Ar$ diffusion and age constraints in muscovite from the Ruby Mountains, Nevada [M.S. Thesis]: Auburn University.

Halsor, S.P., Bornhorst, T.J., Beebe, M., Richardson, K., and Strowd, W., 1988, Geology of the Delamar silver mine, Idaho-A volcanic dome complex and associated hydrothermal system: Economic Geology, v. 83, p. 1159-1169.

Hames, W.E., Unger, D., Saunders, J., Kamenov, G., 2009. Early Yellowstone hotspot magmatism and gold metallogeny: Journal of Volcanology and Geothermal Research, v. 188, p. 214 – 224.

Hames, W.E., 2021, K/Ar and $^{40}Ar/^{39}Ar$ dating methods, *in* Alderton, D., Elias, S.A., eds., Encyclopedia of Geology (second edition): United Kingdom, v. 6, p. 50-65.

Harrison, T.M., 1982, Diffusion of ^{40}Ar in hornblende: Contribution to Mineralogy and Petrology, v. 78, p. 324-331, doi: https://doi.org/10.1007/BF00398927.

Hedenquist, J.W., and Lowenstern, J.B., 1994, The role of magmas in the formation of hydrothermal ore deposits: Nature, v. 370, p. 519-527.

Henry, C.D., Castor, S.B., McIntosh, W.C., Heizler, M.T., Cuney, M., Chemillac, R., 2006, Timing of oldest Steens basalt magmatism from precise dating of silicic volcanic rocks, McDermitt Caldera and Northwest Nevada volcanic field. Eos Trans. AGU 87, 52.

Hill, R.I., 1993, Mantle plumes and continental tectonics: Lithos, v. 30, p. 193-206.

Jarboe, N.A., Coe, R.S., Renne, P.R., 2013, The age of the Steens reversal and the Columbia River Basalt Group: Chemical Geology, v. 274, p.158-168, doi: https://doi.org/10.1016/j.chemgeo.2010.04.001.

John, D.A., Garside, L.J., and Wallace, A.R., 1999, Magmatic and tectonic setting of late Cenozoic epithermal gold-silver deposits in northern Nevada rifts, *in* Kizis, J.A., Jr., ed., Low-sulfidation gold deposits in northern Nevada: Geological Society of Nevada, 1999 Spring Field Trip Guidebook, Special Publication No. 29, p. 64-158.

John, D.A., and Wallace, A.R., 2000, Epithermal gold-silver deposits related to the northern Nevada rift. *In* Cluer, J.K., Price, J.G., Struhsacker, E.M., Hardyman, R.F., and Morris, C.L., eds., Geology and ore deposits 2000-The Great Basin and beyond: Geological Society of Nevada, Symposium Proceedings, this volume.

John, D.A., Wallace, A.R., Ponce, D.A., Fleck, R.B., and Conrad, J.E., 2000, New perspectives on the geology and origin of the northern Nevada Rift, *in* Cluer, J.K., Price, J.G., Struhsacker, E.M., Hardyman, R.F., and Morris, C.L., eds., Geology and Ore Deposits 2000: The Great Basin and Beyond: Geological Society of Nevada Symposium Proceedings, May 15-18, 2000, p. 127-154.

John, D.A., 2001, Miocene and early Pliocene epithermal gold silver deposits in the northern Great Basin, western USA: Characteristics, distribution, and relationship to magmatism: Economic Geology, v. 96, p.1827M.

Karlstrom, K.E., Harlan, S.S., Williams, M.L., McLelland, J., Geissman, J.W., and Åhåll, K.-I., 1999, Refining Rodinia: Geologic evidence for the Australia-Western U.S. connection in the Proterozoic: Geological Society of America Today, v. 9, no. 10, p. 1–7.

KITCO, 2024, Live Gold Prices: https://www.kitco.com/ (accessed July 2023).

Lee, J.-Y., Marti, K., Severinghaus, J.P., Kawamura, K., Yoo, H.-S., Lee, J.B., and Kim, J.S., 2006, A redetermination of the isotopic abundances of atmospheric Ar: Geochimica et Cosmochimica Acta, v. 70, p. 4507-4512. https://doi.org/10.1016/j.gca.2006.06.1563.4.1.

Lindgren, W., 1900, The gold and silver veins of the Silver City, DeLamar, and other mining districts in Idaho. US geological Survey 20th Annual Report, Part 3, p.65-256.

Lingdren, W., 1933, Mineral deposits: New York, McGraw-Hill, 4th ed., 930 p.

Ludwig, K.R., 2012, User's manual for Isoplot 3.75: A geochronological toolkit for Microsoft Excel: Berkeley Geochronology Center Special Publication No. 5, 75 p. http://www.bgc.org/isoplot_etc/isoplot/Isoplot3_75-4_15manual.pdf.

Merrihue, C., and Turner, G., 1966, Potassium-argon dating by activation with fast neutrons: Journal of Geophysical Research, v. 71, p. 2852-2857.

Miller, C.F., and Barton, M.D., 1990, Phanerozoic plutonism in the Cordilleran interior, U.S.A.: Geological Society of America Special Paper 241, p. 213–232.

Min, K., Mundil, R., Renne, P.R., and Ludwig, K.R., 2000, A test for systematic errors in $^{40}Ar/^{39}Ar$ geochronology through comparison with U/Pb analysis of a 1.1-Ga rhyolite; Geochemica et Cosmochimica Acta, v. 64, p. 73-98.

Monroe, L.H., 2021, Using petrographic and geochemical analysis to elucidate the genesis of Au-Ag epithermal deposits on Florida Mountain, Silver City District, Idaho: [M.Sc Thesis]: Auburn University.

Morgan, L.A., and McIntosh, W.C., 2005, $^{40}Ar/^{39}Ar$ ages of silicic volcanic rocks in the Heise volcanic field, eastern Snake River Plain, Idaho: timing of volcanism and tectonism. Geological Society of America Bulletin 117 (3/4). p. 288-306.

Morris, G.A., Larson, P.B., and Hooper, P.R., 2001, “Subduction style” magmatism in a non-subduction setting: the Colville Igneous Complex, NE Washington state, USA: Journal of Petrology, v. 41, p. 43–67.

Nesse, W., 2012, Introduction to Mineralogy: Oxford University Press,

Noble, D.C., McCormack, J.K., McKee, E.H., Silberman, M.L., and Wallace, A.B., 1988, Time of mineralization in the evolution of the McDermitt caldera complex, Nevada-Oregon, and the relation of middle Miocene mineralization in the northern Great Basin to coeval regional basaltic magmatic activity: Economic Geology, v. 83, p. 859–863.

Pansze, A.J., 1975, Geology and ore deposits of the Silver City-Delamar-Flint region, Owyhee County, Idaho: Idaho Bureau of Mines and Geology Pamp

Parsons, T., Thompson, and G.A., Sleep, N.H., 1994, Mantle plume influence on the Neogene uplift and extension of the U.S. western Cordillera?: Geology, v. 22, p. 83–86.

Pierce, K.L. and Morgan, L.A., 1992, The track of the Yellowstone hot spot: Volcanism, faulting, and uplift: Geological Society of America Memoirs, v. 179.

Pierce, K.L., and Morgan, L.A., 2009, Is the track of the Yellowstone hotspot driven by a deep mantle plume? – Review of volcanism, faulting, and uplift in light of new data: Journal of Volcanology and Geothermal Research, v. 188, p. 1-25, doi: https://doi.org/10.1016/j.jvolgeores.2009.07.009.

Proffett, J.M., Jr., 1977, Cenozoic geology of the Yerington district, Nevada, and implications for the nature and origin of Basin and Range faulting: Geological Society of America Bulletin, v. 88, p. 247–266.

Renne, P.R., Swisher, C.C., Deino, A.L., Karner, D.B., Owens, T.L., DePaolo, D.J., 1998, Intercalibration of standards, absolute ages, and uncertainties in $^{40}Ar/^{39}Ar$ Dating: Chemical Geology, v. 145, p. 117–152.

Simmons, F.S., White N.C., and John, D.A., 2005, Geological characteristics of epithermal precious and base metal deposits: Economic Geology 100th anniversary volume, p. 485-522.

Sawkins, F.J., O’Neil, J.R., and Thompson, J.M., 1979, Fluid inclusion and geochemical studies of vein gold deposits, Baguio district, Philippines: Economic Geology, v. 74, p. 1420-1434.

Schaen, A.J., et al., 2020, Interpreting and reporting $^{40}Ar/^{39}Ar$ geochronological data: Geological Society of America Bulletin, v. 133, p. 461-487, doi: https://doi.org/10.1130/B35560.1.

Seedorff, E., 1991, Magmatism, extension, and ore deposits of Eocene to Holocene age in the Great Basin—mutual effects and preliminary proposed genetic relationships, in Raines, G.L., Lisle, R.E., Schafer, R.W., and Wilkinson, W.H., eds., Geology and ore deposits of the Great Basin. Symposium proceedings: Reno, Geological Society of Nevada and U.S. Geological Survey, p. 133–178.

Singer, D.A., 1995, World class base and precious metal deposits-a quantitative analysis: Economic Geology, v. 90, p. 88-104.

Sillitoe, R.H., 1989, Gold deposits in western Pacific island arcs; the magmatic connection: Economic Geology Monographs v. 6, p. 274–291.

Sillitoe, R.H., and Hedenquist, J.W., 2003, Linkages between volcano-tectonic settings, ore fluid compositions and epithermal precious metal deposits: Society of Economic Geologists Special Publication, v. 10, p. 315-343.

Stewart, J.H., 1980, Geology of Nevada: Nevada Bureau of Mines and Geol-ogy: Special Publication 4, p. 136.

——1988, Tectonics of the Walker Lane belt, western Great Basin: Mesozoicand Cenozoic deformation in a zone of shear, in Ernst, W. G., ed., The geo-tectonic development of California: Englewood Cliffs, New Jersey, Prentice-Hall, p. 71–86.

Taylor, B.E., 2007, Epithermal gold deposits, in Goodfellow, W.D., ed., Mineral Deposits of Canada: A synthesis of major deposit-types, district metallogeny, the evolution of geological provinces, and exploration methods: Geological Association of Canada, Mineral Deposits Division, Special Publication No. 5, p. 113-139.

Unger, D.L., 2008, Geochemistry, geochronology, and ore petrology of low-sulfidation Au-Ag ores in the northern Great Basin region of Nevada-Idaho: MS thesis Auburn University.

Wilson, J.T., 1963, Evidence from islands on the spreading of the ocean floor: Nature, 197. 536–538, doi: https://doi-org.spot.lib.auburn.edu/10.1098/rsta.1965.0029.

Willden, R., 1964, Geology and mineral deposits of Humboldt County, Nevada: Nevada Bureau of Mines and Geology Bulletin v. 59, p. 154.

Wright, T.L., and Stewart, D.B., 1968, X-ray and optical study of alkali feldspar: I. Determination of composition an structural state from refined unit-cell parameters and 2V[1]: The American Mineralogist, v. 53, p. 38-87.

Zoback, M.L., and Thompsan, G.A., 1978, Basin and Range rifting in northern Nevada: Clues from a mid-miocene rift and its subsequent offsets: Geology, v. 6, p. 111-116.

Zoback, M.L., McKee, E.H., Blakely, R.J., and Thompsan, G.A., 1994, The northern Nevada rift: Regional tectonomagmatic relations and middle Miocene stress direction: Geological Society of America Bulletin, v. 106, p. 371-382.

APPENDIX 1

Electron Microprobe spot-analysis data of the adularia and alkali feldspar from the Jumbo Mine, Trade Dollar Mine, and Silver City Granite, and calculated cation numbers. Spot analyses were conducted with 15kV accelerated voltage, ~20 nA beam current and 1μm beam size. Results are reported as oxide wt%, the calculations for the cations in formula are based on 8 oxygens. Below is a table describing the respective crystal and standard used to conduct measurements via oxide wt%.

Oxide	Crystal	Standard
SiO_2	TAP	Amelia Albite
Al_2O_3	TAP	Anorthite
FeO	LIF	Fayalite
MgO	TAP	Springwater Olivine
CaO	PET	Anorthite
Na_2O	TAP	Amelia Albite
K_2O	PET	Microcline

Sample/Spot ID	JMA	JMA	JMA	JMA	JMA	JMA	JMA	JMA
Oxide Weight Percent								
SiO_2	66.45	64.10	65.21	64.61	62.55	64.23	63.12	63.88
Al_2O_3	18.27	18.71	18.84	18.20	18.34	19.00	18.50	18.72
FeO	0.00	0.03	0.00	0.08	0.03	0.00	0.00	0.02
MgO	0.03	0.06	0.02	0.03	0.00	0.00	0.00	0.00
CaO	0.01	0.04	0.00	0.01	0.03	0.01	0.01	0.02
Na_2O	0.44	0.21	0.22	0.25	0.55	0.29	0.37	0.25
K_2O	16.95	17.06	17.35	16.91	17.30	16.74	17.37	17.08
Total	102.21	100.37	101.77	100.13	98.84	100.26	99.41	100.04
Cations in Formula								
SiO_2	3.01	2.91	2.96	2.93	2.83	2.91	2.86	2.90
Al_2O_3	0.98	1.00	1.01	0.97	0.98	1.01	0.99	1.00
FeO	0.00	0.00	0.00	0.00	0.00	0.00	0.00	0.00
MgO	0.00	0.00	0.00	0.00	0.00	0.00	0.00	0.00
CaO	0.00	0.00	0.00	0.00	0.00	0.00	0.00	0.00
Na_2O	0.04	0.02	0.02	0.02	0.05	0.03	0.03	0.02
K_2O	0.98	0.99	1.00	0.98	1.00	0.97	1.00	0.99
Sum IV	3.99	3.90	3.96	3.90	3.81	3.93	3.85	3.90
Sum Alk.	1.02	1.01	1.02	1.00	1.05	0.99	1.04	1.01
Ab%	3.78%	1.86%	1.91%	2.23%	4.57%	2.54%	3.15%	2.21%
An%	0.06%	0.19%	0.00%	0.03%	0.14%	0.03%	0.03%	0.09%
Or%	96.15%	97.95%	98.09%	97.74%	95.30%	97.44%	96.82%	97.69%

Sample/Spot ID	TDB_a	TDB_a	TDB_a	TDB_a	TDB_a
Oxide Weight Percent					
SiO_2	63.68	64.73	64.68	65.22	63.94
Al_2O_3	18.72	18.58	18.6	17.78	18.22
FeO	0.00	0.10	0.00	0.05	0.00
MgO	0.00	0.01	0.00	0.01	0.01
CaO	0.03	0.02	0.00	0.01	0.00
Na_2O	0.24	0.32	0.40	0.31	0.38
K_2O	17.55	17.19	17.15	17.21	17.85
Total	100.24	100.95	100.95	100.70	100.46
Cations in Formula					
SiO_2	2.96	3.01	3.01	3.03	2.97
Al_2O_3	1.03	1.02	1.02	0.97	1.00
FeO	0.00	0.00	0.00	0.00	0.00
MgO	0.00	0.00	0.00	0.00	0.00
CaO	0.00	0.00	0.00	0.00	0.00
Na_2O	0.02	0.03	0.04	0.03	0.03
K_2O	1.04	1.02	1.02	1.02	1.06
Sum IV	3.99	4.03	4.03	4.01	3.97
Sum Alk.	1.06	1.05	1.05	1.05	1.09
Ab%	2.03%	2.75%	3.44%	2.67%	3.10%
An%	0.00%	0.01%	0.00%	0.02%	0.02%
Or%	97.97%	97.25%	96.56%	97.33%	96.90%

Sample/Spot ID	TDG-k	TDG-k	TDG-k	TDG-k	TDG-k	TDG-k	TDG-k	TDG-k	TDG-k	TDG-k	TDG-k	TDG-k	TDG-k	TDG-k
Oxide Weight Percent														
SiO_2	59.59	58.22	60.11	64.92	63.46	59.41	63.37	63.37	63.72	61.55	60.44	62.38	62.54	60.76
Al_2O_3	19.11	18.28	18.92	19.68	19.19	20.09	19.18	20.09	19.31	19.57	19.43	19.57	19.52	19.33
FeO	0.00	0	0.00	0.10	0.02	0.01	0.00	0.00	0.02	0.00	0.04	0.00	0.07	0.00
MgO	0.03	0	0.00	0.00	0.00	0.00	0.00	0.00	0.00	0.00	0.00	0.01	0.01	0.00
CaO	0.03	0.06	0.11	0.08	0.08	0.13	0.07	0.08	0.04	0.11	0.09	0.10	0.07	0.03
Na_2O	0.57	1.10	0.86	1.45	1.82	1.40	0.93	0.93	0.83	1.39	1.53	0.96	1.09	1.22
K_2O	16.32	14.54	16.77	14.93	15.37	15.23	16.18	15.22	16.14	16.54	16.36	15.88	16.82	15.91
Total	98.01	95.07	97.84	102.3	101.14	97.19	100.75	100.86	101.3	100.04	98.94	100.02	101.12	98.15
Cations in Formula														
SiO_2	2.89	2.91	2.90	2.95	2.93	2.86	2.94	2.92	2.94	2.90	2.88	2.92	2.91	2.90
Al_2O_3	1.09	1.08	1.08	1.05	1.05	1.14	1.05	1.09	1.05	1.08	1.09	1.08	1.07	1.09
FeO	0.00	0.00	0.00	0.00	0.00	0.00	0.00	0.00	0.00	0.00	0.00	0.00	0.00	0.00
MgO	0.00	0.00	0.00	0.00	0.00	0.00	0.00	0.00	0.00	0.00	0.00	0.00	0.00	0.00
CaO	0.00	0.00	0.01	0.00	0.00	0.01	0.00	0.00	0.00	0.01	0.00	0.00	0.00	0.00
Na_2O	0.05	0.11	0.08	0.13	0.16	0.13	0.08	0.08	0.07	0.13	0.14	0.09	0.10	0.11
K_2O	1.01	0.93	1.03	0.86	0.91	0.94	0.96	0.90	0.95	0.99	1.00	0.95	1.00	0.97
Sum IV	3.98	3.98	3.98	4.00	3.98	4.01	3.99	4.02	3.99	3.98	3.98	4.00	3.98	3.99
Sum Alk.	1.06	1.04	1.12	1.00	1.07	1.07	1.05	0.98	1.03	1.13	1.14	1.04	1.10	1.08
Ab%	5.00%	10.30%	7.23%	12.77%	15.18%	12.19%	8.01%	8.45%	7.26%	11.30%	12.42%	8.39%	8.91%	10.39%
An%	0.17%	0.32%	0.49%	0.41%	0.37%	0.64%	0.34%	0.39%	0.19%	0.51%	0.41%	0.47%	0.31%	0.15%
Or%	94.84%	89.38%	92.28%	86.81%	84.45%	87.17%	91.65%	91.16%	92.55%	88.19%	87.16%	91.14%	90.78%	89.47%

APPENDIX 2

Single crystal total fusion (SCTF) and incremental heating (IH) data for the Jumbo Mine, Trade Dollar Mine, and Silver City Granite. Sample name, heating style, and calculated J-value for its corresponding layer can be found in the top left. SCTF data always precedes IH data. Samples were irradiated at the Oregon State's TRIGA reactor in Corvallis, Oregon. Synthetic CaF_2 was included with the irradiation to determine calcium production factors, and Fish Canyon sanidine (from an aliquot prepared at New Mexico Tech) was used to monitor production of $^{39}Ar_k$, with an assigned age of 28.2 Ma (Schaen et al., 2020). Radial J-values for the samples appear to be negligible. Aliquots of air from an air pipette were measured daily to evaluate mass discrimination, and procedural blanks were measured following every five analyses of unknowns. Samples were analyzed following gas extraction with a CO_2 laser using an automated extraction line, with data collection on an electron multiplier detector. Dates presented are in volts unless otherwise indicated, and are corrected for backgrounds, mass discrimination, and decay of short-lived isotopes.

Analytical Conditions for the SCTF and IH heating experiments.

Irradiation Package: AU-40
Median Date of Irradiation: 1/31/24
Total 40K Decay constant:
5.463 ± 0.107 × 10–10 yr–1 (2σ); Min and Renne (2000)
Monitors, Ages (as summarized in Schaen et al., 2020):
GA1550 Biotite Age (Ma): 9.944E+07
FC Sanidine Age (Ma): 2.820E+07
Final Date of Analyses: ca. March 10th, 2024
Measured 40/36 of Air during analyses: 293.0±1.0
Assumed 40Ar/36Ar of Air (Lee et al., 2006): 298.56
Irradiation Production Factors:
(36/37)Ca: 0.0003046±0.0000084
(39/37)Ca: 0.0007380±0.0000370
(40/39)K: 0±0.0044
(38/39)Cl: 0.01±0.01

Unless indicated otherwise, the data for individual measurements are in volts and errors are the standard deviation of measurement and do not include the error in estimating the J-Value (~0.15-0.25% at the 95% confidence level). Statistical combinations of ages (plateau ages, etc.) do include the error in J-values. P = Laser Power Level (10 = 100%), t = laser heating time (s). Data are corrected for blank, mass discrimination, and interfering nuclear reactions.

The rubric for irradiation filenames is: 'AU + package"+ "layer, radial position" + "phase" + "planchet hole # and sequence", saved as a text file. All samples for this study were within layers 9 and 10, with positions labeled as in sketch to the right, and the monitor data for these layers are included in the dataset below.

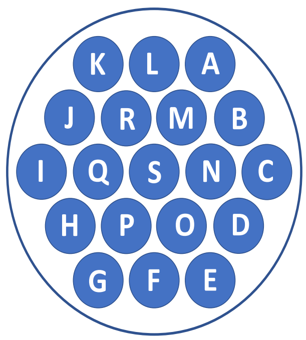

	P	t	40	39	38	37	36	Moles 40Ar	40Ar/36Ar	40Ar/38Ar
Representative analyses of analytical 'blank' during the course of monitor analyses.										
blank.4.20.23.j.txt	0	0	0.00510 ± 0.000071	0.00014 ± 0.000017	0.00004 ± 0.000005	0.00009 ± 0.000011	0.0000387 ± 0.0000039	3.47E-17	132	
blank.4.21.23.a.txt	0	0	0.00436 ± 0.000091	0.00012 ± 0.000021	0.00003 ± 0.000006	0.00008 ± 0.000007	0.0000364 ± 0.0000028	2.96E-17	120	
Representative analyses of analytical 'blank' during the course of sample analyses.										
blank.5.15.24.b.txt	0	0	0.00665 ± 0.000116	0.00017 ± 0.000021	0.00005 ± 0.000006	0.00011 ± 0.000009	0.000041 ± 0.000003	4.20E-17	163.25 ± 0.44	2.043 ± 45427.4718
blank.5.15.24.c.txt	0	0	0.00626 ± 0.000132	0.00022 ± 0.000011	0.00004 ± 0.000005	0.00012 ± 0.000005	0.000037 ± 0.000004	3.96E-17	169.92 ± 0.54	1.359 ± 45427.4866
Representative Analyses of Air aliquots during analsyes of monitors and samples.										
air.2.27.24.a.txt	0	0	12.13927 ± 0.005414	-0.00024 ± 0.000059	0.00782 ± 0.000061	0.00009 ± 0.000015	0.0413213 ± 0.000194	7.67E-14	293.78 ± 1551.67	1.0 ± 45349.4
air.2.27.24.b.txt	0	0	12.18806 ± 0.006932	-0.00032 ± 0.000112	0.00779 ± 0.000081	0.00011 ± 0.000015	0.0414321 ± 0.000145	7.70E-14	294.17 ± 1563.66	1.0 ± 45349.6

Analyses of the Flux Monitor FC-2 (single crystal, Fish Canyon Sanidine, prepared by R. Esser of New Mexico Tech ca. 1998).

	P	t	40Ar(*+atm)	39ArK	38Ar(Atm+Cl)	37ArCa	36Ar(atm)	Moles 40Ar	% Rad.	R	J	% s.d.
au40.1a.san.3a.txt	3	30	16.84833 ± 0.013553	4.55474 ± 0.003055	0.05476 ± 0.000219	0.03213 ± 0.000077	0.001473 ± 0.000016	1.07E-13	97%	3.604130	0.004308 ± 0.000005	0.1%
au40.1a.san.4a.txt	3	30	17.31609 ± 0.011385	4.78500 ± 0.001336	0.05858 ± 0.000333	0.03529 ± 0.000176	0.000242 ± 0.000017	1.09E-13	100%	3.604561	0.004307 ± 0.000003	0.1%
au40.1a.san.5a.txt	3	30	14.46336 ± 0.007216	3.29608 ± 0.002806	0.04142 ± 0.000269	0.04925 ± 0.000274	0.008703 ± 0.000069	9.14E-14	82%	3.609164	0.004302 ± 0.000009	0.2%
au40.1a.san.6a.txt	3	30	19.90752 ± 0.015267	5.48427 ± 0.004507	0.06639 ± 0.000294	0.03487 ± 0.000150	0.000253 ± 0.000018	1.26E-13	100%	3.616906	0.004292 ± 0.000005	0.1%
au40.1a.san.7a.txt	3	30	21.54430 ± 0.015338	5.92630 ± 0.002984	0.07678 ± 0.000405	0.03868 ± 0.000269	0.000642 ± 0.000029	1.36E-13	99%	3.603985	0.004308 ± 0.000004	0.1%
au40.1e.san.12a.txt	3	30	14.36074 ± 0.011717	3.93485 ± 0.004237	0.04869 ± 0.000332	0.03109 ± 0.000163	0.000989 ± 0.000015	9.08E-14	98%	3.576079	0.004341 ± 0.000006	0.1%
au40.1e.san.13a.txt	3	30	11.40315 ± 0.013942	3.05281 ± 0.003993	0.03716 ± 0.000191	0.02231 ± 0.000155	0.001308 ± 0.000018	7.21E-14	97%	3.609321	0.004301 ± 0.000008	0.2%
au40.1e.san.14a.txt	3	30	7.71759 ± 0.010659	2.12890 ± 0.002103	0.02584 ± 0.000227	0.01334 ± 0.000070	0.000101 ± 0.000013	4.88E-14	100%	3.611655	0.004299 ± 0.000008	0.2%
au40.1e.san.8a.txt	3	30	16.61426 ± 0.010223	4.58841 ± 0.004967	0.05535 ± 0.000277	0.03094 ± 0.000137	0.000114 ± 0.000015	1.05E-13	100%	3.614215	0.004296 ± 0.000005	0.1%
au40.1i.san.15a.txt	3	30	14.39066 ± 0.014458	3.95110 ± 0.001927	0.04803 ± 0.000300	0.06875 ± 0.000189	0.000690 ± 0.000015	9.10E-14	99%	3.592173	0.004322 ± 0.000005	0.1%
au40.1i.san.16a.txt	3	30	5.44491 ± 0.008040	1.50489 ± 0.002199	0.01827 ± 0.000145	0.01092 ± 0.000184	0.000028 ± 0.000011	3.44E-14	100%	3.613366	0.004297 ± 0.000009	0.2%
au40.1i.san.17a.txt	3	30	17.40029 ± 0.021887	4.75570 ± 0.004474	0.05720 ± 0.000305	0.04087 ± 0.000186	0.000881 ± 0.000016	1.10E-13	99%	3.604869	0.004307 ± 0.000007	0.2%
au40.1i.san.18a.txt	3	30	12.83408 ± 0.024824	3.52430 ± 0.003962	0.04277 ± 0.000222	0.02943 ± 0.000135	0.000475 ± 0.000023	8.11E-14	99%	3.602512	0.004310 ± 0.000010	0.2%
au40.1i.san.19a.txt	3	30	12.60902 ± 0.026111	3.46244 ± 0.005650	0.04222 ± 0.000317	0.02687 ± 0.000140	0.000278 ± 0.000020	7.97E-14	99%	3.618670	0.004290 ± 0.000012	0.3%
au40.1s.san.21a.txt	3	30	20.26388 ± 0.023110	5.62113 ± 0.003997	0.06824 ± 0.000465	0.03715 ± 0.000145	0.000150 ± 0.000016	1.28E-13	100%	3.597675	0.004315 ± 0.000006	0.1%
au40.1s.san.22a.txt	3	30	14.11563 ± 0.026451	3.87589 ± 0.007189	0.04624 ± 0.000264	0.02446 ± 0.000135	0.000238 ± 0.000024	8.92E-14	100%	3.624384	0.004284 ± 0.000012	0.3%
au40.1s.san.24a.txt	3	30	16.47714 ± 0.025212	4.48640 ± 0.005083	0.05386 ± 0.000199	0.04177 ± 0.000251	0.000811 ± 0.000016	1.04E-13	99%	3.620133	0.004289 ± 0.000008	0.2%
au40.2c.san.25a.txt	3	30	9.18126 ± 0.017248	2.54423 ± 0.003961	0.03057 ± 0.000264	0.01899 ± 0.000242	0.000137 ± 0.000014	5.80E-14	100%	3.593421	0.004321 ± 0.000011	0.2%
au40.2c.san.26a.txt	3	30	18.53616 ± 0.044296	5.14823 ± 0.007421	0.06240 ± 0.000300	0.04001 ± 0.000254	0.000089 ± 0.000021	1.17E-13	100%	3.596101	0.004317 ± 0.000012	0.3%
au40.2c.san.27a.txt	3	30	15.01589 ± 0.037896	4.19185 ± 0.004935	0.05153 ± 0.000351	0.02781 ± 0.000114	0.000104 ± 0.000015	9.49E-14	100%	3.575457	0.004342 ± 0.000012	0.3%
au40.2c.san.28a.txt	3	30	13.13527 ± 0.026207	3.65962 ± 0.003927	0.04475 ± 0.000317	0.02541 ± 0.000149	0.000075 ± 0.000017	8.30E-14	100%	3.583800	0.004332 ± 0.000010	0.2%
au40.2c.san.29a.txt	3	30	7.98226 ± 0.020021	2.21860 ± 0.002744	0.02673 ± 0.000146	0.01459 ± 0.000212	0.000064 ± 0.000013	5.05E-14	100%	3.589927	0.004325 ± 0.000012	0.3%
au40.2g.san.30a.txt	3	30	15.53024 ± 0.027602	4.03010 ± 0.002748	0.04902 ± 0.000150	0.02978 ± 0.000203	0.003745 ± 0.000021	9.82E-14	93%	3.579667	0.004337 ± 0.000009	0.2%
au40.2g.san.31a.txt	3	30	8.05198 ± 0.029040	2.23376 ± 0.005084	0.02714 ± 0.000191	0.01493 ± 0.000229	0.000089 ± 0.000013	5.09E-14	100%	3.593535	0.004320 ± 0.000019	0.4%
au40.2g.san.32a.txt	3	30	4.84790 ± 0.014353	1.33853 ± 0.001924	0.01631 ± 0.000137	0.01011 ± 0.000140	0.000212 ± 0.000008	3.06E-14	99%	3.575584	0.004342 ± 0.000015	0.3%
au40.2g.san.33a.txt	3	30	12.73507 ± 0.036582	3.49358 ± 0.005894	0.04267 ± 0.000222	0.02336 ± 0.000148	0.000750 ± 0.000023	8.05E-14	98%	3.582434	0.004334 ± 0.000015	0.3%
au40.2g.san.34a.txt	3	30	14.36666 ± 0.042363	4.00148 ± 0.008765	0.04791 ± 0.000312	0.02685 ± 0.000082	0.000248 ± 0.000020	9.08E-14	99%	3.572631	0.004346 ± 0.000016	0.4%
au40.2k.san.35a.txt	3	30	9.65387 ± 0.021672	2.69303 ± 0.004619	0.03246 ± 0.000173	0.01994 ± 0.000242	0.000051 ± 0.000014	6.10E-14	100%	3.579851	0.004337 ± 0.000012	0.3%
au40.2k.san.36a.txt	3	30	8.56325 ± 0.026445	2.38390 ± 0.004886	0.02865 ± 0.000165	0.01680 ± 0.000179	0.000078 ± 0.000013	5.41E-14	100%	3.583133	0.004333 ± 0.000016	0.4%
au40.2k.san.37a.txt	3	30	7.15617 ± 0.019705	1.91472 ± 0.003440	0.02363 ± 0.000168	0.01515 ± 0.000165	0.001067 ± 0.000014	4.52E-14	96%	3.573554	0.004345 ± 0.000015	0.3%
au40.2k.san.38a.txt	3	30	17.79813 ± 0.064856	4.89901 ± 0.009393	0.05875 ± 0.000316	0.04671 ± 0.000250	0.000626 ± 0.000026	1.13E-13	99%	3.596112	0.004317 ± 0.000018	0.4%
au40.2k.san.39a.txt	3	30	14.27233 ± 0.047438	3.96089 ± 0.008348	0.04756 ± 0.000214	0.02721 ± 0.000121	0.000164 ± 0.000021	9.02E-14	100%	3.591691	0.004323 ± 0.000017	0.4%
au40.2s.san.40a.txt	3	30	12.59530 ± 0.035363	3.47077 ± 0.006179	0.04206 ± 0.000306	0.02553 ± 0.000157	0.000595 ± 0.000029	7.96E-14	99%	3.578980	0.004338 ± 0.000015	0.3%
au40.2s.san.41a.txt	3	30	5.49050 ± 0.017212	1.52170 ± 0.003450	0.01817 ± 0.000131	0.01003 ± 0.000048	0.000094 ± 0.000013	3.47E-14	99%	3.590472	0.004324 ± 0.000017	0.4%
au40.2s.san.42a.txt	3	30	13.04090 ± 0.036357	3.62042 ± 0.005103	0.04361 ± 0.000155	0.02639 ± 0.000161	0.000081 ± 0.000022	8.24E-14	100%	3.596111	0.004317 ± 0.000014	0.3%
au40.2s.san.43a.txt	3	30	6.91446 ± 0.022323	1.91648 ± 0.003663	0.02328 ± 0.000241	0.01732 ± 0.000186	0.000144 ± 0.000010	4.37E-14	99%	3.586595	0.004329 ± 0.000016	0.4%
au40.2s.san.44a.txt	3	30	8.20743 ± 0.026711	2.28018 ± 0.004260	0.02746 ± 0.000097	0.01838 ± 0.000186	0.000188 ± 0.000010	5.19E-14	99%	3.575883	0.004342 ± 0.000016	0.4%

Sample ID/Increment	P	40Ar(*+atm)	39ArK	38Ar(Atm+Cl)	37ArCa	36Ar(Atm)	Moles 40Ar	% Rad.	R	Age (Ma)	% s.d.
JMA-002, SCTF Analys J-Value=0.004331±0.000012											
au40.2f.adl.51a.txt	3	2.65595 ± 0.005288	1.24950 ± 0.001836	0.01511 ± 0.00008	0.00037 ± 0.000018	0.000165 ± 0.000010	1.68E-14	98.2%	2.086580	16.47 ± 0.05	0.27%
au40.2f.adl.52a.txt	3	4.54716 ± 0.011013	2.12539 ± 0.002449	0.02556 ± 0.00015	0.00033 ± 0.000023	0.000269 ± 0.000019	2.87E-14	98.3%	2.102058	16.59 ± 0.05	0.30%
au40.2f.adl.53a.txt	3	4.31415 ± 0.010712	2.04744 ± 0.003219	0.02458 ± 0.00017	0.00175 ± 0.000032	0.000149 ± 0.000012	2.73E-14	99.0%	2.085690	16.46 ± 0.05	0.31%
au40.2f.adl.54a.txt	3	4.24350 ± 0.010937	2.01141 ± 0.002424	0.02423 ± 0.00010	0.00066 ± 0.000021	0.000102 ± 0.000013	2.68E-14	99.3%	2.094765	16.54 ± 0.05	0.30%
au40.2f.adl.55a.txt	3	5.51665 ± 0.012774	2.59472 ± 0.004568	0.03135 ± 0.00018	0.00126 ± 0.000028	0.000373 ± 0.000010	3.49E-14	98.0%	2.083713	16.45 ± 0.05	0.30%
au40.2f.adl.56a.txt	3	1.26551 ± 0.003405	0.58796 ± 0.001422	0.00688 ± 0.00006	0.00042 ± 0.000020	0.000077 ± 0.000013	8.00E-15	98.2%	2.113891	16.69 ± 0.08	0.48%
au40.2f.adl.57a.txt	3	7.94693 ± 0.020751	3.26253 ± 0.004725	0.04012 ± 0.00017	0.00593 ± 0.000048	0.004174 ± 0.000041	5.02E-14	84.5%	2.057924	16.25 ± 0.06	0.40%
au40.2f.adl.58a.txt	3	1.51147 ± 0.004951	0.72150 ± 0.001684	0.00852 ± 0.00007	0.00028 ± 0.000019	0.000001 ± 0.000013	9.55E-15	100.0%	2.094571	16.53 ± 0.08	0.47%
au40.2f.adl.59a.txt	3	1.90261 ± 0.005828	0.87716 ± 0.001415	0.01071 ± 0.00012	0.00044 ± 0.000018	0.000160 ± 0.000010	1.20E-14	97.5%	2.115326	16.70 ± 0.07	0.39%
au40.2f.adl.60a.txt	3	4.10703 ± 0.009018	1.92224 ± 0.002622	0.02330 ± 0.00015	0.00105 ± 0.000030	0.000280 ± 0.000008	2.60E-14	98.0%	2.093575	16.53 ± 0.04	0.27%
au40.2f.adl.61a.txt	3	5.22850 ± 0.012901	2.45264 ± 0.002815	0.02936 ± 0.00015	0.00077 ± 0.000024	0.000306 ± 0.000010	3.31E-14	98.3%	2.094899	16.54 ± 0.05	0.28%
au40.2f.adl.62a.txt	3	1.39213 ± 0.003268	0.58681 ± 0.000979	0.00717 ± 0.00009	0.00198 ± 0.000074	0.000647 ± 0.000011	8.80E-15	86.3%	2.046859	16.16 ± 0.07	0.43%
au40.2f.adl.63a.txt	3	7.70834 ± 0.017198	3.62009 ± 0.006063	0.04378 ± 0.00025	0.00163 ± 0.000021	0.000555 ± 0.000018	4.87E-14	97.9%	2.084064	16.45 ± 0.05	0.29%
au40.2f.adl.64a.txt	3	4.76597 ± 0.012017	2.26470 ± 0.004499	0.02731 ± 0.00016	0.00043 ± 0.000028	0.000051 ± 0.000010	3.01E-14	99.7%	2.097756	16.56 ± 0.05	0.33%
au40.2f.adl.65a.txt	3	4.06546 ± 0.010006	1.78040 ± 0.001971	0.02188 ± 0.00008	0.00191 ± 0.000032	0.001217 ± 0.000012	2.57E-14	91.2%	2.081628	16.43 ± 0.05	0.31%
au40.2f.adl.66a.txt	3	1.05726 ± 0.001994	0.49515 ± 0.000544	0.00576 ± 0.00005	0.00026 ± 0.000008	0.000088 ± 0.000010	6.68E-15	97.5%	2.082620	16.44 ± 0.06	0.37%
au40.2f.adl.67a.txt	3	0.68412 ± 0.001862	0.28528 ± 0.000792	0.00333 ± 0.00003	0.00068 ± 0.000039	0.000319 ± 0.000009	4.32E-15	86.2%	2.067755	16.32 ± 0.11	0.65%
au40.2f.adl.68a.txt	3	3.44129 ± 0.010737	1.62431 ± 0.002023	0.01981 ± 0.00014	0.00085 ± 0.000024	0.000129 ± 0.000012	2.18E-14	98.9%	2.095216	16.54 ± 0.06	0.36%
au40.2f.adl.69a.txt	3	2.71493 ± 0.007774	1.28309 ± 0.002095	0.01489 ± 0.00007	0.00056 ± 0.000025	0.000097 ± 0.000011	1.72E-14	98.9%	2.093636	16.53 ± 0.06	0.36%
au40.2f.adl.70a.txt	3	4.00416 ± 0.010755	1.87972 ± 0.003977	0.02227 ± 0.00012	0.00062 ± 0.000026	0.000280 ± 0.000010	2.53E-14	97.9%	2.086210	16.47 ± 0.06	0.36%
au40.2f.adl.71a.txt	3	4.96185 ± 0.008642	2.34599 ± 0.001678	0.02829 ± 0.00017	0.00088 ± 0.000016	0.000201 ± 0.000014	3.14E-14	98.8%	2.089716	16.50 ± 0.03	0.21%
au40.2f.adl.72a.txt	3	3.65683 ± 0.009842	1.73052 ± 0.003398	0.02064 ± 0.00021	0.00164 ± 0.000034	0.000147 ± 0.000012	2.31E-14	98.8%	2.088105	16.48 ± 0.06	0.35%
au40.2f.adl.73a.txt	3	4.64686 ± 0.013340	2.15021 ± 0.003552	0.02612 ± 0.00018	0.00093 ± 0.000023	0.000503 ± 0.000010	2.94E-14	96.8%	2.091976	16.51 ± 0.06	0.35%
au40.2f.adl.74a.txt	3	2.30255 ± 0.005942	1.08341 ± 0.002071	0.01267 ± 0.00005	0.00074 ± 0.000035	0.000135 ± 0.000012	1.46E-14	98.3%	2.088383	16.49 ± 0.06	0.36%
au40.2f.adl.75a.txt	3	1.72924 ± 0.004465	0.81877 ± 0.001197	0.01003 ± 0.00012	0.00049 ± 0.000019	0.000064 ± 0.000011	1.09E-14	98.9%	2.088887	16.49 ± 0.06	0.36%
au40.2f.adl.76a.txt	3	0.83094 ± 0.001966	0.38976 ± 0.000710	0.00473 ± 0.00005	0.00027 ± 0.000022	0.000083 ± 0.000009	5.25E-15	97.0%	2.068931	16.33 ± 0.07	0.45%
au40.2f.adl.77a.txt	3	3.71852 ± 0.006100	1.74442 ± 0.002669	0.02117 ± 0.00016	0.00967 ± 0.000103	0.000162 ± 0.000013	2.35E-14	98.7%	2.104655	16.61 ± 0.04	0.25%
au40.2f.adl.78a.txt	3	5.09337 ± 0.009362	2.39885 ± 0.002785	0.02857 ± 0.00016	0.00099 ± 0.000032	0.000308 ± 0.000009	3.22E-14	98.2%	2.085336	16.46 ± 0.04	0.23%
au40.2f.adl.79a.txt	3	5.67932 ± 0.012636	2.65337 ± 0.004712	0.03202 ± 0.00025	0.00309 ± 0.000045	0.000338 ± 0.000015	3.59E-14	98.2%	2.102912	16.60 ± 0.05	0.30%
au40.2f.adl.80a.txt	3	3.64728 ± 0.007885	1.73154 ± 0.002907	0.02092 ± 0.00016	0.00022 ± 0.000022	0.000081 ± 0.000012	2.31E-14	99.3%	2.092540	16.52 ± 0.05	0.29%
au40.2f.adl.81a.txt	3	2.77675 ± 0.006255	1.29749 ± 0.001841	0.01526 ± 0.00010	0.00061 ± 0.000019	0.000240 ± 0.000008	1.76E-14	97.4%	2.085514	16.46 ± 0.05	0.29%
au40.2f.adl.82a.txt	3	2.38565 ± 0.006435	1.12315 ± 0.001809	0.01350 ± 0.00008	0.00035 ± 0.000012	0.000087 ± 0.000006	1.51E-14	98.9%	2.101125	16.59 ± 0.05	0.33%
au40.2f.adl.83a.txt	3	3.52914 ± 0.008771	1.67287 ± 0.002834	0.02012 ± 0.00015	0.00023 ± 0.000015	0.000056 ± 0.000008	2.23E-14	99.5%	2.099692	16.57 ± 0.05	0.31%
au40.2f.adl.84a.txt	3	2.06279 ± 0.005958	0.98004 ± 0.001536	0.01183 ± 0.00012	0.00022 ± 0.000010	0.000027 ± 0.000009	1.30E-14	99.6%	2.096662	16.55 ± 0.06	0.36%
au40.2f.adl.85a.txt	3	0.66461 ± 0.001659	0.30715 ± 0.000801	0.00357 ± 0.00004	0.00047 ± 0.000029	0.000046 ± 0.000009	4.20E-15	97.9%	2.119505	16.73 ± 0.09	0.56%
au40.2f.adl.86a.txt	3	2.35303 ± 0.005582	1.10802 ± 0.001401	0.01327 ± 0.00014	0.00055 ± 0.000018	0.000096 ± 0.000010	1.49E-14	98.8%	2.098141	16.56 ± 0.05	0.30%
au40.2f.adl.87a.txt	3	2.34108 ± 0.005493	1.10019 ± 0.002064	0.01316 ± 0.00006	0.00232 ± 0.000056	0.000200 ± 0.000009	1.48E-14	97.5%	2.074288	16.38 ± 0.05	0.33%
au40.2f.adl.89a.txt	3	1.32416 ± 0.004327	0.62787 ± 0.000862	0.00766 ± 0.00011	0.00010 ± 0.000009	0.000035 ± 0.000012	8.37E-15	99.2%	2.092738	16.52 ± 0.07	0.45%
au40.2f.adl.90a.txt	3	2.20766 ± 0.004435	1.04254 ± 0.001915	0.01258 ± 0.00010	0.00033 ± 0.000024	0.000084 ± 0.000009	1.40E-14	98.9%	2.093708	16.53 ± 0.05	0.30%
au40.2f.adl.91a.txt	3	1.82656 ± 0.004220	0.86064 ± 0.000803	0.01040 ± 0.00008	0.00013 ± 0.000016	0.000084 ± 0.000012	1.15E-14	98.6%	2.093659	16.53 ± 0.05	0.32%
au40.2f.adl.92a.txt	3	0.91660 ± 0.002506	0.43386 ± 0.001058	0.00511 ± 0.00003	0.00007 ± 0.000013	0.000017 ± 0.000010	5.79E-15	99.4%	2.100902	16.58 ± 0.08	0.50%
au40.2f.adl.93a.txt	3	0.42836 ± 0.001257	0.19951 ± 0.000463	0.00238 ± 0.00004	0.00024 ± 0.000015	0.000035 ± 0.000011	2.71E-15	97.6%	2.095356	16.54 ± 0.14	0.86%
au40.2f.adl.94a.txt	3	1.78039 ± 0.004508	0.82866 ± 0.001335	0.00991 ± 0.00009	0.00012 ± 0.000013	0.000150 ± 0.000013	1.13E-14	97.5%	2.095153	16.54 ± 0.06	0.38%
au40.2h.adl.95a.txt	3	4.57957 ± 0.009253	2.16731 ± 0.002297	0.02602 ± 0.00016	0.00024 ± 0.000014	0.000146 ± 0.000015	2.90E-14	99.1%	2.093064	16.52 ± 0.04	0.25%
au40.2h.adl.96a.txt	3	1.29978 ± 0.002810	0.61045 ± 0.001524	0.00743 ± 0.00014	0.00005 ± 0.000011	0.000022 ± 0.000013	8.22E-15	99.5%	2.118680	16.72 ± 0.07	0.44%
au40.2h.adl.97a.txt	3	1.50666 ± 0.004058	0.70780 ± 0.001091	0.00831 ± 0.00005	0.00009 ± 0.000022	0.000084 ± 0.000010	9.52E-15	98.4%	2.093664	16.53 ± 0.06	0.37%
au40.2h.adl.98a.txt	3	1.59659 ± 0.003987	0.75475 ± 0.001275	0.00896 ± 0.00009	0.00021 ± 0.000022	0.000056 ± 0.000012	1.01E-14	99.0%	2.093655	16.53 ± 0.06	0.38%
au40.2h.adl.99a.txt	3	0.52650 ± 0.001112	0.24091 ± 0.000805	0.00279 ± 0.00004	0.00018 ± 0.000015	0.000040 ± 0.000013	3.33E-15	97.8%	2.136881	16.87 ± 0.14	0.82%
au40.2h.adl.100a.txt	3	0.87067 ± 0.002672	0.40935 ± 0.000695	0.00487 ± 0.00005	0.00022 ± 0.000020	0.000021 ± 0.000009	5.50E-15	99.3%	2.112126	16.67 ± 0.08	0.47%
	The following data were excluded from presentation and considered to not represent adularia.										
au40.2f.adl.88a.txt	3	0.17544 ± 0.000532	0.07603 ± 0.000400	0.00091 ± 0.00002	0.00010 ± 0.000012	0.000015 ± 0.000011	1.11E-15	97.5%	2.249681	17.753 ± 0.348	1.95%

Sample ID/Increment	P	40Ar(*+atm)	39ArK	38Ar(Atm+Cl)	37ArCa	36Ar(Atm)	Moles 40Ar	% Rad.	R	Age (Ma)	% s.d.
TDGK-001, SCTF Anal J-Value=0.004331±0.000012											
au40.2i.ksp.11a.txt	3.5	15.43254 ± 0.056642	2.09195 ± 0.007089	0.02551 ± 0.000253	0.14232 ± 0.000787	0.001980 ± 0.000021	9.76E-14	96.2%	7.1038	55.47 ± 0.29	1%
au40.2i.ksp.12a.txt	3.5	12.62844 ± 0.079693	1.67605 ± 0.006773	0.02028 ± 0.000078	0.00717 ± 0.000074	0.001050 ± 0.000016	7.98E-14	97.5%	7.3498	57.36 ± 0.44	1%
au40.2i.ksp.13a.txt	3.5	10.47532 ± 0.039912	3.26636 ± 0.011476	0.04054 ± 0.000204	0.06893 ± 0.000334	0.004222 ± 0.000053	6.62E-14	88.1%	2.8270	22.28 ± 0.14	1%
au40.2i.ksp.14a.txt	3.5	4.28958 ± 0.018498	0.53439 ± 0.001801	0.00765 ± 0.000057	0.22558 ± 0.000752	0.005965 ± 0.000052	2.71E-14	58.9%	4.7680	37.42 ± 0.42	1%
au40.2i.ksp.15a.txt	3.5	13.37913 ± 0.059094	1.66721 ± 0.005076	0.02094 ± 0.000150	0.00595 ± 0.000073	0.006439 ± 0.000050	8.46E-14	85.8%	6.8839	53.78 ± 0.34	1%
au40.2i.ksp.31a.txt	3.5	0.82584 ± 0.000945	0.10327 ± 0.000312	0.00143 ± 0.000016	0.20619 ± 0.000574	0.001449 ± 0.000013	5.22E-15	48.1%	4.0353	31.72 ± 0.36	1%
au40.2i.ksp.32a.txt	3.5	2.41287 ± 0.008745	0.14535 ± 0.000602	0.00216 ± 0.000046	0.24725 ± 0.000616	0.002178 ± 0.000028	1.53E-14	73.3%	12.3417	95.32 ± 0.84	1%
au40.2i.ksp.33a.txt	3.5	1.98862 ± 0.001825	0.24455 ± 0.000481	0.00367 ± 0.000023	0.33912 ± 0.000823	0.003810 ± 0.000039	1.26E-14	43.4%	3.6570	28.77 ± 0.41	1%
au40.2i.ksp.34a.txt	3.5	2.12462 ± 0.005099	0.27383 ± 0.000608	0.00395 ± 0.000045	0.45258 ± 0.001587	0.004328 ± 0.000038	1.34E-14	39.8%	3.2411	25.52 ± 0.39	2%
au40.2i.ksp.35a.txt	3.5	10.89992 ± 0.024814	1.88833 ± 0.002994	0.02454 ± 0.000192	0.19318 ± 0.000492	0.008646 ± 0.000074	6.89E-14	76.6%	4.4288	34.78 ± 0.16	0%
au40.2i.ksp.36a.txt	3.5	3.67365 ± 0.015703	1.02351 ± 0.002876	0.01317 ± 0.000066	0.18937 ± 0.000781	0.004904 ± 0.000040	2.32E-14	60.6%	2.1904	17.28 ± 0.17	1%
au40.2i.ksp.37a.txt	3.5	1.99064 ± 0.007418	0.21600 ± 0.000890	0.00307 ± 0.000028	0.37332 ± 0.001735	0.002662 ± 0.000040	1.26E-14	60.5%	5.7366	44.93 ± 0.60	1%
au40.2i.ksp.38a.txt	3.5	1.96394 ± 0.007888	0.23129 ± 0.000846	0.00305 ± 0.000037	0.21225 ± 0.000935	0.002691 ± 0.000037	1.24E-14	59.5%	5.1387	40.29 ± 0.53	1%
au40.2i.ksp.39a.txt	3.5	1.33639 ± 0.004950	0.21400 ± 0.000891	0.00293 ± 0.000034	0.44441 ± 0.001549	0.002105 ± 0.000024	8.45E-15	53.5%	3.5311	27.78 ± 0.39	1%
au40.2i.ksp.40a.txt	3.5	3.30713 ± 0.011231	0.88623 ± 0.002115	0.01118 ± 0.000073	0.37341 ± 0.001157	0.004341 ± 0.000032	2.09E-14	61.2%	2.3230	18.33 ± 0.15	1%
au40.2i.ksp.41a.txt	3.5	2.18961 ± 0.006087	0.30002 ± 0.000827	0.00444 ± 0.000052	0.47624 ± 0.001318	0.004018 ± 0.000044	1.38E-14	45.8%	3.4881	27.45 ± 0.42	2%
au40.2i.ksp.42a.txt	3.5	2.13415 ± 0.008568	0.37485 ± 0.001265	0.00500 ± 0.000070	0.51491 ± 0.002106	0.003245 ± 0.000036	1.35E-14	55.1%	3.2623	25.68 ± 0.33	1%
au40.2i.ksp.43a.txt	3.5	0.21299 ± 0.000921	0.02530 ± 0.000175	0.00037 ± 0.000019	0.05591 ± 0.000377	0.000441 ± 0.000013	1.35E-15	38.8%	3.4710	27.31 ± 1.36	5%
au40.2i.ksp.44a.txt	3.5	0.67181 ± 0.002793	0.25016 ± 0.000617	0.00306 ± 0.000071	0.03649 ± 0.000294	0.000502 ± 0.000017	4.25E-15	77.9%	2.1053	16.62 ± 0.19	1%
au40.2i.ksp.45a.txt	3.5	3.38712 ± 0.014827	0.43424 ± 0.001563	0.00522 ± 0.000066	0.00512 ± 0.000083	0.000237 ± 0.000007	2.14E-14	97.9%	7.6401	59.59 ± 0.35	1%
au40.2i.ksp.46a.txt	3.5	1.67888 ± 0.005935	0.23007 ± 0.000726	0.00276 ± 0.000064	0.00076 ± 0.000024	0.000110 ± 0.000007	1.06E-14	98.1%	7.1563	55.88 ± 0.28	0%
au40.2i.ksp.47a.txt	3.5	0.13226 ± 0.000471	0.01302 ± 0.000148	0.00017 ± 0.000017	0.02995 ± 0.000261	0.000230 ± 0.000008	8.36E-16	48.6%	5.1562	40.43 ± 1.71	4%
au40.2i.ksp.48a.txt	3.5	0.22174 ± 0.000775	0.01508 ± 0.000087	0.00024 ± 0.000013	0.05086 ± 0.000507	0.000398 ± 0.000008	1.40E-15	47.0%	7.2314	56.45 ± 1.48	3%
au40.2i.ksp.49a.txt	3.5	0.20685 ± 0.000736	0.02636 ± 0.000096	0.00035 ± 0.000016	0.05267 ± 0.000395	0.000200 ± 0.000007	1.31E-15	71.4%	5.7902	45.34 ± 0.68	1%
au40.2i.ksp.50a.txt	3.5	3.86936 ± 0.012530	0.50384 ± 0.001082	0.00620 ± 0.000090	0.00523 ± 0.000083	0.000340 ± 0.000008	2.45E-14	97.4%	7.4812	58.37 ± 0.24	0%
au40.2i.ksp.51a.txt	3.5	0.96181 ± 0.002372	0.36710 ± 0.000886	0.00455 ± 0.000056	0.00250 ± 0.000058	0.000716 ± 0.000016	6.08E-15	78.0%	2.0447	16.14 ± 0.13	1%
au40.2i.ksp.52a.txt	3.5	1.87228 ± 0.006612	0.23605 ± 0.000867	0.00283 ± 0.000058	0.00066 ± 0.000031	0.000165 ± 0.000008	1.18E-14	97.4%	7.7250	60.24 ± 0.32	1%
au40.2i.ksp.53a.txt	3.5	0.10886 ± 0.000351	0.01655 ± 0.000071	0.00021 ± 0.000011	0.03965 ± 0.000260	0.000144 ± 0.000007	6.88E-16	61.0%	4.2353	33.27 ± 1.06	3%
au40.2i.ksp.54a.txt	3.5	1.65811 ± 0.007085	0.24253 ± 0.000693	0.00300 ± 0.000049	0.00090 ± 0.000019	0.000206 ± 0.000007	1.05E-14	96.3%	6.5862	51.49 ± 0.28	1%
au40.2i.ksp.55a.txt	3.5	0.27961 ± 0.001014	0.02825 ± 0.000210	0.00041 ± 0.000012	0.05651 ± 0.000381	0.000526 ± 0.000016	1.77E-15	44.4%	4.5854	36.00 ± 1.50	4%
au40.2i.ksp.56a.txt	3.5	1.57406 ± 0.007169	0.21892 ± 0.000590	0.00263 ± 0.000045	0.01267 ± 0.000216	0.000093 ± 0.000012	9.95E-15	98.3%	7.0702	55.21 ± 0.32	1%
au40.2i.ksp.57a.txt	3.5	0.24156 ± 0.001225	0.03472 ± 0.000173	0.00046 ± 0.000017	0.07957 ± 0.000335	0.000330 ± 0.000008	1.53E-15	59.7%	4.3646	34.28 ± 0.68	2%
au40.2i.ksp.58a.txt	3.5	0.29445 ± 0.001221	0.04506 ± 0.000247	0.00059 ± 0.000019	0.05379 ± 0.000347	0.000396 ± 0.000009	1.86E-15	60.3%	4.0493	31.83 ± 0.59	2%
au40.2i.ksp.59a.txt	3.5	0.33512 ± 0.001195	0.07101 ± 0.000235	0.00087 ± 0.000021	0.04201 ± 0.000325	0.000447 ± 0.000008	2.12E-15	60.5%	2.9120	22.94 ± 0.34	1%
au40.2i.ksp.60a.txt	3.5	1.80140 ± 0.005894	0.69059 ± 0.001778	0.00847 ± 0.000131	0.00013 ± 0.000024	0.001415 ± 0.000027	1.14E-14	76.8%	2.0029	15.81 ± 0.12	1%

Sample ID/Increment	P	40Ar(*+atm)	39ArK	38Ar(Atm+Cl)	37ArCa	36Ar(Atm)	Moles 40Ar	% Rad.	R	Age (Ma)	% s.d.
TDGA-001, SCTF Anal	J-Value=0.0043191±0.0000051										
au40.1b.adl.71a.txt	3.5	3.91224 ± 0.002917	1.84566 ± 0.001286	0.02211 ± 0.000092	0.00038 ± 0.000031	0.000744 ± 0.000009	2.47E-14	94.4%	2.0006	15.79 ± 0.02	0%
au40.1b.adl.72a.txt	3.5	4.65349 ± 0.004226	1.61537 ± 0.001336	0.02032 ± 0.000149	0.00011 ± 0.000023	0.004811 ± 0.000040	2.94E-14	69.5%	2.0007	15.79 ± 0.06	0%
au40.1b.adl.73a.txt	3.5	9.45231 ± 0.022160	3.94832 ± 0.005956	0.04837 ± 0.000269	0.00021 ± 0.000028	0.005081 ± 0.000045	5.98E-14	84.1%	2.0137	15.90 ± 0.06	0%
au40.1b.adl.74a.txt	3.5	6.27363 ± 0.019046	2.71646 ± 0.005994	0.03318 ± 0.000193	0.00028 ± 0.000020	0.002768 ± 0.000042	3.97E-14	87.0%	2.0084	15.85 ± 0.08	0%
au40.1b.adl.75a.txt	3.5	4.57526 ± 0.018301	1.86988 ± 0.004195	0.02297 ± 0.000111	0.00012 ± 0.000023	0.002690 ± 0.000030	2.89E-14	82.6%	2.0217	15.96 ± 0.10	1%
au40.1b.adl.76a.txt	3.5	4.71088 ± 0.016563	1.46873 ± 0.003582	0.01885 ± 0.000219	0.00010 ± 0.000017	0.005804 ± 0.000054	2.98E-14	63.6%	2.0398	16.10 ± 0.14	1%
au40.1b.adl.77a.txt	3.5	2.62142 ± 0.009611	1.12954 ± 0.003008	0.01369 ± 0.000107	0.00019 ± 0.000021	0.001168 ± 0.000022	1.66E-14	86.8%	2.0152	15.91 ± 0.09	1%
au40.1b.adl.78a.txt	3.5	5.44211 ± 0.018141	2.49963 ± 0.005876	0.03030 ± 0.000255	0.00017 ± 0.000028	0.001350 ± 0.000025	3.44E-14	92.7%	2.0175	15.93 ± 0.07	0%
au40.1b.adl.79a.txt	3.5	2.39557 ± 0.007625	1.04398 ± 0.002432	0.01309 ± 0.000118	0.00012 ± 0.000019	0.000941 ± 0.000017	1.51E-14	88.4%	2.0283	16.01 ± 0.08	1%
au40.1b.adl.80a.txt	3.5	4.32505 ± 0.014834	1.93371 ± 0.004621	0.02346 ± 0.000137	0.00015 ± 0.000026	0.001426 ± 0.000026	2.73E-14	90.3%	2.0188	15.94 ± 0.08	1%
au40.1b.adl.81a.txt	3.5	4.51579 ± 0.020953	1.84542 ± 0.005970	0.02266 ± 0.000141	0.00021 ± 0.000020	0.002734 ± 0.000029	2.85E-14	82.1%	2.0092	15.86 ± 0.12	1%
au40.1b.adl.82a.txt	3.5	4.09789 ± 0.019232	1.97698 ± 0.006382	0.02401 ± 0.000184	0.00012 ± 0.000023	0.000334 ± 0.000007	2.59E-14	97.6%	2.0229	15.97 ± 0.09	1%
au40.1b.adl.83a.txt	3.5	4.92985 ± 0.022778	2.26805 ± 0.006988	0.02749 ± 0.000183	0.00021 ± 0.000032	0.001274 ± 0.000024	3.12E-14	92.4%	2.0077	15.85 ± 0.10	1%
au40.1b.adl.84a.txt	3.5	2.23450 ± 0.008757	1.08309 ± 0.003864	0.01306 ± 0.000104	0.00005 ± 0.000022	0.000142 ± 0.000008	1.41E-14	98.1%	2.0243	15.98 ± 0.09	1%
au40.1b.adl.85a.txt	3.5	2.52226 ± 0.009849	1.04669 ± 0.002881	0.01293 ± 0.000106	0.00007 ± 0.000028	0.001384 ± 0.000033	1.59E-14	83.8%	2.0191	15.94 ± 0.12	1%
au40.1b.adl.86a.txt	3.5	4.16828 ± 0.014354	1.98120 ± 0.004598	0.02413 ± 0.000188	0.00007 ± 0.000019	0.000592 ± 0.000007	2.64E-14	95.8%	2.0156	15.91 ± 0.07	0%
au40.1b.adl.87a.txt	3.5	4.63924 ± 0.015531	2.17038 ± 0.004813	0.02626 ± 0.000168	0.00026 ± 0.000025	0.000940 ± 0.000022	2.93E-14	94.0%	2.0095	15.86 ± 0.07	0%
au40.1b.adl.88a.txt	3.5	3.24960 ± 0.012409	1.46715 ± 0.003968	0.01764 ± 0.000131	0.00010 ± 0.000020	0.001031 ± 0.000023	2.05E-14	90.6%	2.0072	15.84 ± 0.09	1%
au40.1b.adl.89a.txt	3.5	4.42068 ± 0.016588	1.58104 ± 0.003473	0.01975 ± 0.000172	0.00011 ± 0.000027	0.004126 ± 0.000043	2.79E-14	72.4%	2.0249	15.98 ± 0.12	1%
au40.1b.adl.90a.txt	3.5	3.05853 ± 0.010233	1.45693 ± 0.003909	0.01775 ± 0.000084	0.00411 ± 0.000050	0.000410 ± 0.000008	1.93E-14	96.0%	2.0164	15.92 ± 0.07	0%
au40.1b.adl.91a.txt	3.5	3.55034 ± 0.011709	1.57318 ± 0.002635	0.01904 ± 0.000140	0.00011 ± 0.000018	0.001349 ± 0.000030	2.24E-14	88.8%	2.0034	15.82 ± 0.08	1%
au40.1b.adl.92a.txt	3.5	5.89025 ± 0.017696	2.09818 ± 0.005648	0.02621 ± 0.000278	0.00011 ± 0.000018	0.005558 ± 0.000049	3.72E-14	72.1%	2.0245	15.98 ± 0.11	1%
au40.1b.adl.93a.txt	3.5	2.34127 ± 0.008633	0.97002 ± 0.003191	0.01197 ± 0.000079	0.00006 ± 0.000018	0.001306 ± 0.000024	1.48E-14	83.5%	2.0157	15.91 ± 0.11	1%
au40.1b.adl.94a.txt	3.5	1.87818 ± 0.007135	0.84103 ± 0.002586	0.01026 ± 0.000095	0.00005 ± 0.000020	0.000549 ± 0.000018	1.19E-14	91.4%	2.0401	16.10 ± 0.10	1%
au40.1b.adl.95a.txt	3.5	2.21670 ± 0.009026	1.08544 ± 0.003140	0.01325 ± 0.000090	0.00005 ± 0.000025	0.000073 ± 0.000012	1.40E-14	99.0%	2.0223	15.96 ± 0.08	1%
au40.1c.adl.96a.txt	3.5	1.52667 ± 0.005854	0.70490 ± 0.001742	0.00846 ± 0.000074	0.00007 ± 0.000024	0.000337 ± 0.000008	9.65E-15	93.5%	2.0245	15.98 ± 0.08	1%
au40.1c.adl.96b.txt	3.5	1.02824 ± 0.003995	0.50639 ± 0.001358	0.00614 ± 0.000061	0.00011 ± 0.000024	0.000025 ± 0.000010	6.50E-15	99.3%	2.0160	15.91 ± 0.09	1%
au40.1c.adl.97a.txt	3.5	3.34894 ± 0.013505	1.45341 ± 0.003363	0.01784 ± 0.000103	0.00013 ± 0.000015	0.001368 ± 0.000014	2.12E-14	87.9%	2.0260	15.99 ± 0.09	1%
au40.1c.adl.98a.txt	3.5	2.65208 ± 0.010118	1.25683 ± 0.002839	0.01534 ± 0.000104	0.00009 ± 0.000022	0.000398 ± 0.000009	1.68E-14	95.6%	2.0165	15.92 ± 0.08	0%
au40.1c.adl.99a.txt	3.5	1.56873 ± 0.005149	0.68947 ± 0.002158	0.00850 ± 0.000121	0.00022 ± 0.000024	0.000564 ± 0.000010	9.92E-15	89.4%	2.0336	16.05 ± 0.09	1%
au40.1c.adl.101a.txt	3.5	1.05813 ± 0.003820	0.42149 ± 0.000959	0.00518 ± 0.000055	0.00006 ± 0.000015	0.000640 ± 0.000013	6.69E-15	82.1%	2.0615	16.27 ± 0.11	1%
au40.1c.adl.102a.txt	3.5	1.85033 ± 0.005236	0.89155 ± 0.001983	0.01072 ± 0.000119	0.00012 ± 0.000028	0.000203 ± 0.000007	1.17E-14	96.8%	2.0081	15.85 ± 0.06	0%
au40.1c.adl.104a.txt	3.5	3.16693 ± 0.010806	1.29226 ± 0.002869	0.01597 ± 0.000177	0.00025 ± 0.000022	0.001927 ± 0.000026	2.00E-14	82.0%	2.0101	15.87 ± 0.09	1%
au40.1c.adl.105a.txt	3.5	1.22347 ± 0.003627	0.57056 ± 0.001364	0.00689 ± 0.000080	0.00005 ± 0.000025	0.000275 ± 0.000007	7.73E-15	93.4%	2.0020	15.80 ± 0.07	0%
au40.1c.adl.106a.txt	3.5	0.87406 ± 0.003535	0.32110 ± 0.001124	0.00413 ± 0.000080	0.00006 ± 0.000019	0.000749 ± 0.000018	5.53E-15	74.7%	2.0329	16.05 ± 0.17	1%
au40.1c.adl.107a.txt	3.5	0.74113 ± 0.002975	0.35391 ± 0.001651	0.00435 ± 0.000049	0.00006 ± 0.000021	0.000075 ± 0.000010	4.69E-15	97.0%	2.0311	16.03 ± 0.12	1%
au40.1c.adl.108a.txt	3.5	0.86840 ± 0.003414	0.40890 ± 0.000970	0.00479 ± 0.000078	0.00001 ± 0.000024	0.000147 ± 0.000006	5.49E-15	95.0%	2.0173	15.92 ± 0.08	1%
au40.1c.adl.109a.txt	3.5	0.95518 ± 0.003285	0.44820 ± 0.001145	0.00538 ± 0.000058	0.00006 ± 0.000014	0.000174 ± 0.000007	6.04E-15	94.6%	2.0164	15.92 ± 0.08	1%
au40.1c.adl.110a.txt	3.5	0.93498 ± 0.003466	0.36352 ± 0.001304	0.00417 ± 0.000059	0.00009 ± 0.000030	0.000664 ± 0.000018	5.91E-15	79.0%	2.0326	16.04 ± 0.16	1%
	The following data were excluded from presentation and considered to not represent adularia.										
au40.1c.adl.103a.txt	3.5	3.80853 ± 0.011636	0.48739 ± 0.000409	0.00575 ± 0.000094	0.00091 ± 0.000033	0.000094 ± 0.000006	2.41E-14	99.3%	7.7572	60.49 ± 0.20	0%

Sample ID/Increment Info	P	t	40Ar(*+atm)	39ArK	38Ar(Atm+Cl)	37ArCa	36Ar(Atm)	Moles 40Ar*	% Rad.	R	Age (Ma)	% s.d.
JMA-002, IH Analyses	J-Value=0.004331±0.000012											
au40.2f.adl.45a.txt	0.6	30	0.12292 ± 0.000388	0.02141 ± 0.000086	0.00034 ± 0.000016	0.00149 ± 0.000031	0.000308 ± 0.000014	7.77E-16	25.9%	1.4917	11.79 ± 1.58	13%
au40.2f.adl.45b.txt	0.8	30	0.03101 ± 0.000258	0.01307 ± 0.000103	0.00015 ± 0.000009	0.00012 ± 0.000012	0.000012 ± 0.000009	1.96E-16	88.5%	2.0999	16.64 ± 1.64	10%
au40.2f.adl.45c.txt	1	30	0.07318 ± 0.000356	0.03358 ± 0.000142	0.00039 ± 0.000012	0.00023 ± 0.000018	0.000007 ± 0.000010	4.63E-16	97.2%	2.1181	16.78 ± 0.69	4%
au40.2f.adl.45d.txt	1.2	30	0.10829 ± 0.000484	0.05087 ± 0.000295	0.00060 ± 0.000014	0.00014 ± 0.000016	-0.000002 ± 0.000009	6.85E-16	100.6%	2.1291	16.87 ± 0.45	3%
au40.2f.adl.45e.txt	1.5	30	0.19606 ± 0.000434	0.08878 ± 0.000294	0.00103 ± 0.000020	0.00011 ± 0.000012	0.000019 ± 0.000008	1.24E-15	97.2%	2.1462	16.94 ± 0.22	1%
au40.2f.adl.45f.txt	1.8	30	0.37087 ± 0.000836	0.17420 ± 0.000558	0.00208 ± 0.000020	0.00003 ± 0.000017	-0.000009 ± 0.000008	2.34E-15	100.7%	2.1290	16.80 ± 0.12	1%
au40.2f.adl.45g.txt	2.1	30	0.63814 ± 0.001805	0.29710 ± 0.000923	0.00359 ± 0.000025	0.00003 ± 0.000015	0.000048 ± 0.000009	4.03E-15	97.8%	2.0999	16.57 ± 0.10	1%
au40.2f.adl.45h.txt	2.5	30	1.06978 ± 0.001661	0.50150 ± 0.000822	0.00581 ± 0.000050	0.00000 ± 0.000012	0.000038 ± 0.000009	6.76E-15	98.9%	2.1107	16.66 ± 0.06	0%
au40.2f.adl.45i.txt	2.9	30	0.10677 ± 0.000384	0.04413 ± 0.000223	0.00052 ± 0.000018	-0.00001 ± 0.000019	0.000057 ± 0.000006	6.75E-16	84.2%	2.0382	16.09 ± 0.35	2%
au40.2f.adl.45j.txt	3	30	0.02498 ± 0.000143	0.00803 ± 0.000070	0.00010 ± 0.000016	0.00003 ± 0.000018	0.000030 ± 0.000010	1.58E-16	64.9%	2.0196	15.94 ± 2.87	18%

Sample ID/Increment Info	P	t	40Ar(*+atm)	39ArK	38Ar(Atm+Cl)	37ArCa	36Ar(Atm)	Moles 40Ar*	% Rad.	R	Age (Ma)	% s.d.
JMA-002, IH Analyses	J-Value=0.004331±0.000012											
au40.2f.adl.46a.txt	0.6	30	0.05592 ± 0.000293	0.01150 ± 0.000065	0.00016 ± 0.000008	0.00036 ± 0.000013	0.000094 ± 0.000006	3.53E-16	50.2%	2.4417	19.26 ± 1.26	7%
au40.2f.adl.46b.txt	0.8	30	0.02434 ± 0.000208	0.01035 ± 0.000095	0.00012 ± 0.000013	0.00013 ± 0.000024	0.000019 ± 0.000005	1.54E-16	77.5%	1.8226	14.39 ± 1.19	8%
au40.2f.adl.46c.txt	1	30	0.07342 ± 0.000345	0.03376 ± 0.000180	0.00038 ± 0.000010	0.00010 ± 0.000008	0.000010 ± 0.000004	4.64E-16	95.8%	2.0839	16.51 ± 0.31	2%
au40.2f.adl.46d.txt	1.2	30	0.13131 ± 0.000332	0.05944 ± 0.000357	0.00067 ± 0.000018	0.00008 ± 0.000018	0.000025 ± 0.000004	8.30E-16	94.4%	2.0849	16.52 ± 0.19	1%
au40.2f.adl.46e.txt	1.5	30	0.20496 ± 0.000501	0.09678 ± 0.000292	0.00111 ± 0.000014	0.00004 ± 0.000016	0.000008 ± 0.000003	1.30E-15	98.9%	2.0942	16.59 ± 0.11	1%
au40.2f.adl.46f.txt	1.8	30	0.35671 ± 0.001006	0.16956 ± 0.000432	0.00198 ± 0.000022	0.00006 ± 0.000018	0.000013 ± 0.000006	2.25E-15	98.9%	2.0816	16.43 ± 0.10	1%
au40.2f.adl.46g.txt	2	30	0.38007 ± 0.001316	0.17977 ± 0.000408	0.00213 ± 0.000033	-0.00001 ± 0.000015	0.000024 ± 0.000009	2.40E-15	98.1%	2.0749	16.44 ± 0.14	1%
au40.2f.adl.46h.txt	2.25	30	0.45749 ± 0.001385	0.21736 ± 0.000643	0.00273 ± 0.000048	-0.00002 ± 0.000019	0.000017 ± 0.000008	2.89E-15	98.9%	2.0812	16.49 ± 0.11	1%
au40.2f.adl.46i.txt	2.5	30	0.99805 ± 0.001813	0.46822 ± 0.000931	0.00547 ± 0.000033	0.00005 ± 0.000007	0.000062 ± 0.000005	6.31E-15	98.2%	2.0926	16.52 ± 0.05	0%
au40.2f.adl.46j.txt	2.9	30	0.19037 ± 0.000267	0.08895 ± 0.000327	0.00107 ± 0.000016	0.00005 ± 0.000019	0.000020 ± 0.000010	1.20E-15	97.0%	2.0755	16.45 ± 0.27	2%
au40.2f.adl.46k.txt	3	30	0.01979 ± 0.000203	0.00858 ± 0.000111	0.00011 ± 0.000011	0.00003 ± 0.000008	0.000001 ± 0.000005	1.25E-16	98.7%	2.2748	17.95 ± 1.44	8%

Sample ID/Increment Info	P	t	40Ar(*+atm)	39ArK	38Ar(Atm+Cl)	37ArCa	36Ar(Atm)	Moles 40Ar*	% Rad.	R	Age (Ma)	% s.d.
JMA-002, IH Analyses	J-Value=0.004331±0.000012											
au40.2f.adl.47a.txt	0.6	30	0.04336 ± 0.000244	0.01560 ± 0.000092	0.00021 ± 0.000012	0.00021 ± 0.000022	0.000062 ± 0.000006	2.74E-16	58.0%	1.6145	12.76 ± 0.90	7%
au40.2f.adl.47b.txt	0.8	30	0.05848 ± 0.000408	0.02393 ± 0.000105	0.00028 ± 0.000016	0.00010 ± 0.000014	0.000012 ± 0.000005	3.70E-16	93.7%	2.2904	18.07 ± 0.56	3%
au40.2f.adl.47c.txt	1	30	0.14732 ± 0.000483	0.06812 ± 0.000179	0.00078 ± 0.000017	0.00011 ± 0.000018	-0.000011 ± 0.000009	9.31E-16	102.1%	2.1627	17.07 ± 0.30	2%
au40.2f.adl.47d.txt	1.2	30	0.20663 ± 0.000285	0.09730 ± 0.000294	0.00113 ± 0.000014	0.00009 ± 0.000012	0.000013 ± 0.000006	1.31E-15	98.2%	2.0855	16.46 ± 0.16	1%
au40.2f.adl.47a.txt	1.5	30	1.85180 ± 0.004314	0.86392 ± 0.001591	0.01041 ± 0.000081	0.00063 ± 0.000021	0.000089 ± 0.000006	1.17E-14	98.6%	2.1131	16.68 ± 0.05	0%
au40.2f.adl.47b.txt	1.8	30	0.47271 ± 0.001321	0.22595 ± 0.000406	0.00262 ± 0.000036	0.00000 ± 0.000016	0.000007 ± 0.000010	2.99E-15	99.6%	2.0833	16.51 ± 0.12	1%
au40.2f.adl.47c.txt	2	30	0.87477 ± 0.001953	0.40834 ± 0.000825	0.00502 ± 0.000059	0.00000 ± 0.000013	0.000062 ± 0.000011	5.53E-15	97.9%	2.0971	16.62 ± 0.08	1%
au40.2f.adl.47d.txt	2.25	30	1.55988 ± 0.004148	0.74427 ± 0.001389	0.00899 ± 0.000082	0.00002 ± 0.000010	0.000030 ± 0.000009	9.86E-15	99.4%	2.0839	16.51 ± 0.06	0%
au40.2f.adl.47e.txt	2.5	30	2.74825 ± 0.007516	1.30926 ± 0.001982	0.01580 ± 0.000091	-0.00001 ± 0.000015	0.000012 ± 0.000012	1.74E-14	99.9%	2.0963	16.61 ± 0.06	0%
au40.2f.adl.47f.txt	2.9	30	1.39005 ± 0.003080	0.65976 ± 0.001031	0.00790 ± 0.000045	-0.00004 ± 0.000016	0.000001 ± 0.000012	8.79E-15	100.0%	2.1063	16.69 ± 0.06	0%
au40.2f.adl.47g.txt	3	30	0.33507 ± 0.000746	0.15878 ± 0.000327	0.00194 ± 0.000041	0.00000 ± 0.000013	0.000017 ± 0.000009	2.12E-15	98.5%	2.0778	16.46 ± 0.14	1%

Sample ID/Increment Info	P	t	40Ar(*+atm)	39ArK	38Ar(Atm+Cl)	37ArCa	36Ar(Atm)	Moles 40Ar*	% Rad.	R	Age (Ma)	% s.d.
JMA-002, IH Analyses	J-Value=0.004331±0.000012											
au40.2f.adl.48a.txt	0.6	30	0.00213 ± 0.000126	0.00011 ± 0.000068	0.00001 ± 0.000010	0.00013 ± 0.000013	0.000009 ± 0.000006	1.35E-17	-28.5%	-5.2193	-41.85 -± 187.89	449%
au40.2f.adl.48b.txt	0.8	30	0.02582 ± 0.000219	0.00956 ± 0.000092	0.00011 ± 0.000009	0.00015 ± 0.000014	0.000014 ± 0.000005	1.63E-16	83.6%	2.2585	17.82 ± 1.36	8%
au40.2f.adl.48c.txt	1	30	0.05852 ± 0.000243	0.02588 ± 0.000104	0.00029 ± 0.000014	0.00010 ± 0.000019	0.000010 ± 0.000005	3.70E-16	94.7%	2.1423	16.91 ± 0.48	3%
au40.2f.adl.48d.txt	1.2	30	0.11839 ± 0.000456	0.05561 ± 0.000283	0.00064 ± 0.000023	0.00009 ± 0.000013	-0.000012 ± 0.000009	7.48E-16	102.9%	2.1288	16.80 ± 0.39	2%
au40.2f.adl.48e.txt	1.5	30	0.33425 ± 0.000901	0.15917 ± 0.000223	0.00184 ± 0.000025	0.00006 ± 0.000019	-0.000001 ± 0.000008	2.11E-15	100.1%	2.1000	16.57 ± 0.13	1%
au40.2f.adl.48f.txt	1.8	30	0.92089 ± 0.001738	0.43888 ± 0.000704	0.00517 ± 0.000038	0.00004 ± 0.000008	-0.000002 ± 0.000009	5.82E-15	100.1%	2.0983	16.56 ± 0.06	0%
au40.2f.adl.48g.txt	2	30	1.75009 ± 0.003233	0.83252 ± 0.001166	0.00976 ± 0.000095	0.00007 ± 0.000012	-0.000007 ± 0.000009	1.11E-14	100.1%	2.1022	16.59 ± 0.05	0%
au40.2f.adl.48h.txt	2.25	30	0.73977 ± 0.001727	0.35189 ± 0.000497	0.00425 ± 0.000033	-0.00002 ± 0.000010	-0.000003 ± 0.000008	4.68E-15	100.1%	2.1023	16.66 ± 0.07	0%
au40.2f.adl.48i.txt	2.55	30	0.08000 ± 0.000378	0.03781 ± 0.000163	0.00044 ± 0.000014	0.00000 ± 0.000012	0.000016 ± 0.000006	5.06E-16	93.9%	1.9876	15.75 ± 0.36	2%
au40.2f.adl.48j.txt	2.9	30	0.01960 ± 0.000137	0.00847 ± 0.000129	0.00012 ± 0.000010	-0.00001 ± 0.000022	0.000001 ± 0.000005	1.24E-16	98.1%	2.2690	17.90 ± 1.41	8%
au40.2f.adl.48k.txt	3	30	0.00606 ± 0.000127	0.00192 ± 0.000084	0.00003 ± 0.000009	0.00005 ± 0.000018	0.000008 ± 0.000005	3.83E-17	61.8%	1.9509	15.40 ± 6.70	43%

Sample ID/Increment Info	P	t	40Ar(*+atm)	39ArK	38Ar(Atm+Cl)	37ArCa	36Ar(Atm)	Moles 40Ar*	% Rad.	R	Age (Ma)	% s.d.
JMA-002, IH Analyses	J-Value=0.004331±0.000012											
au40.2f.adl.49a.txt	0.6	30	0.00688 ± 0.000136	0.00084 ± 0.000084	0.00002 ± 0.000012	0.00008 ± 0.000018	0.000018 ± 0.000005	4.35E-17	21.7%	1.7925	14.16 ± 16.28	115%
au40.2f.adl.49b.txt	0.8	30	0.01623 ± 0.000188	0.00637 ± 0.000062	0.00008 ± 0.000012	0.00003 ± 0.000014	0.000010 ± 0.000006	1.03E-16	81.4%	2.0724	16.42 ± 2.34	14%
au40.2f.adl.49c.txt	1	30	0.03728 ± 0.000255	0.01661 ± 0.000130	0.00019 ± 0.000009	0.00007 ± 0.000012	0.000007 ± 0.000006	2.36E-16	94.4%	2.1199	16.73 ± 0.81	5%
au40.2f.adl.49d.txt	1.2	30	0.06535 ± 0.000431	0.03048 ± 0.000174	0.00035 ± 0.000011	0.00005 ± 0.000017	0.000001 ± 0.000005	4.13E-16	99.5%	2.1329	16.83 ± 0.44	3%
au40.2f.adl.49e.txt	1.5	30	0.16549 ± 0.000241	0.07810 ± 0.000215	0.00094 ± 0.000019	0.00002 ± 0.000018	0.000013 ± 0.000007	1.05E-15	97.7%	2.0693	16.40 ± 0.20	1%
au40.2f.adl.49f.txt	1.8	30	0.24466 ± 0.000574	0.11622 ± 0.000236	0.00139 ± 0.000018	0.00008 ± 0.000011	0.000006 ± 0.000005	1.55E-15	99.3%	2.0898	16.49 ± 0.12	1%
au40.2f.adl.49g.txt	2	30	0.39344 ± 0.001111	0.18743 ± 0.000479	0.00222 ± 0.000028	0.00004 ± 0.000022	-0.000005 ± 0.000008	2.49E-15	100.4%	2.0991	16.57 ± 0.12	1%
au40.2f.adl.49h.txt	2.25	30	1.29508 ± 0.002512	0.61532 ± 0.001252	0.00748 ± 0.000110	0.00007 ± 0.000019	0.000003 ± 0.000010	8.19E-15	99.9%	2.1031	16.60 ± 0.06	0%
au40.2f.adl.49i.txt	2.55	30	0.14366 ± 0.000599	0.06826 ± 0.000322	0.00078 ± 0.000022	-0.00001 ± 0.000011	0.000006 ± 0.000005	9.08E-16	98.8%	2.0787	16.47 ± 0.19	1%
au40.2f.adl.49j.txt	2.9	30	0.06802 ± 0.000341	0.03138 ± 0.000131	0.00038 ± 0.000013	0.00004 ± 0.000012	0.000004 ± 0.000005	4.30E-16	98.5%	2.1339	16.84 ± 0.42	3%
au40.2f.adl.49k.txt	3	30	0.05568 ± 0.000280	0.02562 ± 0.000136	0.00031 ± 0.000010	0.00004 ± 0.000016	0.000003 ± 0.000006	3.52E-16	98.3%	2.1377	16.87 ± 0.58	3%

Sample ID/Increment Info	P	t	40Ar(*+atm)	39ArK	38Ar(Atm+Cl)	37ArCa	36Ar(Atm)	Moles 40Ar*	% Rad.	R	Age (Ma)	% s.d.
JMA-002, IH Analyses	J-Value=0.004331±0.000012											
au40.2f.adl.50a.txt	0.6	30	0.00391 ± 0.000129	0.00180 ± 0.000061	0.00003 ± 0.000010	0.00006 ± 0.000018	-0.000016 ± 0.000007	2.47E-17	224.1%	2.1736	17.15 ± 9.10	53%
au40.2f.adl.50b.txt	0.8	30	0.02607 ± 0.000167	0.01247 ± 0.000072	0.00013 ± 0.000012	-0.00001 ± 0.000013	-0.000025 ± 0.000008	1.65E-16	128.1%	2.0898	16.49 ± 1.54	9%
au40.2f.adl.50c.txt	1	30	0.04331 ± 0.000220	0.02035 ± 0.000141	0.00024 ± 0.000009	0.00006 ± 0.000016	-0.000006 ± 0.000005	2.74E-16	103.8%	2.1286	16.80 ± 0.61	4%
au40.2f.adl.50d.txt	1.2	30	0.18927 ± 0.000303	0.09032 ± 0.000213	0.00105 ± 0.000014	0.00007 ± 0.000013	-0.000011 ± 0.000008	1.20E-15	101.8%	2.0956	16.54 ± 0.22	1%
au40.2f.adl.50e.txt	1.4	30	0.39562 ± 0.000856	0.18871 ± 0.000766	0.00222 ± 0.000032	0.00008 ± 0.000012	-0.000021 ± 0.000009	2.50E-15	101.6%	2.0964	16.55 ± 0.13	1%
au40.2f.adl.50f.txt	1.6	30	0.25481 ± 0.000645	0.12157 ± 0.000488	0.00145 ± 0.000021	0.00013 ± 0.000013	-0.000012 ± 0.000008	1.61E-15	101.4%	2.0961	16.54 ± 0.17	1%
au40.2f.adl.50g.txt	1.8	30	0.23157 ± 0.000410	0.11086 ± 0.000367	0.00132 ± 0.000020	0.00005 ± 0.000013	-0.000017 ± 0.000007	1.46E-15	102.2%	2.0890	16.49 ± 0.16	1%
au40.2f.adl.50h.txt	2	30	0.29555 ± 0.000540	0.14081 ± 0.000379	0.00161 ± 0.000016	0.00006 ± 0.000013	-0.000019 ± 0.000009	1.87E-15	101.9%	2.0989	16.57 ± 0.16	1%
au40.2f.adl.50i.txt	2.1	30	0.22796 ± 0.000269	0.10917 ± 0.000238	0.00129 ± 0.000020	0.00004 ± 0.000012	-0.000003 ± 0.000009	1.44E-15	100.4%	2.0880	16.48 ± 0.19	1%
au40.2f.adl.50j.txt	2.2	30	0.21318 ± 0.000377	0.10226 ± 0.000291	0.00119 ± 0.000024	0.00006 ± 0.000017	-0.000015 ± 0.000008	1.35E-15	102.0%	2.0847	16.45 ± 0.20	1%
au40.2f.adl.50k.txt	2.3	30	0.19196 ± 0.000298	0.09151 ± 0.000379	0.00114 ± 0.000032	0.00002 ± 0.000011	-0.000016 ± 0.000010	1.21E-15	102.5%	2.0978	16.56 ± 0.26	2%
au40.2f.adl.50l.txt	2.4	30	0.23282 ± 0.000226	0.11077 ± 0.000279	0.00127 ± 0.000025	0.00004 ± 0.000012	-0.000002 ± 0.000005	1.47E-15	100.2%	2.1018	16.59 ± 0.12	1%
au40.2f.adl.50m.txt	2.5	30	0.19990 ± 0.000380	0.09515 ± 0.000248	0.00112 ± 0.000018	0.00000 ± 0.000024	0.000005 ± 0.000006	1.26E-15	99.2%	2.0847	16.45 ± 0.15	1%
au40.2f.adl.50n.txt	2.65	30	0.28866 ± 0.000604	0.13724 ± 0.000290	0.00162 ± 0.000020	0.00007 ± 0.000015	-0.000007 ± 0.000009	1.82E-15	100.7%	2.1034	16.60 ± 0.16	1%
au40.2f.adl.50o.txt	2.8	30	0.38194 ± 0.001049	0.18236 ± 0.000416	0.00214 ± 0.000024	0.00004 ± 0.000010	-0.000018 ± 0.000010	2.41E-15	101.4%	2.0944	16.53 ± 0.14	1%
au40.2f.adl.50p.txt	2.9	30	0.33361 ± 0.000806	0.15940 ± 0.000296	0.00189 ± 0.000029	0.00004 ± 0.000020	0.000003 ± 0.000008	2.11E-15	99.7%	2.0876	16.48 ± 0.13	1%
au40.2f.adl.50q.txt	3	30	0.21173 ± 0.000344	0.10051 ± 0.000233	0.00115 ± 0.000018	0.00005 ± 0.000020	0.000006 ± 0.000005	1.34E-15	99.2%	2.0901	16.50 ± 0.13	1%

Sample ID/Increment Info	P	t	40Ar(*+atm)	39ArK	38Ar(Atm+Cl)	37ArCa	36Ar(Atm)	Moles 40Ar*	% Rad.	R	Age (Ma)	% s.d.
TDGA-001, IH Analyses	J-Value=0.0043191±0.0000051											
au40.1b.adl.66a.txt	0.6	30	0.17610 ± 0.000818	0.08271 ± 0.000329	0.00102 ± 0.000032	0.00003 ± 0.000014	0.000012 ± 0.000011	1.11E-15	98.0%	2.0856	16.46 ± 0.33	2%
au40.1b.adl.66b.txt	0.8	30	1.35451 ± 0.003654	0.57811 ± 0.001419	0.00710 ± 0.000097	0.00006 ± 0.000014	0.000677 ± 0.000019	8.56E-15	85.2%	1.9969	15.76 ± 0.10	1%
au40.1b.adl.66c.txt	1	30	2.55243 ± 0.007704	1.16690 ± 0.002517	0.01420 ± 0.000115	0.00011 ± 0.000027	0.000746 ± 0.000015	1.61E-14	91.4%	1.9984	15.78 ± 0.07	0%
au40.1b.adl.66d.txt	1.2	30	0.41960 ± 0.001256	0.15656 ± 0.000341	0.00205 ± 0.000057	-0.00003 ± 0.000020	0.000345 ± 0.000018	2.65E-15	75.7%	2.0282	16.01 ± 0.29	2%
au40.1b.adl.66e.txt	1.4	30	0.66233 ± 0.002278	0.28008 ± 0.000901	0.00336 ± 0.000095	-0.00001 ± 0.000024	0.000323 ± 0.000014	4.19E-15	85.6%	2.0243	15.98 ± 0.15	1%
au40.1b.adl.66f.txt	1.6	30	2.76695 ± 0.007317	1.31498 ± 0.002354	0.01609 ± 0.000122	0.00013 ± 0.000013	0.000440 ± 0.000008	1.75E-14	95.3%	2.0054	15.83 ± 0.05	0%
au40.1b.adl.66g.txt	1.8	30	1.37069 ± 0.005943	0.64932 ± 0.001897	0.00779 ± 0.000114	0.00004 ± 0.000029	0.000216 ± 0.000008	8.66E-15	95.3%	2.0125	15.89 ± 0.09	1%
au40.1b.adl.66h.txt	2	30	0.59015 ± 0.002386	0.28115 ± 0.000909	0.00340 ± 0.000046	0.00008 ± 0.000021	0.000083 ± 0.000006	3.73E-15	95.9%	2.0120	15.88 ± 0.10	1%
au40.1b.adl.66i.txt	2.25	30	0.60640 ± 0.002426	0.28258 ± 0.001106	0.00349 ± 0.000062	0.00002 ± 0.000017	0.000125 ± 0.000007	3.83E-15	93.9%	2.0150	15.91 ± 0.11	1%
au40.1b.adl.66j.txt	2.5	30	0.13811 ± 0.000713	0.06529 ± 0.000396	0.00072 ± 0.000017	0.00000 ± 0.000026	0.000023 ± 0.000006	8.73E-16	95.0%	2.0096	15.86 ± 0.25	2%
au40.1b.adl.66k.txt	2.8	30	0.14753 ± 0.000388	0.07085 ± 0.000325	0.00079 ± 0.000018	0.00004 ± 0.000021	-0.000004 ± 0.000009	9.33E-16	100.9%	2.0823	16.43 ± 0.31	2%
au40.1b.adl.66l.txt	3.1	30	0.10136 ± 0.000335	0.04968 ± 0.000294	0.00065 ± 0.000028	-0.00005 ± 0.000030	0.000018 ± 0.000006	6.41E-16	94.7%	1.9329	15.26 ± 0.32	2%
au40.1b.adl.66m.txt	3.3	30	0.02613 ± 0.000198	0.01223 ± 0.000094	0.00013 ± 0.000011	0.00004 ± 0.000018	0.000012 ± 0.000005	1.65E-16	86.1%	1.8390	14.52 ± 1.02	7%
au40.1b.adl.66n.txt	3.4	30	0.02369 ± 0.000177	0.01115 ± 0.000155	0.00010 ± 0.000015	-0.00002 ± 0.000019	-0.000018 ± 0.000011	1.50E-16	122.8%	2.1231	16.76 ± 2.27	14%
au40.1b.adl.66o.txt	3.5	30	0.03256 ± 0.000292	0.01567 ± 0.000131	0.00020 ± 0.000017	-0.00004 ± 0.000023	0.000015 ± 0.000006	2.06E-16	86.0%	1.7874	14.12 ± 0.88	6%

Sample ID/Increment Info	P	t	40Ar(*+atm)	39ArK	38Ar(Atm+Cl)	37ArCa	36Ar(Atm)	Moles 40Ar*	% Rad.	R	Age (Ma)	% s.d.
TDGA-001, IH Analyses	J-Value=0.0043191±0.0000051											
au40.1b.adl.67a.txt	0.6	30	0.23840 ± 0.000715	0.11523 ± 0.000391	0.00139 ± 0.000037	0.00003 ± 0.000017	0.000014 ± 0.000005	1.51E-15	98.3%	2.0339	16.05 ± 0.13	1%
au40.1b.adl.67b.txt	0.7	30	0.49812 ± 0.002346	0.24825 ± 0.000902	0.00293 ± 0.000050	0.00010 ± 0.000025	-0.000007 ± 0.000011	3.15E-15	100.4%	2.0066	15.84 ± 0.14	1%
au40.1b.adl.67c.txt	0.8	30	1.33927 ± 0.005418	0.65805 ± 0.001755	0.00782 ± 0.000081	0.00009 ± 0.000018	0.000053 ± 0.000009	8.47E-15	98.8%	2.0116	15.88 ± 0.08	1%
au40.1b.adl.67d.txt	0.9	30	1.10524 ± 0.004458	0.54157 ± 0.001564	0.00652 ± 0.000130	0.00001 ± 0.000014	0.000066 ± 0.000005	6.99E-15	98.2%	2.0049	15.83 ± 0.08	1%
au40.1b.adl.67e.txt	1.05	30	0.14053 ± 0.000442	0.04985 ± 0.000284	0.00060 ± 0.000023	-0.00012 ± 0.000025	0.000112 ± 0.000008	8.88E-16	76.5%	2.1555	17.01 ± 0.39	2%
au40.1b.adl.67f.txt	1.2	30	0.05990 ± 0.000253	0.02906 ± 0.000157	0.00033 ± 0.000015	0.00002 ± 0.000015	0.000018 ± 0.000007	3.79E-16	91.1%	1.8771	14.82 ± 0.54	4%
au40.1b.adl.67g.txt	1.4	30	0.10304 ± 0.000356	0.05031 ± 0.000176	0.00057 ± 0.000016	0.00007 ± 0.000013	0.000006 ± 0.000007	6.51E-16	98.2%	2.0110	15.87 ± 0.31	2%
au40.1b.adl.67h.txt	1.6	30	0.81719 ± 0.002593	0.39636 ± 0.001426	0.00479 ± 0.000059	0.00007 ± 0.000017	0.000064 ± 0.000007	5.17E-15	97.7%	2.0137	15.90 ± 0.09	1%
au40.1b.adl.67i.txt	1.85	30	0.67099 ± 0.001761	0.32207 ± 0.001144	0.00377 ± 0.000075	0.00003 ± 0.000019	0.000060 ± 0.000011	4.24E-15	97.4%	2.0284	16.01 ± 0.11	1%
au40.1b.adl.67j.txt	2.1	30	0.32758 ± 0.000927	0.15865 ± 0.000565	0.00190 ± 0.000030	0.00003 ± 0.000025	0.000020 ± 0.000006	2.07E-15	98.2%	2.0277	16.01 ± 0.11	1%
au40.1b.adl.67k.txt	2.4	30	0.29697 ± 0.000996	0.14668 ± 0.000324	0.00161 ± 0.000032	0.00001 ± 0.000022	0.000014 ± 0.000005	1.88E-15	98.6%	1.9968	15.76 ± 0.10	1%
au40.1b.adl.67l.txt	2.7	30	0.13517 ± 0.000567	0.06583 ± 0.000326	0.00074 ± 0.000013	0.00000 ± 0.000019	-0.000009 ± 0.000008	8.55E-16	101.9%	2.0532	16.21 ± 0.29	2%

Au40.1b.adk.67.e.txt and au40.1b.adl.67f.txt were excluded from the discussion, as they were anomalously higher and lower (respectively) than the determined plateau ages. These releases are likely due to errors in measurement and blank correction as they comprise a very small fraction of the total $^{39}Ar_k$.

Sample ID/Increment Info	P	t	40Ar(*+atm)	39ArK	38Ar(Atm+Cl)	37ArCa	36Ar(Atm)	Moles 40Ar*	% Rad.	R	Age (Ma)	% s.d.
TDGA-001, IH Analyses	J-Value=0.0043191±0.0000051											
au40.1b.adl.113a.txt	0.6	30	0.28705 ± 0.000950	0.09829 ± 0.000381	0.00115 ± 0.000018	0.00008 ± 0.000024	0.000306 ± 0.000013	1.81E-15	68.5%	1.9998	15.79 ± 0.34	2%
au40.1b.adl.113b.txt	0.7	30	0.26044 ± 0.001380	0.12626 ± 0.000352	0.00146 ± 0.000024	0.00003 ± 0.000016	0.000029 ± 0.000008	1.65E-15	96.8%	1.9959	15.76 ± 0.17	1%
au40.1b.adl.113c.txt	0.8	30	0.47025 ± 0.001523	0.23281 ± 0.000828	0.00276 ± 0.000039	0.00001 ± 0.000023	0.000018 ± 0.000010	2.97E-15	98.9%	1.9970	15.76 ± 0.13	1%
au40.1b.adl.113d.txt	0.9	30	1.32296 ± 0.005014	0.64584 ± 0.001905	0.00785 ± 0.000095	0.00004 ± 0.000025	0.000083 ± 0.000012	8.36E-15	98.1%	2.0104	15.87 ± 0.09	1%
au40.1b.adl.113e.txt	1.05	30	0.66137 ± 0.002716	0.32207 ± 0.000817	0.00386 ± 0.000064	-0.00002 ± 0.000018	0.000053 ± 0.000009	4.18E-15	97.6%	2.0047	15.82 ± 0.10	1%
au40.1b.adl.113f.txt	1.2	30	0.13804 ± 0.000612	0.06631 ± 0.000352	0.00084 ± 0.000031	0.00005 ± 0.000015	0.000020 ± 0.000006	8.73E-16	95.7%	1.9931	15.73 ± 0.23	1%
au40.1b.adl.113g.txt	1.35	30	0.44027 ± 0.001526	0.21235 ± 0.000761	0.00234 ± 0.000040	0.00000 ± 0.000021	0.000040 ± 0.000006	2.78E-15	97.3%	2.0171	15.92 ± 0.10	1%
au40.1b.adl.113h.txt	1.5	30	0.33940 ± 0.001373	0.16358 ± 0.000299	0.00195 ± 0.000049	0.00002 ± 0.000025	0.000036 ± 0.000006	2.15E-15	96.8%	2.0089	15.86 ± 0.11	1%
au40.1b.adl.113i.txt	1.65	30	0.67687 ± 0.002661	0.32833 ± 0.000908	0.00396 ± 0.000074	0.00004 ± 0.000020	0.000047 ± 0.000005	4.28E-15	97.9%	2.0188	15.94 ± 0.09	1%
au40.1b.adl.113k.txt	2	30	0.42281 ± 0.001375	0.20590 ± 0.000868	0.00250 ± 0.000049	0.00002 ± 0.000024	0.000030 ± 0.000005	2.67E-15	97.9%	2.0111	15.88 ± 0.10	1%
au40.1b.adl.113l.txt	2.3	30	0.29338 ± 0.000623	0.14165 ± 0.000502	0.00171 ± 0.000042	0.00000 ± 0.000029	0.000030 ± 0.000006	1.85E-15	97.0%	2.0095	15.86 ± 0.13	1%
au40.1b.adl.113m.txt	2.6	30	0.09341 ± 0.000398	0.04593 ± 0.000276	0.00052 ± 0.000017	0.00004 ± 0.000024	0.000010 ± 0.000005	5.90E-16	96.8%	1.9691	15.55 ± 0.30	2%
au40.1b.adl.113n.txt	3	30	0.04967 ± 0.000322	0.02383 ± 0.000187	0.00027 ± 0.000013	0.00000 ± 0.000029	0.000010 ± 0.000006	3.14E-16	93.8%	1.9554	15.44 ± 0.66	4%
au40.1b.adl.113o.txt	3.5	30	0.13658 ± 0.000802	0.06684 ± 0.000176	0.00076 ± 0.000014	-0.00002 ± 0.000014	-0.000014 ± 0.000012	8.63E-16	103.0%	2.0434	16.13 ± 0.44	3%

Sample ID/Increment Info	P	t	40Ar(*+atm)	39ArK	38Ar(Atm+Cl)	37ArCa	36Ar(Atm)	Moles 40Ar*	% Rad.	R	Age (Ma)	% s.d.
TDGA-001, IH Analyses	J-Value=0.0043191±0.0000051											
au40.1b.adl.114a.txt	0.6	30	0.34139 ± 0.000629	0.07232 ± 0.000360	0.00095 ± 0.000022	0.00000 ± 0.000018	0.000619 ± 0.000011	2.16E-15	46.4%	2.1911	17.29 ± 0.40	2%
au40.1b.adl.114b.txt	0.7	30	0.38730 ± 0.001639	0.19082 ± 0.000817	0.00230 ± 0.000058	0.00000 ± 0.000027	0.000021 ± 0.000005	2.45E-15	98.4%	1.9971	15.77 ± 0.12	1%
au40.1b.adl.114c.txt	0.8	30	0.92430 ± 0.003479	0.45561 ± 0.001069	0.00558 ± 0.000083	-0.00001 ± 0.000014	0.000048 ± 0.000006	5.84E-15	98.5%	1.9979	15.77 ± 0.08	0%
au40.1b.adl.114d.txt	0.9	30	0.94431 ± 0.002890	0.46586 ± 0.001542	0.00567 ± 0.000087	0.00000 ± 0.000014	0.000030 ± 0.000006	5.97E-15	99.1%	2.0081	15.85 ± 0.08	0%
au40.1b.adl.114e.txt	1	30	0.77179 ± 0.002669	0.37340 ± 0.001430	0.00448 ± 0.000059	-0.00002 ± 0.000015	0.000056 ± 0.000006	4.88E-15	97.9%	2.0228	15.97 ± 0.09	1%
au40.1b.adl.114f.txt	1.1	30	0.12329 ± 0.000449	0.05825 ± 0.000168	0.00068 ± 0.000014	0.00003 ± 0.000021	0.000026 ± 0.000006	7.79E-16	93.9%	1.9870	15.69 ± 0.25	2%
au40.1b.adl.114g.txt	1.25	30	0.57071 ± 0.001570	0.28074 ± 0.000773	0.00340 ± 0.000067	-0.00005 ± 0.000013	0.000021 ± 0.000006	3.61E-15	98.9%	2.0103	15.87 ± 0.08	1%
au40.1b.adl.114h.txt	1.4	30	0.74908 ± 0.002398	0.36923 ± 0.000979	0.00454 ± 0.000049	0.00000 ± 0.000024	0.000029 ± 0.000006	4.74E-15	98.9%	2.0054	15.83 ± 0.08	0%
au40.1b.adl.114i.txt	1.6	30	0.60000 ± 0.001996	0.29554 ± 0.000605	0.00359 ± 0.000041	-0.00006 ± 0.000010	0.000025 ± 0.000006	3.79E-15	98.8%	2.0056	15.83 ± 0.08	0%
au40.1b.adl.114j.txt	1.8	30	0.43381 ± 0.001451	0.21228 ± 0.000546	0.00256 ± 0.000042	0.00004 ± 0.000023	0.000027 ± 0.000006	2.74E-15	98.2%	2.0058	15.83 ± 0.10	1%
au40.1b.adl.114k.txt	2	30	0.53460 ± 0.002492	0.26095 ± 0.000835	0.00301 ± 0.000032	0.00000 ± 0.000010	0.000039 ± 0.000006	3.38E-15	97.9%	2.0049	15.83 ± 0.11	1%
au40.1b.adl.114l.txt	2.3	30	0.23265 ± 0.001067	0.11377 ± 0.000435	0.00141 ± 0.000031	0.00001 ± 0.000019	0.000023 ± 0.000006	1.47E-15	97.1%	1.9856	15.67 ± 0.16	1%
au40.1b.adl.114m.txt	2.6	30	0.13070 ± 0.000671	0.06139 ± 0.000309	0.00069 ± 0.000022	-0.00003 ± 0.000013	0.000023 ± 0.000006	8.26E-16	94.7%	2.0160	15.91 ± 0.26	2%
au40.1b.adl.114n.txt	3	30	0.02499 ± 0.000202	0.01114 ± 0.000146	0.00013 ± 0.000015	0.00003 ± 0.000021	-0.000015 ± 0.000010	1.58E-16	117.2%	2.2429	17.70 ± 2.03	11%
au40.1b.adl.114o.txt	3.5	30	0.02235 ± 0.000211	0.01033 ± 0.000052	0.00013 ± 0.000014	0.00000 ± 0.000025	0.000014 ± 0.000006	1.41E-16	82.1%	1.7750	14.02 ± 1.30	9%

Sample ID/Increment Info	P	t	40Ar(*+atm)	39ArK	38Ar(Atm+Cl)	37ArCa	36Ar(Atm)	Moles 40Ar*	% Rad.	R	Age (Ma)	% s.d.
TDGA-001, IH Analyses	J-Value=0.0043191±0.0000051											
au40.1b.adl.115a.txt	0.6	30	5.64482 ± 0.019746	0.06589 ± 0.000188	0.00439 ± 0.000033	0.00019 ± 0.000031	0.018373 ± 0.000075	3.57E-14	3.8%	3.2707	25.75 ± 4.44	17%
au40.1b.adl.115b.txt	0.7	30	0.31111 ± 0.001354	0.13495 ± 0.000574	0.00167 ± 0.000034	0.00006 ± 0.000014	0.000128 ± 0.000007	1.97E-15	87.9%	2.0257	15.99 ± 0.16	1%
au40.1b.adl.115c.txt	0.8	30	0.54173 ± 0.002097	0.18390 ± 0.000406	0.00232 ± 0.000054	-0.00007 ± 0.000045	0.000579 ± 0.000020	3.42E-15	68.4%	2.0151	15.91 ± 0.27	2%
au40.1b.adl.115d.txt	0.9	30	0.61819 ± 0.001935	0.28168 ± 0.000951	0.00342 ± 0.000060	0.00000 ± 0.000025	0.000167 ± 0.000007	3.91E-15	92.0%	2.0200	15.95 ± 0.10	1%
au40.1b.adl.115e.txt	1	30	1.52725 ± 0.004584	0.69607 ± 0.001308	0.00845 ± 0.000070	0.00012 ± 0.000031	0.000342 ± 0.000008	9.65E-15	93.4%	2.0488	16.172 ± 0.07	0%
au40.1b.adl.115f.txt	1.1	30	0.82066 ± 0.002259	0.38740 ± 0.000770	0.00478 ± 0.000070	0.00003 ± 0.000022	0.000106 ± 0.000006	5.19E-15	96.2%	2.0376	16.084 ± 0.07	0%
au40.1b.adl.115g.txt	1.25	30	0.85562 ± 0.002340	0.39429 ± 0.000391	0.00475 ± 0.000067	0.00000 ± 0.000027	0.000203 ± 0.000008	5.41E-15	93.0%	2.0178	15.93 ± 0.07	0%
au40.1b.adl.115h.txt	1.4	30	2.16438 ± 0.007334	0.99696 ± 0.002551	0.01206 ± 0.000074	0.00002 ± 0.000020	0.000581 ± 0.000018	1.37E-14	92.1%	1.9988	15.78 ± 0.08	1%
au40.1b.adl.115i.txt	1.6	30	3.06668 ± 0.011943	1.34955 ± 0.003526	0.01637 ± 0.000137	0.00003 ± 0.000024	0.001148 ± 0.000024	1.94E-14	88.9%	2.0210	15.95 ± 0.09	1%
au40.1b.adl.115j.txt	1.8	30	1.95728 ± 0.007224	0.94723 ± 0.003156	0.01144 ± 0.000075	0.00001 ± 0.000021	0.000160 ± 0.000015	1.24E-14	97.6%	2.0165	15.92 ± 0.09	1%
au40.1b.adl.115k.txt	2	30	0.86469 ± 0.003747	0.42551 ± 0.001405	0.00510 ± 0.000066	-0.00001 ± 0.000020	0.000022 ± 0.000012	5.47E-15	99.3%	2.0169	15.92 ± 0.11	1%
au40.1b.adl.115l.txt	2.3	30	0.63971 ± 0.002108	0.31414 ± 0.001043	0.00373 ± 0.000044	0.00000 ± 0.000025	0.000007 ± 0.000010	4.04E-15	99.7%	2.0301	16.02 ± 0.11	1%
au40.1b.adl.115m.txt	2.6	30	0.27201 ± 0.001229	0.13299 ± 0.000546	0.00166 ± 0.000061	-0.00002 ± 0.000017	0.000002 ± 0.000011	1.72E-15	99.8%	2.0405	16.11 ± 0.22	1%
au40.1b.adl.115n.txt	3	30	0.34270 ± 0.000999	0.16521 ± 0.000516	0.00197 ± 0.000041	0.00000 ± 0.000021	0.000024 ± 0.000006	2.17E-15	97.9%	2.0310	16.03 ± 0.11	1%
au40.1b.adl.115o.txt	3.5	30	0.09570 ± 0.000445	0.04548 ± 0.000232	0.00050 ± 0.000017	-0.00003 ± 0.000025	0.000011 ± 0.000006	6.05E-16	96.6%	2.0322	16.04 ± 0.31	2%

Sample ID/Increment Info	P	t	40Ar(*+atm)	39ArK	38Ar(Atm+Cl)	37ArCa	36Ar(Atm)	Moles 40Ar*	% Rad.	R	Age (Ma)	% s.d.
TDGK-001, IH Analyses	J-Value=0.004331±0.000012											
au40.2i.ksp.3a.txt	0.4	30	0.00041 ± 0.000161	-0.00002 ± 0.000038	-0.00001 ± 0.000012	0.00005 ± 0.000026	0.000006 ± 0.000005	2.62E-18	-318.1%	56.3997	400.07 ± 1020.16	255%
au40.2i.ksp.3b.txt	0.5	30	0.05752 ± 0.000231	0.00452 ± 0.000043	0.00004 ± 0.000012	0.00003 ± 0.000020	-0.000009 ± 0.000009	3.64E-16	104.8%	12.7216	98.18 ± 4.65	5%
au40.2i.ksp.3c.txt	0.6	30	0.20969 ± 0.000615	0.07740 ± 0.000356	0.00087 ± 0.000018	0.00015 ± 0.000021	0.000020 ± 0.000006	1.33E-15	97.2%	2.6333	20.76 ± 0.21	1%
au40.2i.ksp.3d.txt	0.7	30	1.05627 ± 0.004800	0.23904 ± 0.001055	0.00296 ± 0.000064	0.00039 ± 0.000034	0.000101 ± 0.000011	6.68E-15	97.2%	4.2940	33.73 ± 0.24	1%
au40.2i.ksp.3e.txt	0.75	30	1.87464 ± 0.007615	0.36272 ± 0.001053	0.00431 ± 0.000094	0.00065 ± 0.000030	0.000064 ± 0.000006	1.19E-14	99.0%	5.1164	40.12 ± 0.21	1%
au40.2i.ksp.3a.txt	0.8	30	1.54328 ± 0.005189	0.23198 ± 0.001079	0.00279 ± 0.000064	0.00046 ± 0.000026	0.000052 ± 0.000006	9.76E-15	99.0%	6.5867	51.49 ± 0.31	1%
au40.2i.ksp.3b.txt	0.85	30	0.71558 ± 0.002615	0.10780 ± 0.000381	0.00123 ± 0.000025	0.00027 ± 0.000031	-0.000008 ± 0.000008	4.52E-15	100.4%	6.6381	51.89 ± 0.32	1%
au40.2i.ksp.3c.txt	0.9	30	2.89299 ± 0.010790	0.41953 ± 0.000949	0.00504 ± 0.000105	0.00071 ± 0.000017	0.000034 ± 0.000009	1.83E-14	99.6%	6.8718	53.69 ± 0.24	0%
au40.2i.ksp.3d.txt	0.95	30	1.84839 ± 0.005989	0.27102 ± 0.000631	0.00325 ± 0.000024	0.00037 ± 0.000020	0.000050 ± 0.000007	1.17E-14	99.2%	6.7655	52.87 ± 0.22	0%
au40.2i.ksp.3e.txt	1	30	2.04538 ± 0.006972	0.30432 ± 0.000827	0.00371 ± 0.000056	0.00048 ± 0.000038	0.000079 ± 0.000006	1.29E-14	98.9%	6.6450	51.94 ± 0.23	0%
au40.2i.ksp.3f.txt	1.1	30	3.70901 ± 0.012049	0.53906 ± 0.001279	0.00645 ± 0.000078	0.00093 ± 0.000048	0.000182 ± 0.000007	2.34E-14	98.6%	6.7810	52.99 ± 0.22	0%
au40.2i.ksp.3g.txt	1.2	30	2.52222 ± 0.008932	0.36048 ± 0.000855	0.00424 ± 0.000064	0.00058 ± 0.000035	0.000020 ± 0.000009	1.59E-14	99.8%	6.9803	54.52 ± 0.24	0%
au40.2i.ksp.3h.txt	1.3	30	1.84332 ± 0.005386	0.25668 ± 0.000855	0.00289 ± 0.000045	0.00032 ± 0.000024	0.000044 ± 0.000007	1.17E-14	99.3%	7.1302	55.67 ± 0.26	0%
au40.2i.ksp.3i.txt	1.45	30	0.55377 ± 0.001777	0.07856 ± 0.000360	0.00084 ± 0.000011	0.00010 ± 0.000020	-0.000018 ± 0.000009	3.50E-15	101.0%	7.0491	55.05 ± 0.40	1%
au40.2i.ksp.3j.txt	1.6	30	0.11095 ± 0.000306	0.01613 ± 0.000082	0.00017 ± 0.000013	0.00003 ± 0.000024	0.000003 ± 0.000006	7.01E-16	99.2%	6.8272	53.34 ± 0.85	2%
au40.2i.ksp.3k.txt	1.8	30	0.13462 ± 0.000774	0.01955 ± 0.000180	0.00020 ± 0.000011	0.00004 ± 0.000020	0.000013 ± 0.000006	8.51E-16	97.2%	6.6909	52.29 ± 0.88	2%

Sample ID/Increment Info	P	t	40Ar(*+atm)	39ArK	38Ar(Atm+Cl)	37ArCa	36Ar(Atm)	Moles 40Ar*	% Rad.	R	Age (Ma)	% s.d.
TDGK-001, IH Analyses	J-Value=0.004331±0.000012											
au40.2i.ksp.5a.txt	0.4	30	0.01037 ± 0.000165	0.00149 ± 0.000079	-0.00005 ± 0.000018	-0.00004 ± 0.000021	0.000019 ± 0.000008	6.56E-17	47.3%	3.2824	25.84 ± 13.29	51%
au40.2i.ksp.5b.txt	0.45	30	0.00887 ± 0.000152	0.00354 ± 0.000040	0.00003 ± 0.000013	0.00003 ± 0.000022	0.000003 ± 0.000010	5.61E-17	91.0%	2.2798	17.99 ± 6.50	36%
au40.2i.ksp.5c.txt	0.5	30	0.04172 ± 0.000376	0.01765 ± 0.000058	0.00019 ± 0.000012	0.00010 ± 0.000031	0.000016 ± 0.000005	2.64E-16	88.3%	2.0886	16.48 ± 0.70	4%
au40.2i.ksp.5d.txt	0.55	30	0.15444 ± 0.000557	0.04852 ± 0.000204	0.00053 ± 0.000012	0.00016 ± 0.000028	0.000042 ± 0.000008	9.76E-16	91.9%	2.9263	23.05 ± 0.41	2%
au40.2i.ksp.5e.txt	0.6	30	0.16039 ± 0.000223	0.04857 ± 0.000204	0.00059 ± 0.000020	0.00020 ± 0.000018	0.000041 ± 0.000010	1.01E-15	92.4%	3.0522	24.04 ± 0.51	2%
au40.2i.ksp.5f.txt	0.65	30	0.11090 ± 0.000536	0.03890 ± 0.000276	0.00051 ± 0.000024	0.00010 ± 0.000028	0.000015 ± 0.000009	7.01E-16	96.1%	2.7398	21.59 ± 0.60	3%
au40.2i.ksp.5g.txt	0.7	30	0.17904 ± 0.000641	0.05038 ± 0.000197	0.00057 ± 0.000012	0.00021 ± 0.000022	0.000017 ± 0.000008	1.13E-15	97.3%	3.4567	27.20 ± 0.41	1%
au40.2i.ksp.5h.txt	0.75	30	0.90965 ± 0.002718	0.16567 ± 0.000300	0.00208 ± 0.000046	0.00045 ± 0.000031	0.000427 ± 0.000017	5.75E-15	86.1%	4.7294	37.12 ± 0.28	1%
au40.2i.ksp.5i.txt	0.8	30	0.16307 ± 0.000518	0.04622 ± 0.000142	0.00052 ± 0.000014	0.00025 ± 0.000017	0.000019 ± 0.000006	1.03E-15	96.6%	3.4085	26.83 ± 0.33	1%
au40.2i.ksp.5j.txt	0.85	30	0.24007 ± 0.000983	0.06542 ± 0.000246	0.00081 ± 0.000023	0.00017 ± 0.000018	0.000080 ± 0.000007	1.52E-15	90.1%	3.3084	26.04 ± 0.28	1%
au40.2i.ksp.5k.txt	0.9	30	0.12507 ± 0.000682	0.04043 ± 0.000184	0.00046 ± 0.000016	0.00006 ± 0.000031	0.000004 ± 0.000008	7.91E-16	99.1%	3.0666	24.15 ± 0.48	2%
au40.2i.ksp.5l.txt	0.95	30	1.21542 ± 0.004964	0.23695 ± 0.000896	0.00297 ± 0.000037	0.00059 ± 0.000022	0.000826 ± 0.000009	7.68E-15	79.9%	4.0991	32.21 ± 0.24	1%
au40.2i.ksp.5m.txt	1	30	0.33548 ± 0.001442	0.10538 ± 0.000151	0.00119 ± 0.000019	0.00033 ± 0.000018	0.000044 ± 0.000010	2.12E-15	96.1%	3.0603	24.10 ± 0.25	1%
au40.2i.ksp.5n.txt	1.15	30	0.62286 ± 0.002062	0.16827 ± 0.000629	0.00191 ± 0.000029	0.00098 ± 0.000024	0.000070 ± 0.000011	3.94E-15	96.7%	3.5787	28.16 ± 0.21	1%
au40.2i.ksp.5o.txt	1.2	30	0.86723 ± 0.003007	0.16407 ± 0.000352	0.00203 ± 0.000063	0.00047 ± 0.000032	0.000237 ± 0.000007	5.48E-15	91.9%	4.8597	38.13 ± 0.20	1%
au40.2i.ksp.5p.txt	1.25	30	0.65811 ± 0.002253	0.11563 ± 0.000294	0.00143 ± 0.000034	0.00029 ± 0.000039	0.000068 ± 0.000006	4.16E-15	96.9%	5.5174	43.23 ± 0.22	1%
au40.2i.ksp.5q.txt	1.3	30	1.27956 ± 0.004186	0.21310 ± 0.000564	0.00257 ± 0.000066	0.00048 ± 0.000030	0.000142 ± 0.000006	8.09E-15	96.7%	5.8079	45.48 ± 0.21	0%
au40.2i.ksp.5r.txt	1.4	30	1.74889 ± 0.004475	0.28964 ± 0.000765	0.00353 ± 0.000058	0.00070 ± 0.000017	0.000190 ± 0.000011	1.11E-14	96.8%	5.8441	45.76 ± 0.20	0%
au40.2i.ksp.5s.txt	1.5	30	8.51419 ± 0.022579	1.32069 ± 0.002878	0.01627 ± 0.000072	0.00408 ± 0.000085	0.000856 ± 0.000023	5.38E-14	97.0%	6.2555	48.93 ± 0.18	0%
au40.2i.ksp.5t.txt	1.6	30	4.71063 ± 0.015590	0.68605 ± 0.002266	0.00833 ± 0.000062	0.00131 ± 0.000039	0.000192 ± 0.000007	2.98E-14	98.8%	6.7839	53.01 ± 0.25	0%
au40.2i.ksp.5u.txt	1.8	30	4.66894 ± 0.012915	0.72364 ± 0.001535	0.00876 ± 0.000073	0.00174 ± 0.000089	0.000362 ± 0.000020	2.95E-14	97.7%	6.3045	49.31 ± 0.19	0%
au40.2i.ksp.5v.txt	2	30	3.09993 ± 0.009418	0.47466 ± 0.001002	0.00573 ± 0.000102	0.00095 ± 0.000035	0.000214 ± 0.000017	1.96E-14	98.0%	6.3980	50.03 ± 0.21	0%
au40.2i.ksp.5w.txt	2.2	30	0.97232 ± 0.003962	0.14155 ± 0.000584	0.00166 ± 0.000036	0.00030 ± 0.000026	0.000047 ± 0.000012	6.15E-15	98.6%	6.7719	52.92 ± 0.37	1%
au40.2i.ksp.5x.txt	2.4	30	1.27980 ± 0.005315	0.17482 ± 0.000750	0.00197 ± 0.000033	0.00044 ± 0.000027	0.000017 ± 0.000009	8.09E-15	99.6%	7.2924	56.92 ± 0.36	1%
au40.2i.ksp.5y.txt	2.6	30	0.62562 ± 0.002571	0.07820 ± 0.000162	0.00085 ± 0.000014	0.00021 ± 0.000027	0.000006 ± 0.000009	3.95E-15	99.7%	7.9779	62.18 ± 0.39	1%

Sample ID/Increment Info	P	t	40Ar(*+atm)	39ArK	38Ar(Atm+Cl)	37ArCa	36Ar(Atm)	Moles 40Ar*	% Rad.	R	Age (Ma)	% s.d.
TDGK-001, IH Analyses	J-Value=0.004331±0.000012											
au40.2i.plag.6a.txt	0.4	30	0.09913 ± 0.000328	0.00227 ± 0.000070	0.00007 ± 0.000014	0.00063 ± 0.000013	0.000226 ± 0.000007	6.27E-16	32.8%	14.3242	110.18 ± 14.55	13%
au40.2i.plag.6b.txt	0.45	30	0.02572 ± 0.000182	0.00133 ± 0.000052	0.00000 ± 0.000011	0.00032 ± 0.000017	0.000065 ± 0.000007	1.63E-16	25.4%	4.9313	38.68 ± 13.89	36%
au40.2i.plag.6c.txt	0.5	30	0.03378 ± 0.000269	0.00315 ± 0.000044	0.00003 ± 0.000010	0.00101 ± 0.000025	0.000073 ± 0.000007	2.14E-16	35.9%	3.8828	30.53 ± 5.46	18%
au40.2i.plag.6d.txt	0.55	30	0.04614 ± 0.000209	0.00705 ± 0.000063	0.00011 ± 0.000013	0.00306 ± 0.000066	0.000072 ± 0.000006	2.92E-16	54.0%	3.5777	28.15 ± 2.08	7%
au40.2i.plag.6e.txt	0.6	30	0.04543 ± 0.000241	0.00851 ± 0.000105	0.00010 ± 0.000015	0.00575 ± 0.000088	0.000055 ± 0.000007	2.87E-16	64.4%	3.5033	27.57 ± 1.90	7%
au40.2i.plag.6f.txt	0.65	30	0.04845 ± 0.000316	0.00819 ± 0.000062	0.00009 ± 0.000013	0.01342 ± 0.000137	0.000072 ± 0.000007	3.06E-16	55.8%	3.4560	27.20 ± 2.03	7%
au40.2i.plag.6g.txt	0.7	30	0.01378 ± 0.000174	0.00302 ± 0.000044	0.00001 ± 0.000013	0.00672 ± 0.000151	0.000014 ± 0.000006	8.71E-17	69.5%	3.3743	26.56 ± 4.97	19%
au40.2i.plag.6h.txt	0.75	30	0.01763 ± 0.000151	0.00328 ± 0.000049	0.00003 ± 0.000015	0.00867 ± 0.000159	0.000004 ± 0.000010	1.11E-16	93.9%	5.2937	41.50 ± 6.92	17%
au40.2i.plag.6i.txt	0.8	30	0.02682 ± 0.000172	0.00473 ± 0.000051	0.00000 ± 0.000021	0.01370 ± 0.000184	0.000020 ± 0.000007	1.70E-16	78.1%	4.7011	36.90 ± 3.27	9%
au40.2i.plag.6j.txt	0.85	30	0.08601 ± 0.000225	0.01210 ± 0.000102	0.00013 ± 0.000013	0.01892 ± 0.000197	0.000050 ± 0.000010	5.44E-16	82.8%	6.0309	47.20 ± 1.92	4%
au40.2i.plag.6k.txt	0.9	30	0.04301 ± 0.000362	0.00659 ± 0.000065	0.00007 ± 0.000013	0.01309 ± 0.000156	0.000018 ± 0.000006	2.72E-16	87.3%	5.8863	46.08 ± 2.26	5%
au40.2i.plag.6l.txt	0.95	30	0.03772 ± 0.000188	0.00630 ± 0.000087	0.00006 ± 0.000013	0.01285 ± 0.000177	0.000029 ± 0.000006	2.38E-16	77.5%	4.8311	37.91 ± 2.21	6%
au40.2i.plag.6m.txt	1	30	0.07707 ± 0.000159	0.01238 ± 0.000096	0.00013 ± 0.000015	0.02106 ± 0.000286	0.000043 ± 0.000010	4.87E-16	83.6%	5.3644	42.04 ± 2.00	5%
au40.2i.plag.6n.txt	1.15	30	0.24673 ± 0.000953	0.03581 ± 0.000282	0.00045 ± 0.000015	0.16053 ± 0.000440	0.000231 ± 0.000008	1.56E-15	72.4%	5.4066	42.37 ± 0.71	2%
au40.2i.plag.6o.txt	1.2	30	0.04593 ± 0.000367	0.00617 ± 0.000083	0.00007 ± 0.000014	0.04198 ± 0.000409	0.000014 ± 0.000011	2.90E-16	90.8%	7.4079	57.81 ± 4.11	7%
au40.2i.plag.6p.txt	1.25	30	0.02286 ± 0.000218	0.00315 ± 0.000050	0.00003 ± 0.000015	0.02103 ± 0.000208	-0.000006 ± 0.000009	1.45E-16	107.8%	7.8875	61.49 ± 6.47	11%
au40.2i.plag.6q.txt	1.3	30	0.03704 ± 0.000169	0.00461 ± 0.000047	0.00005 ± 0.000012	0.03494 ± 0.000247	0.000019 ± 0.000006	2.34E-16	84.9%	7.5491	58.89 ± 3.04	5%
au40.2i.plag.6r.txt	1.4	30	0.01743 ± 0.000134	0.00238 ± 0.000042	0.00001 ± 0.000012	0.01566 ± 0.000256	0.000017 ± 0.000007	1.10E-16	71.2%	5.8395	45.72 ± 6.44	14%
au40.2i.plag.6s.txt	1.5	30	0.02768 ± 0.000221	0.00339 ± 0.000048	0.00004 ± 0.000014	0.02330 ± 0.000224	0.000004 ± 0.000009	1.75E-16	95.3%	8.4552	65.84 ± 6.07	9%
au40.2i.plag.6t.txt	1.6	30	0.02863 ± 0.000311	0.00353 ± 0.000042	0.00002 ± 0.000017	0.02736 ± 0.000367	0.000019 ± 0.000007	1.81E-16	80.9%	7.2959	56.95 ± 4.58	8%
au40.2i.plag.6u.txt	1.8	30	0.03060 ± 0.000207	0.00387 ± 0.000047	0.00004 ± 0.000012	0.02802 ± 0.000189	0.000028 ± 0.000006	1.93E-16	73.1%	6.4681	50.58 ± 3.54	7%
au40.2i.plag.6v.txt	2	30	0.01286 ± 0.000103	0.00166 ± 0.000045	0.00002 ± 0.000014	0.01262 ± 0.000205	0.000018 ± 0.000006	8.13E-17	58.5%	5.2367	41.05 ± 9.06	22%
au40.2i.plag.6w.txt	2.2	30	0.00698 ± 0.000117	0.00081 ± 0.000044	0.00000 ± 0.000014	0.00712 ± 0.000142	-0.000020 ± 0.000009	4.41E-17	182.7%	9.4388	73.34 ± 26.83	37%
au40.2i.plag.6x.txt	2.4	30	0.00285 ± 0.000122	0.00032 ± 0.000048	-0.00001 ± 0.000012	0.00262 ± 0.000101	0.000000 ± 0.000006	1.80E-17	95.5%	9.4028	73.07 ± 45.90	63%

Sample ID/Increment Info	P	t	40Ar(*+atm)	39ArK	38Ar(Atm+Cl)	37ArCa	36Ar(Atm)	Moles 40Ar*	% Rad.	R	Age (Ma)	% s.d.
TDGK-001, IH Analyses	J-Value=0.004331±0.000012											
au40.2i.plag.7a.txt	0.4	30	0.00142 ± 0.000092	0.00004 ± 0.000042	-0.00002 ± 0.000013	-0.00004 ± 0.000019	0.000004 ± 0.000006	9.00E-18	14.4%	5.4878	43.00 ± 600.75	1397%
au40.2i.plag.7b.txt	0.45	30	0.23382 ± 0.000776	0.00249 ± 0.000045	0.00011 ± 0.000014	0.00071 ± 0.000028	0.000509 ± 0.000008	1.48E-15	35.6%	33.5340	248.24 ± 16.50	7%
au40.2i.plag.7c.txt	0.5	30	0.06932 ± 0.000171	0.00218 ± 0.000051	0.00004 ± 0.000012	0.00065 ± 0.000030	0.000135 ± 0.000006	4.38E-16	42.5%	13.5559	104.44 ± 9.50	9%
au40.2i.plag.7d.txt	0.55	30	0.04766 ± 0.000333	0.00475 ± 0.000069	0.00006 ± 0.000013	0.00140 ± 0.000040	0.000080 ± 0.000007	3.01E-16	50.1%	5.0537	39.63 ± 3.53	9%
au40.2i.plag.7e.txt	0.6	30	0.05824 ± 0.000228	0.00845 ± 0.000124	0.00009 ± 0.000013	0.00364 ± 0.000098	0.000102 ± 0.000007	3.68E-16	48.2%	3.3582	26.43 ± 2.03	8%
au40.2i.plag.7f.txt	0.65	30	0.06868 ± 0.000233	0.01143 ± 0.000136	0.00014 ± 0.000014	0.00774 ± 0.000060	0.000105 ± 0.000006	4.34E-16	54.9%	3.3607	26.45 ± 1.46	6%
au40.2i.plag.7g.txt	0.7	30	0.01557 ± 0.000152	0.00383 ± 0.000046	0.00004 ± 0.000016	0.00377 ± 0.000047	0.000004 ± 0.000010	9.84E-17	92.2%	3.8452	30.23 ± 5.85	19%
au40.2i.plag.7h.txt	0.75	30	0.02411 ± 0.000173	0.00521 ± 0.000062	0.00005 ± 0.000013	0.00887 ± 0.000224	0.000028 ± 0.000009	1.52E-16	65.4%	3.1847	25.08 ± 4.26	17%
au40.2i.plag.7i.txt	0.8	30	0.01567 ± 0.000238	0.00396 ± 0.000040	0.00004 ± 0.000011	0.00948 ± 0.000195	0.000018 ± 0.000006	9.90E-17	66.2%	2.8397	22.38 ± 3.75	17%
au40.2i.plag.7j.txt	0.85	30	0.01499 ± 0.000154	0.00411 ± 0.000050	0.00005 ± 0.000012	0.01250 ± 0.000240	0.000006 ± 0.000007	9.48E-17	88.4%	3.5042	27.57 ± 4.04	15%
au40.2i.plag.7k.txt	0.9	30	0.06527 ± 0.000276	0.01266 ± 0.000097	0.00018 ± 0.000013	0.04819 ± 0.000411	0.000047 ± 0.000011	4.13E-16	78.8%	4.4173	34.69 ± 2.04	6%
au40.2i.plag.7l.txt	0.95	30	0.01871 ± 0.000166	0.00501 ± 0.000064	0.00005 ± 0.000013	0.01973 ± 0.000259	0.000014 ± 0.000006	1.18E-16	78.2%	3.2861	25.87 ± 2.95	11%
au40.2i.plag.7m.txt	1	30	0.01807 ± 0.000237	0.00487 ± 0.000056	0.00005 ± 0.000013	0.01795 ± 0.000132	0.000004 ± 0.000009	1.14E-16	93.8%	3.8200	30.04 ± 4.10	14%
au40.2i.plag.7n.txt	1.15	30	0.03767 ± 0.000312	0.00865 ± 0.000118	0.00011 ± 0.000013	0.03124 ± 0.000139	0.000010 ± 0.000009	2.38E-16	92.3%	4.3565	34.22 ± 2.42	7%
au40.2i.plag.7o.txt	1.2	30	0.09746 ± 0.000446	0.01351 ± 0.000125	0.00017 ± 0.000016	0.04176 ± 0.000228	0.000153 ± 0.000006	6.16E-16	53.8%	4.1659	32.73 ± 1.28	4%
au40.2i.plag.7p.txt	1.25	30	0.02015 ± 0.000138	0.00515 ± 0.000071	0.00005 ± 0.000016	0.01248 ± 0.000206	-0.000004 ± 0.000010	1.27E-16	105.8%	4.1384	32.52 ± 4.41	14%
au40.2i.plag.7q.txt	1.3	30	0.04527 ± 0.000201	0.01169 ± 0.000100	0.00013 ± 0.000012	0.01785 ± 0.000156	0.000031 ± 0.000007	2.86E-16	80.0%	3.2409	25.52 ± 1.38	5%
au40.2i.plag.7r.txt	1.4	30	0.05998 ± 0.000207	0.01308 ± 0.000083	0.00016 ± 0.000012	0.01823 ± 0.000155	0.000051 ± 0.000006	3.79E-16	75.0%	3.5692	28.08 ± 1.11	4%
au40.2i.plag.7s.txt	1.5	30	0.21339 ± 0.000962	0.03446 ± 0.000177	0.00041 ± 0.000016	0.11003 ± 0.000721	0.000188 ± 0.000011	1.35E-15	74.0%	4.8812	38.30 ± 0.82	2%
au40.2i.plag.7t.txt	1.6	30	0.11343 ± 0.000478	0.01562 ± 0.000111	0.00022 ± 0.000021	0.07571 ± 0.000361	0.000073 ± 0.000007	7.17E-16	81.1%	6.3447	49.62 ± 1.16	2%
au40.2i.plag.7u.txt	1.8	30	0.31211 ± 0.000637	0.04429 ± 0.000230	0.00050 ± 0.000014	0.23478 ± 0.000878	0.000154 ± 0.000007	1.97E-15	85.4%	6.5192	50.97 ± 0.49	1%
au40.2i.plag.7v.txt	2	30	0.05905 ± 0.000316	0.00753 ± 0.000075	0.00008 ± 0.000017	0.05067 ± 0.000349	0.000021 ± 0.000006	3.73E-16	89.4%	7.6514	59.68 ± 1.99	3%
au40.2i.plag.7w.txt	2.2	30	0.05880 ± 0.000302	0.00687 ± 0.000052	0.00006 ± 0.000011	0.04488 ± 0.000463	0.000029 ± 0.000006	3.72E-16	85.2%	7.9242	61.77 ± 2.15	3%
au40.2i.plag.7x.txt	2.4	30	0.06808 ± 0.000139	0.00745 ± 0.000067	0.00007 ± 0.000014	0.04688 ± 0.000397	0.000026 ± 0.000006	4.30E-16	88.8%	8.7187	67.85 ± 1.96	3%

Sample ID/Increment Info	P	t	40Ar(*+atm)	39ArK	38Ar(Atm+Cl)	37ArCa	36Ar(Atm)	Moles 40Ar*	% Rad.	R	Age (Ma)	% s.d.
TDGK-001, IH Analyses	J-Value=0.004331±0.000012											
au40.2i.ksp.8a.txt	0.4	30	2.26251 ± 0.007737	0.00149 ± 0.000071	0.00095 ± 0.000018	0.00001 ± 0.000018	0.005174 ± 0.000040	1.43E-14	32.4%	493.5101	2093.03 ± 371.85	18%
au40.2i.ksp.8b.txt	0.45	30	1.80959 ± 0.007408	0.00700 ± 0.000049	0.00030 ± 0.000013	0.00006 ± 0.000034	0.001139 ± 0.000027	1.14E-14	81.4%	210.5806	1186.50 ± 13.57	1%
au40.2i.ksp.8c.txt	0.5	30	0.54101 ± 0.002138	0.02898 ± 0.000180	0.00037 ± 0.000015	0.00025 ± 0.000025	0.000221 ± 0.000006	3.42E-15	87.9%	16.4184	125.75 ± 1.17	1%
au40.2i.ksp.8d.txt	0.55	30	0.18864 ± 0.000831	0.03339 ± 0.000237	0.00038 ± 0.000015	0.00031 ± 0.000025	0.000051 ± 0.000006	1.19E-15	92.0%	5.1962	40.74 ± 0.56	1%
au40.2i.ksp.8e.txt	0.6	30	0.52059 ± 0.001353	0.06829 ± 0.000360	0.00097 ± 0.000045	0.00054 ± 0.000042	0.000436 ± 0.000007	3.29E-15	75.2%	5.7373	44.93 ± 0.44	1%
au40.2i.ksp.8f.txt	0.65	30	0.79993 ± 0.003076	0.13110 ± 0.000538	0.00157 ± 0.000025	0.00081 ± 0.000015	0.000160 ± 0.000007	5.06E-15	94.1%	5.7405	44.96 ± 0.29	1%
au40.2i.ksp.8g.txt	0.7	30	0.85879 ± 0.002428	0.16269 ± 0.000447	0.00203 ± 0.000043	0.00091 ± 0.000044	0.000164 ± 0.000007	5.43E-15	94.4%	4.9814	39.07 ± 0.19	0%
au40.2i.ksp.8h.txt	0.75	30	0.79812 ± 0.003332	0.16247 ± 0.000517	0.00208 ± 0.000060	0.00079 ± 0.000031	0.000090 ± 0.000006	5.05E-15	96.7%	4.7495	37.27 ± 0.22	1%
au40.2i.ksp.8i.txt	0.8	30	0.61824 ± 0.002247	0.13530 ± 0.000317	0.00163 ± 0.000052	0.00057 ± 0.000023	0.000000 ± 0.000010	3.91E-15	100.0%	4.5689	35.87 ± 0.23	1%
au40.2i.ksp.8j.txt	0.85	30	0.98551 ± 0.003361	0.19237 ± 0.000392	0.00236 ± 0.000056	0.00065 ± 0.000039	0.000046 ± 0.000008	6.23E-15	98.6%	5.0532	39.63 ± 0.18	0%
au40.2i.ksp.8k.txt	0.9	30	0.61713 ± 0.002609	0.12341 ± 0.000577	0.00142 ± 0.000021	0.00046 ± 0.000038	0.000010 ± 0.000006	3.90E-15	99.5%	4.9759	39.03 ± 0.27	1%
au40.2i.ksp.8l.txt	0.95	30	1.29193 ± 0.005097	0.23170 ± 0.000925	0.00274 ± 0.000053	0.00105 ± 0.000011	0.000000 ± 0.000011	8.17E-15	100.0%	5.5763	43.68 ± 0.27	1%
au40.2i.ksp.8m.txt	1	30	2.55144 ± 0.009881	0.37292 ± 0.001060	0.00454 ± 0.000066	0.00293 ± 0.000033	0.000155 ± 0.000007	1.61E-14	98.2%	6.7199	52.52 ± 0.26	0%
au40.2i.ksp.8n.txt	1.15	30	12.48483 ± 0.042998	1.66051 ± 0.004021	0.02009 ± 0.000212	0.00602 ± 0.000072	0.000635 ± 0.000013	7.89E-14	98.5%	7.4061	57.79 ± 0.25	0%
au40.2i.ksp.8o.txt	1.2	30	3.33126 ± 0.012717	0.43431 ± 0.001025	0.00543 ± 0.000058	0.00121 ± 0.000039	0.000127 ± 0.000007	2.11E-14	98.9%	7.5840	59.16 ± 0.27	0%
au40.2i.ksp.8p.txt	1.25	30	4.45423 ± 0.014580	0.57840 ± 0.001305	0.00689 ± 0.000039	0.00140 ± 0.000040	0.000128 ± 0.000007	2.82E-14	99.1%	7.6357	59.56 ± 0.24	0%
au40.2i.ksp.8q.txt	1.3	30	2.37032 ± 0.007971	0.30639 ± 0.000882	0.00351 ± 0.000052	0.00072 ± 0.000028	0.000057 ± 0.000007	1.50E-14	99.3%	7.6814	59.91 ± 0.27	0%
au40.2i.ksp.8r.txt	1.4	30	1.54005 ± 0.005294	0.17669 ± 0.000407	0.00222 ± 0.000039	0.00034 ± 0.000025	0.000053 ± 0.000007	9.74E-15	99.0%	8.6279	67.16 ± 0.30	0%
au40.2i.ksp.8s.txt	1.5	30	1.45328 ± 0.004654	0.16731 ± 0.000460	0.00202 ± 0.000031	0.00031 ± 0.000031	0.000032 ± 0.000007	9.19E-15	99.4%	8.6298	67.17 ± 0.30	0%
au40.2i.ksp.8t.txt	1.6	30	0.73842 ± 0.002372	0.09281 ± 0.000219	0.00107 ± 0.000017	0.00023 ± 0.000040	-0.000013 ± 0.000012	4.67E-15	100.5%	7.9565	62.02 ± 0.38	1%
au40.2i.ksp.8u.txt	1.8	30	0.76139 ± 0.002488	0.09041 ± 0.000388	0.00101 ± 0.000027	0.00020 ± 0.000020	-0.000001 ± 0.000009	4.81E-15	100.0%	8.4217	65.58 ± 0.42	1%
au40.2i.ksp.8v.txt	2	30	0.57230 ± 0.002167	0.07197 ± 0.000247	0.00093 ± 0.000036	0.00017 ± 0.000031	0.000015 ± 0.000007	3.62E-15	99.2%	7.8890	61.50 ± 0.38	1%
au40.2i.ksp.8w.txt	2.2	30	0.23652 ± 0.000939	0.03007 ± 0.000218	0.00034 ± 0.000019	0.00008 ± 0.000020	-0.000014 ± 0.000009	1.50E-15	101.8%	7.8646	61.31 ± 0.88	1%
au40.2i.ksp.8x.txt	2.4	30	0.24012 ± 0.001092	0.02949 ± 0.000137	0.00034 ± 0.000017	0.00011 ± 0.000028	-0.000008 ± 0.000011	1.52E-15	101.0%	8.1434	63.45 ± 0.95	2%
au40.2i.ksp.8y.txt	2.6	30	0.14426 ± 0.000665	0.01794 ± 0.000151	0.00020 ± 0.000010	0.00004 ± 0.000027	0.000002 ± 0.000007	9.12E-16	99.5%	8.0021	62.37 ± 1.06	2%

Sample ID/Increment Info	P	t	40Ar(*+atm)	39ArK	38Ar(Atm+Cl)	37ArCa	36Ar(Atm)	Moles 40Ar*	% Rad.	R	Age (Ma)	% s.d.
TDGK-001, IH Analyses	J-Value=0.004331±0.000012											
au40.2i.plag.16a.txt	0.4	30	0.19262 ± 0.000765	0.00412 ± 0.000052	0.00014 ± 0.000017	0.00086 ± 0.000027	0.000468 ± 0.000009	1.22E-15	28.2%	13.2173	101.90 ± 7.75	8%
au40.2i.plag.16b.txt	0.45	30	0.04121 ± 0.000373	0.00318 ± 0.000045	0.00006 ± 0.000014	0.00073 ± 0.000034	0.000106 ± 0.000006	2.60E-16	23.9%	3.1169	24.55 ± 5.14	21%
au40.2i.plag.16c.txt	0.5	30	0.03567 ± 0.000165	0.00553 ± 0.000084	0.00007 ± 0.000019	0.00095 ± 0.000043	0.000069 ± 0.000011	2.25E-16	43.0%	2.7874	21.97 ± 4.71	21%
au40.2i.plag.16d.txt	0.55	30	0.17396 ± 0.000851	0.02576 ± 0.000197	0.00033 ± 0.000018	0.00808 ± 0.000161	0.000315 ± 0.000014	1.10E-15	46.5%	3.1692	24.96 ± 1.36	5%
au40.2i.plag.16e.txt	0.6	30	0.12542 ± 0.000554	0.01970 ± 0.000136	0.00026 ± 0.000014	0.01043 ± 0.000076	0.000268 ± 0.000011	7.93E-16	36.9%	2.3969	18.91 ± 1.42	8%
au40.2i.plag.16f.txt	0.65	30	0.04261 ± 0.000293	0.00864 ± 0.000087	0.00011 ± 0.000013	0.01206 ± 0.000205	0.000046 ± 0.000012	2.69E-16	67.9%	3.4792	27.38 ± 3.19	12%
au40.2i.plag.16g.txt	0.7	30	0.02087 ± 0.000207	0.00420 ± 0.000056	0.00005 ± 0.000012	0.00845 ± 0.000131	0.000018 ± 0.000010	1.32E-16	74.7%	3.8994	30.66 ± 5.68	19%
au40.2i.plag.16h.txt	0.75	30	0.01765 ± 0.000213	0.00373 ± 0.000060	0.00005 ± 0.000017	0.00864 ± 0.000155	0.000006 ± 0.000010	1.12E-16	89.1%	4.4321	34.81 ± 6.42	18%
au40.2i.plag.16i.txt	0.8	30	0.02144 ± 0.000200	0.00250 ± 0.000043	0.00002 ± 0.000013	0.00534 ± 0.000092	0.000044 ± 0.000007	1.36E-16	39.0%	3.5385	27.84 ± 6.38	23%
au40.2i.plag.16j.txt	0.85	30	0.00788 ± 0.000148	0.00187 ± 0.000060	0.00002 ± 0.000011	0.00512 ± 0.000087	0.000008 ± 0.000006	4.98E-17	71.3%	3.2597	25.66 ± 7.77	30%
au40.2i.plag.16k.txt	0.9	30	0.02479 ± 0.000198	0.00323 ± 0.000052	0.00004 ± 0.000012	0.00765 ± 0.000092	0.000037 ± 0.000007	1.57E-16	56.5%	4.5555	35.77 ± 4.97	14%
au40.2i.plag.16l.txt	0.95	30	0.01024 ± 0.000130	0.00236 ± 0.000045	0.00003 ± 0.000013	0.00521 ± 0.000070	0.000007 ± 0.000006	6.47E-17	80.5%	3.6891	29.02 ± 6.29	22%
au40.2i.plag.16m.txt	1	30	0.00795 ± 0.000150	0.00193 ± 0.000043	0.00002 ± 0.000012	0.00353 ± 0.000059	-0.000028 ± 0.000008	5.02E-17	203.5%	4.2809	33.63 ± 10.20	30%
au40.2i.plag.16n.txt	1.15	30	0.13071 ± 0.000569	0.01554 ± 0.000140	0.00022 ± 0.000011	0.01759 ± 0.000274	0.000278 ± 0.000008	8.26E-16	37.2%	3.2320	25.45 ± 1.41	6%
au40.2i.plag.16o.txt	1.2	30	0.11969 ± 0.000498	0.02209 ± 0.000134	0.00029 ± 0.000021	0.02712 ± 0.000294	0.000181 ± 0.000008	7.57E-16	55.2%	3.1040	24.45 ± 0.91	4%
au40.2i.plag.16p.txt	1.25	30	0.09750 ± 0.000566	0.01619 ± 0.000129	0.00021 ± 0.000014	0.03254 ± 0.000299	0.000146 ± 0.000009	6.16E-16	55.8%	3.5481	27.92 ± 1.33	5%
au40.2i.plag.16q.txt	1.3	30	0.14284 ± 0.000608	0.01968 ± 0.000182	0.00025 ± 0.000019	0.07793 ± 0.000338	0.000222 ± 0.000008	9.03E-16	54.1%	4.2953	33.74 ± 1.11	3%
au40.2i.plag.16r.txt	1.4	30	0.07100 ± 0.000143	0.00976 ± 0.000135	0.00011 ± 0.000014	0.05336 ± 0.000474	0.000085 ± 0.000006	4.49E-16	64.6%	5.2156	40.89 ± 1.71	4%
au40.2i.plag.16s.txt	1.5	30	0.04832 ± 0.000294	0.00663 ± 0.000079	0.00006 ± 0.000013	0.03957 ± 0.000298	0.000041 ± 0.000007	3.05E-16	74.7%	6.0070	47.02 ± 2.50	5%
au40.2i.plag.16t.txt	1.6	30	0.04432 ± 0.000241	0.00581 ± 0.000069	0.00008 ± 0.000014	0.04175 ± 0.000401	0.000038 ± 0.000006	2.80E-16	74.5%	6.3619	49.76 ± 2.59	5%

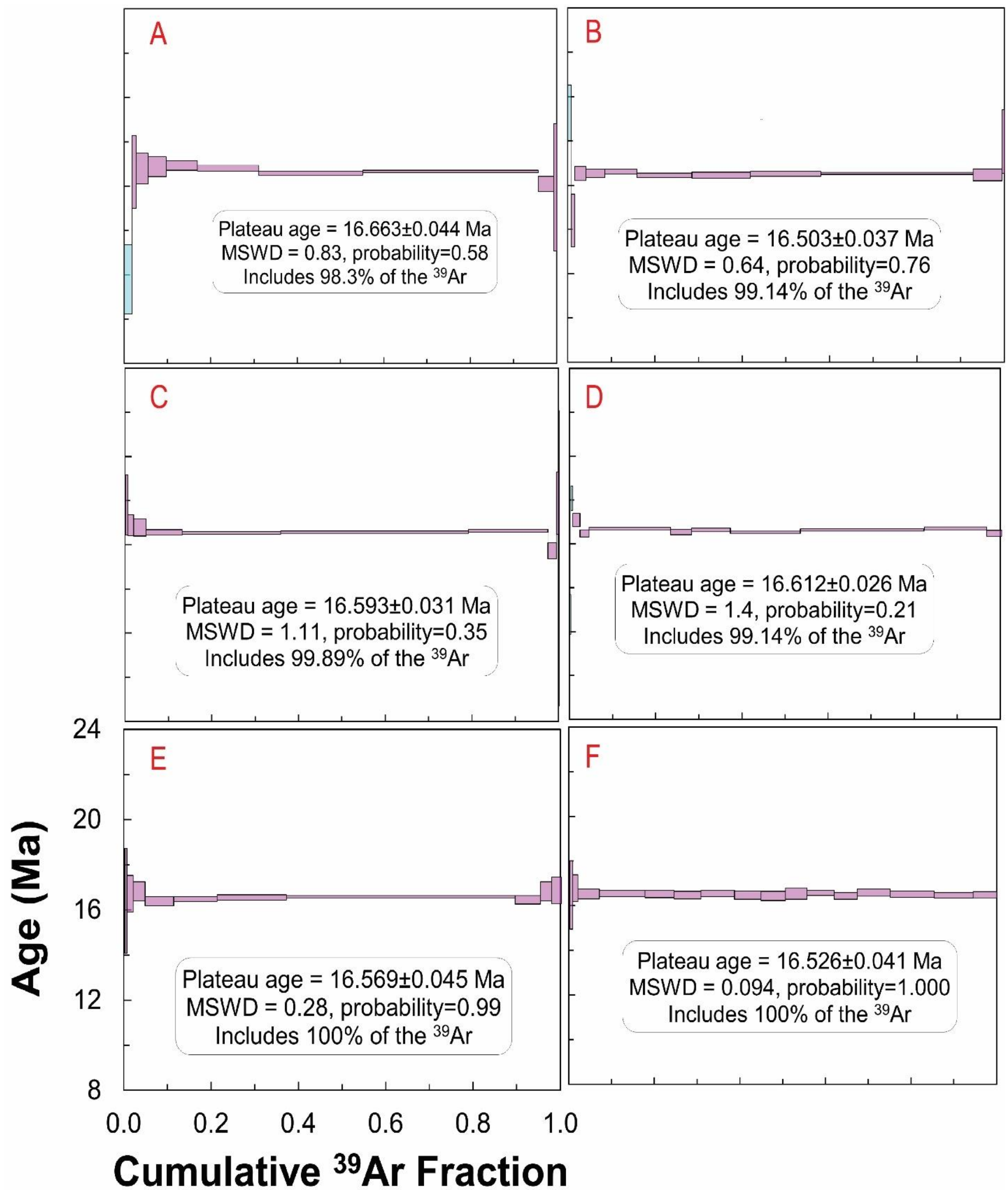

Release spectra for adularia (JMA-002) collected from vein material from the Jumbo Mine. Plateau ages range between 16.66 ± 0.04 to 16.56 ± 0.04 Ma. Box heights represent 1σ, including J-error of 0.000012%. Blue boxes were not included in the plateau age calculation, where purple was included. Analysis Number: A, au40.2f.adl.45; B, au40.2f.adl.46; C, au40.2f.adl.47; D, au40.2f.adl.48; E, au40.2f.adl.49; F, au40.2f.adl.50.

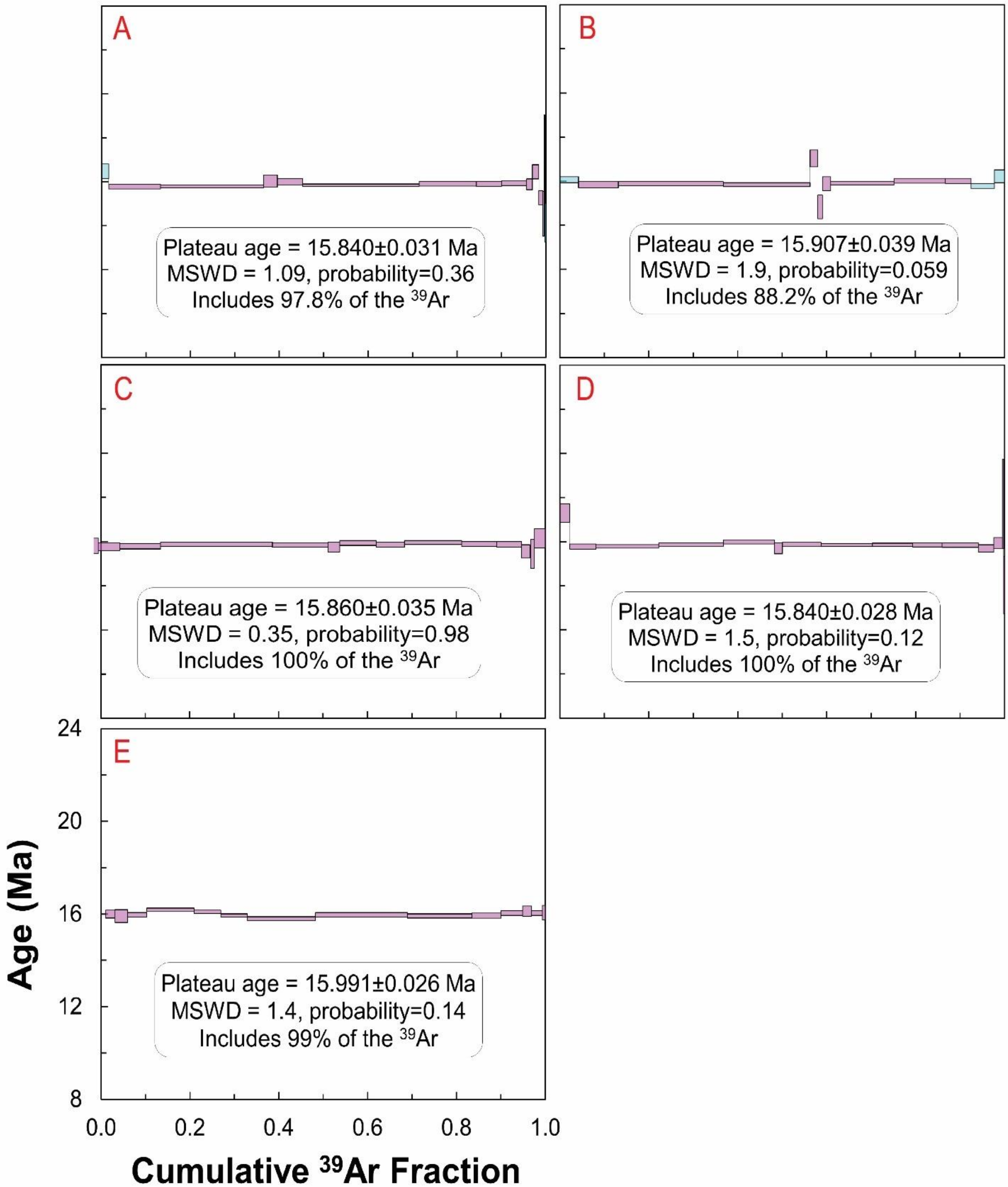

Release spectra for adularia (TDGA-001) collected from vein material from the Trade Dollar Mine. Plateau ages range between 15.99 ± 0.026 to 15.84 ± 0.028 Ma. Box heights represent 1σ, including J-error of 0.000005%. Blue boxes were not included in the plateau age calculation, where purple was included. Analysis Number: A, au40.1b.adl.66; B, au40.1b.adl.67; C, au40.1b.adl.113; D, au40.1b.adl.114; E, au40.1b.adl.115.

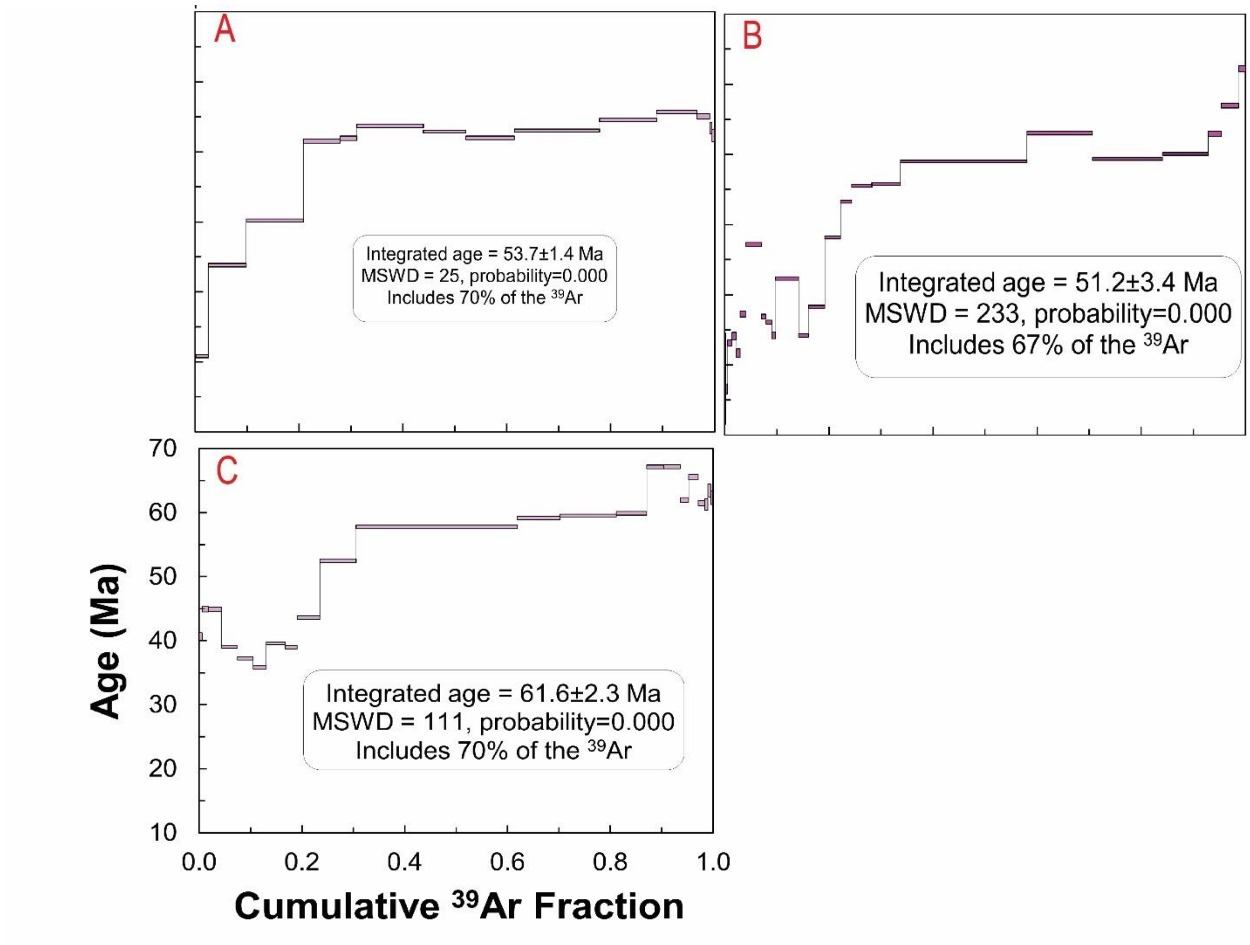

Release spectra for alkali feldspar (TDGK-001) collected from the host rock from the Trade Dollar Mine. The release spectra reflect a diffusion loss profile. Box heights represent 1σ, including J-error of 0.000012%. Analysis Number: A, au40.2i.ksp.3; B, au40.2i.ksp.5; C, au40.2i.ksp.8.

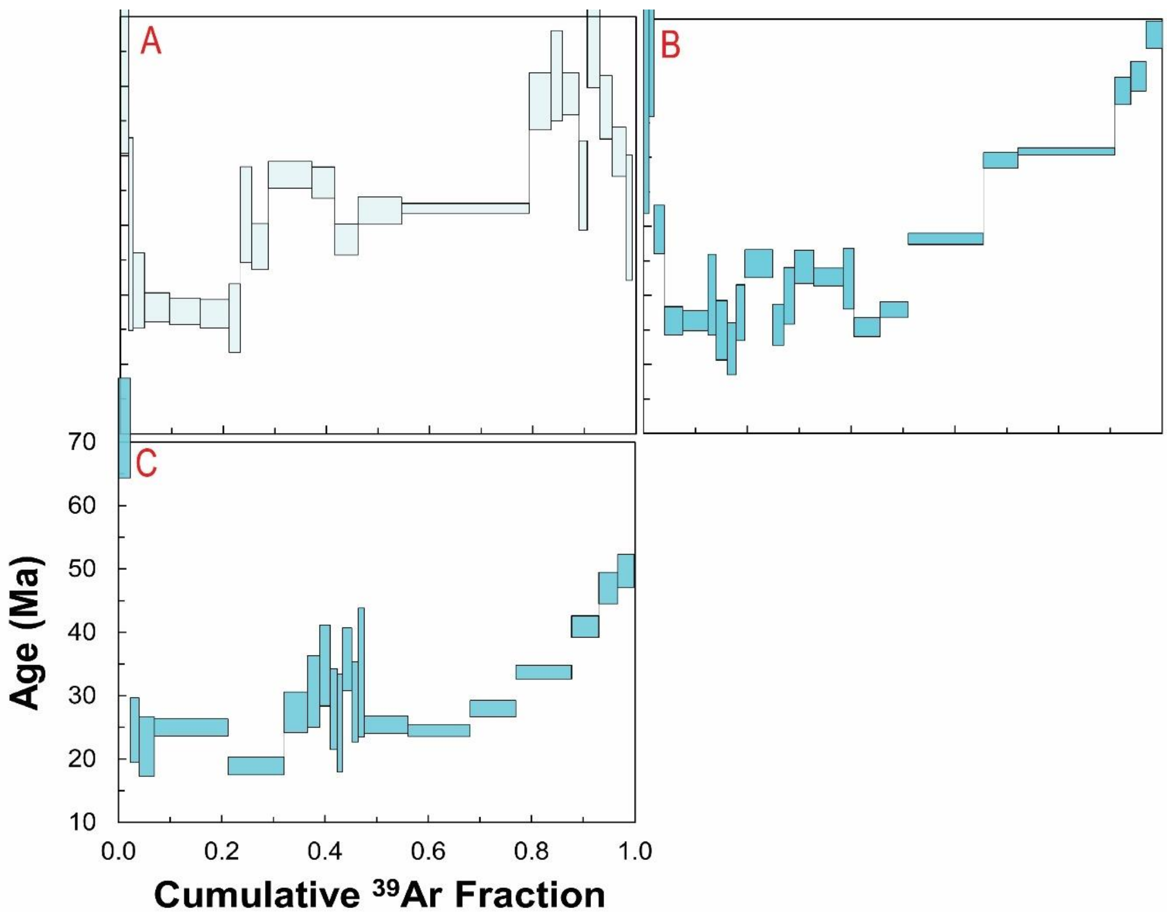

Release spectra for plagioclase feldspar (TDGK-001) collected from the host rock from the Trade Dollar Mine. The release spectra reflect a diffusion loss profile. Box heights represent 1σ, including J-error of 0.000012%. Analysis Number: A, au40.2i.plag.6; B, au40.2i.plag.7; C, au40.2i.plag.16.

APPENDIX 3

Samples of adularia were collected from the Jumbo Mine, Nevada and the Trade Dollar Mine, Idaho. The Jumbo Mine collection site was located at 41° 18’ 1.008” N and 117° 59’ 57.012” W. The Trade Dollar Mine collection site was located at 43° 0’ 29” N and 116° 44’ 19” W.

(A) A phyllite of the Mesozoic metasedimentary hosted Jumbo Mine with a vein (0.0 – 0.5 cm) of adularia which crystallized upon an open fracture. The vein material presents with heavy iron oxide staining. Adularia in this sample are rhombic to sub-rhombic habit, and 0.1 – 0.2 cm in diameter, and perfect cleavage on (001) and good cleavage on (010).

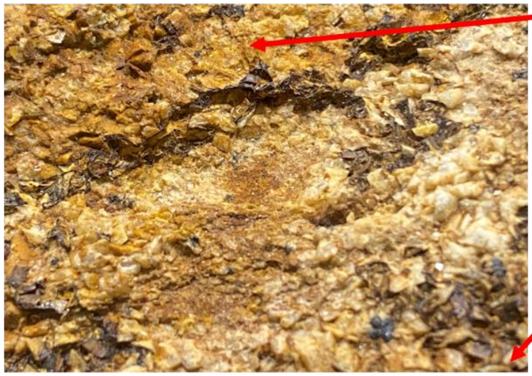

(B) A phyllite of the Mesozoic metasedimentary hosted Jumbo Mine with a vein (0.0 – 0.3 cm) of adularia which crystallized upon an open fracture. The vein material presents with medium to no iron oxide staining.⁺. Adularia in this sample are rhombic to sub-rhombic habit, and 0.1 – 0.2 cm in diameter, and perfect cleavage on (001) and good cleavage on (010).

(C) A block of the Silver City Granite encrusted in adularia, with a vein of adularia crystallized within a fracture of the block. The vein material rings the granite block, and crosscuts through fractures of the block (red circle), with a diameter of (0.1 – 3.0 cm). The feldspars from the Silver City Granite are largely un-altered, 0.1 – 0.3 cm in diameter, are euhedral to subhedral, milky to white, and non-metallic, with visible striations, and perfect cleavage on (001) and good cleavage on (010). The adularia ranges from 0.2 – 3.0 cm in diameter, are rhombic to granular habit, vitreous to milky, and perfect cleavage on (001) and good cleavage on (010). It should be noted that both the TDGA-001 sample and TDGK-001 sample are from this block.

(D) A cut billet of the vein material hosted by the basaltic suite of the Silver City District at the Trade Dollar Mine. This sample is a monolithic breccia with basaltic host rock clasts (0.4 – 4.0 cm in diameter). The basaltic clasts commonly have alteration to sulfides (pyrite) along the rims. The groundmass is fine crystalline adularia (0.01 – 0.1 cm in diameter). The breccia texture was likely generated via hydraulic fracturing of the basaltic host rock preceding Au-Ag mineralization.

(E) Vein material hosted by the basaltic suite of the Silver City District at the Trade Dollar Mine. This sample is a monolithic breccia with basaltic host rock clasts (0.4 – 1.0 cm in diameter). The basaltic clasts commonly have alteration to sulfides (pyrite) along the rims. The groundmass is rhombic to granular adularia (0.01 – 1.0 cm in diameter). The breccia texture was likely generated via hydraulic fracturing of the basaltic host rock preceding Au-Ag mineralization.

(F) Vein material hosted by the basaltic suite of the Silver City District at the Trade Dollar Mine. The vein material crystallized upon the surface of an open fracture of a basaltic host rock, creating a vein diameter of 3.5 cm. Adularia in this sample has a rhombic habit, and appear in a layered texture upon the host rock (pseudo-colloform banding).